

Analysis of sea ice microalgae biomass variability using transmitted irradiance

by

Karley Campbell

A Thesis submitted to the Faculty of Graduate Studies of

The University of Manitoba

in partial fulfilment of the requirements of the degree of

MASTER OF SCIENCE

Department of Environment and Geography

University of Manitoba

Winnipeg

Copyright © 2012 by Karley Campbell

ABSTRACT

The spring bloom of microalgae within the bottom of sea ice provides a significant contribution to primary production in the Arctic Ocean. The aim of this research was to improve observations of the ice algae bloom using a transmitted irradiance technique to remotely estimate biomass, and to examine the influence of physical processes on biomass throughout the sea ice melt season. Results indicate that bottom ice temperature is highly influential in controlling biomass variability and bloom termination. Snow depth is also significant as it buffers ice temperature from the atmosphere and largely controls transmission of photosynthetically active radiation (PAR). The relationship between snow depth and biomass can change over the spring however, limiting biomass accumulation early on while promoting it later. Brine drainage, under-ice current velocity, and surface PAR in the absence of snow cover are also important factors. Overall this research helps to characterize the spring ice algae bloom in the Arctic by improving *in situ* biomass estimates and identifying primary factors controlling it.

ACKNOWLEDGEMENTS

I would like to thank my supervisor Dr. David Barber for his support and guidance in this research endeavour.

I would like to thank my committee members Drs. C.J. Mundy, Michel Gosselin, and Brenda Hann for their contributions of knowledge, editing, and overall support towards this work.

I would like to thank everyone involved with the 2010 and 2011 Arctic-ICE research projects, especially Kristy Hugill for her tireless help with data collection.

I would like to thank the ArcticNet program of the Network of Centres of Excellence, the Canada Research Chairs (CRC) program, the Natural Sciences and Engineering Research Council (NSERC), and the Northern Science Training Program (NSTP) for their financial support.

TABLE OF CONTENTS

ABSTRACT.....	ii
ACKNOWLEDGEMENTS.....	iii
TABLE OF CONTENTS.....	iv
LIST OF TABLES.....	viii
LIST OF FIGURES.....	ix
LIST OF COPYRIGHTED MATERIAL.....	xii
CHAPTER ONE: INTRODUCTION.....	1
1. Rationale and Context.....	1
2. Thesis Objectives.....	2
3.0 Thesis Structure.....	2
Literature Cited.....	4
CHAPTER 2: BACKGROUND.....	5
1. Introduction.....	5
2. Sea Ice Formation, Growth, and Decay.....	5
2.1 Sea Ice Formation.....	5
2.2 Sea Ice Growth.....	6
2.2.1 Crystal Growth.....	6
2.2.2 Brine Inclusions and Drainage.....	8
2.3 Snow on Sea Ice.....	9
2.4 Sea Ice Melt and Decay.....	10
3. Radiative Transfer.....	11
3.1 Albedo.....	11
3.2 Sea Ice Attenuation.....	13
3.2.1 Vertical Attenuation Profile.....	13
3.2.2 Surface Layer: Snowpack Attenuation.....	14
3.2.3 Surface Layer: Sea Ice Attenuation.....	15
3.2.4 Central Ice Attenuation.....	16
3.2.5 Detritus and Other Absorption.....	17
3.3 Seasonal Changes in Attenuation.....	19

4. Ice Algae	19
4.1 Habitat.....	19
4.2 Algae Attenuation Properties.....	20
4.3 Influential Factors on Growth.....	21
4.3.1 Nutrients.....	22
4.3.2 Salinity and Temperature	23
4.3.3 Tide and Brine.....	24
5. Biomass Sampling Techniques	25
5.1 Traditional Methodology.....	25
5.1.1 Algal Sample Collection	25
5.1.2 Chl <i>a</i> Processing	26
5.1.3 Spectrophotometry	26
5.1.4 Fluorometry.....	27
5.2 Developing Methodology	28
5.2.1 Biomass Estimates Using Ratios of Transmitted Irradiance.....	29
5.2.2 Biomass Estimates Using Normalized Difference Indices (NDIs).....	30
Literature Cited	31
CHAPTER THREE: TIME SERIES MEASUREMENTS OF ICE ALGAE BIOMASS USING TRANSMITTED IRRADIANCE AND ASSESSMENT OF INFLUENTIAL PHYSICAL VARIABLES OVER THE SPRING MELT PERIOD	37
Abstract	37
1. Introduction	38
2. Materials and Methods	40
2.1 Study Site.....	40
2.2 Transmitted Irradiance Measurements	41
2.3 Deriving Time Series Chl <i>a</i> from T_{λ}	42
2.3.1 Core Sampling	42
2.3.2 Calculation of Time Series Biomass.....	43
2.4 Physical Sampling	44
2.5 Principal Component Analysis	45
3. Results and Discussion.....	45

3.1 Site Conditions	45
3.2 Optimal NDI	46
3.3 Time Series Chl <i>a</i> Calculation	47
3.4 Environmental Influences on Ice Algae Biomass.....	50
3.4.1 Principal Component Analysis	50
3.4.2 Linear Regression Analysis	53
4. Summary and Conclusions.....	60
Acknowledgements	63
Literature Cited	64
CHAPTER FOUR: CHARACTERIZING THE ICE ALGAE BIOMASS – SNOW DEPTH RELATIONSHIP OVER SPRING MELT USING TRANSMITTED IRRADIANCE	68
Abstract	68
1. Introduction	69
2. Materials and Methods	72
2.1 Study Site.....	72
2.2 Determining Biomass from Transmitted Irradiance	73
2.2.1 Measurement of T_{λ}	74
2.2.2 T_{λ} Calibration.....	74
2.2.3 Normalized Difference Index (NDI) and Biomass Calculation.....	75
2.3 Snow Clear Experimentation.....	76
2.4 Time Series	76
2.5 Transect Sampling	77
2.6 Sampling End Date	78
3. Results	79
3.1 Site Characteristics	79
3.2 Time Series Analysis	81
3.3 Snow Clear Experimentation.....	83
3.4 Transect Analysis.....	87
3.4.1 Seasonal Trends	87
3.4.2 Chl <i>a</i> – H_S association.....	89

4. Discussion	92
4.1 Biomass Response to Snow Removal	92
4.2 Seasonality of the Biomass – H _s Relationship	96
5. Conclusions	99
Acknowledgements	100
Literature Cited	101
CHAPTER FIVE: CONCLUSIONS AND RECOMMENDATIONS	104
5.1 Summary	104
5.2 Future Recommendations.....	105
5.3 Conclusions	106
Literature Cited	109
APPENDIX A: ABBREVIATIONS.....	110

LIST OF TABLES

Table 3.1. Coefficients of determination (r^2 values) between calculated chl a concentration and environmental variables (snow depth, H_S ; surface PAR, S_{PAR} ; PAR integrated transmittance, T_{PAR} ; average brine volume, BV_{AVG} ; bottom ice temperature gradient, TG; and mean daily under-ice velocity, MDV) for 3 sampling periods: early spring (9 May to 9 June, but 9 to 24 May for TG), late spring (10 to 26 June, but 25 May to 26 June for TG) and the total sampling period (9 May to 26 June) when point distributions permitted statistical analysis. Bolded values are significant at $p < 0.05$ 55

Table 4.1. Summary of transect measurements including sample date, transect length and number of chlorophyll a (chl a) biomass, snow depth (H_S) and PAR integrated transmittance (T_{PAR}) observations..... 78

LIST OF FIGURES

Figure 2.1. Close-up of the sea ice skeletal layer at the growth interface where ice crystals develop by production of platelet extensions. From Horner (2000). Copyright (2012) Taylor & Francis Group LLC - Books..... 7

Figure 2.2. (a) Enlargement and (b) shrinkage of sea ice brine pockets in sea ice during an experimental warming and cooling sequence highlighted by arrows 1 and 2, respectively. From Light et al. (2003). Copyright (2012) American Geophysical Union. 8

Figure 2.3. Albedo decline as a function of wavelength with melt season progression on first-year ice: (a) dry snow over ice, (b) melting snow over ice, (c) bare ice, and (d) melting ice. From Grenfell and Perovich (1984). Copyright (2012) American Geophysical Union..... 12

Figure 2.4. (a) Transmittance and (b) spectral diffuse attenuation coefficient (K_{profiler}) of photosynthetically active radiation (PAR) through first-year ice. The vertical profile is divided into optically unique 1. Surface, 2. Internal, 3. Detritus, and 4. Algal regions. From Ehn et al. (2008). Copyright (2012) American Geophysical Union. 14

Figure 2.5. Absorption coefficients for pure ice and seawater, chlorophyll *a* (chl *a*) calculated for a concentration of 100 mg m^{-3} as well as non-algal particles (NAP) and coloured dissolved organic matter (CDOM) using exponential slopes of -0.0123 and -0.0176 respectively. Modified from Ehn (2006). 18

Figure 2.6. Location of bottom ice algal community in a landfast first-year ice ecosystem. Adapted from Arrigo et al. (2010). Copyright (2012) John Wiley and Sons. 20

Figure 2.7. (a) Sub-ice irradiance from algae free surface and (b) relative absorbance by a suspension of ice algae across photosynthetically active radiation (PAR) wavelengths. From Legendre and Gosselin (1991). Copyright (2012) Springer Science 29

Figure 2.8. (a) Correlation surface between core based chl *a* and all possible NDI wavelength (λ) combinations and (b) regression of NDI calculated for wavelengths 485 and 472 with core derived biomass, dashed lines represent model output and circles observed values. From Mundy et al. (2007b). Copyright (2012) American Geophysical Union..... 30

Figure 3.1. Location of 2011 Arctic-ICE Allen Bay camp (74° 43.165' N; 95° 10.099' W)	41
Figure 3.2. Changes in snow depth (H_S , circle) and integrated transmittance of photosynthetically active radiation (T_{PAR} , solid) at the time series site from 9 May to 26 June. H_S values following 9 June are representative of snow or white ice depth.....	47
Figure 3.3. Pearson correlation surface of all possible normalized difference indices (NDIs) with core derived chlorophyll a (chl a) measurements.	47
Figure 3.4. Changes in chlorophyll a (chl a) concentration at the time series site (calculated values, solid) and at high snow depth core locations (measured values, circle) from 9 May to 26 June.	48
Figure 3.5. Principal component analysis of variables sampled on the landfast ice of Allen Bay (Nunavut) from 9 May to 9 June (solid) and from 10 to 26 June (circle). The environmental and biological variables are: snow depth (H_S), incident downwelling of photosynthetically active radiation (S_{PAR}), PAR integrated transmittance (T_{PAR}), bottom ice temperature gradient (TG), mean daily current velocity at 2.5 m depth beneath the air- ice interface (MDV), and bottom ice chlorophyll a (chl a) concentration.	51
Figure 3.6. Relationships between calculated chlorophyll a (chl a) concentration and (a) snow depth (H_S), (b) integrated transmittance of photosynthetically active radiation (T_{PAR}), (c) bottom ice temperature gradient (TG), (d) average percent brine volume of total ice thickness (BV_{AVG}), (e) mean daily current velocity at 2.5 m depth below the air- ice interface (MDV), and (f) incident downwelling PAR (S_{PAR}) before (inclusive; solid) and after (circle) 9 June. Note that in (c), the data are presented before (solid) and after (circle) 25 May.....	54
Figure 3.7. Changes in temperature (T_{10}) and salinity (S_{10}) in the bottom 10 cm of sea ice, and average percent brine volume of the entire ice column (BV_{AVG}) from 9 May to 24 June measured at medium snow depth core locations.....	57
Figure 4.1. Location of 2011 ice camp in Allen Bay, Nunavut, Canada (74° 43.165' N; 95° 10.099' W).	73
Figure 4.2. Daily average values of (a) air temperature, (b) albedo and (c) surface photosynthetically active radiation (S_{PAR}) measured at the meteorological station over the sample period. In (a) and (b), bars represent the standard deviation.	80

Figure 4.3. Time series of bottom ice chlorophyll *a* (chl *a*) biomass and snow depth (H_S) at (a) the snow clear site A and under (b) high, (c) medium and (d) low snow cover sites. Chl *a* biomass was calculated using the normalized difference index (see section 2.2 for details)..... 82

Figure 4.4. Temporal changes in bottom ice chlorophyll *a* (chl *a*) biomass and daily average surface photosynthetically active radiation (S_{PAR}) at snow clear sites (a) A, (b) B (c) C, (d) D, (e) E and (f) F. Sample day one is snow covered, sample day 2 and onwards represent measurements following snow removal. Chl *a* biomass was calculated using the normalized difference index (see section 2.2 for details). The rate of change of chl *a* biomass at each site (R_X) and for the same period at the time series site under medium snow cover (R_{TS}) was determined following equation (4.3), with the exception of site D where R_{TS} was calculated from the time series site under low snow cover. Standard deviations of daily R_X and R_{TS} values about the mean are also provided..... 85

Figure 4.5. Temporal changes and variability in (a) bottom ice chlorophyll *a* (chl *a*) biomass, (b) snow depth (H_S) and (c) PAR integrated transmittance (T_{PAR}) from 29 April to 11 June along transects. Chl *a* biomass was calculated using the normalized difference index (see section 2.2 for details). Boxes represent the median and interquartile ranges, vertical lines the sample range, and outliers are indicated by circles and stars for extreme cases. In (c), note the change in scale on 11 June..... 88

Figure 4.6. Linear regressions between bottom ice chlorophyll *a* (chl *a*) biomass and snow depth (H_S) for transects sampled from the 29 April to 11 June. Open circles represent sites covered with >30 cm of snow. Chl *a* biomass was calculated using the normalized difference index (see section 2.2 for details). Solid lines indicate slope significantly different from zero ($p < 0.05$) while dashed lines represent non-significant relationships ($p > 0.05$). 91

Figure 4.7. Temporal changes in Pearson correlation coefficient (r) between bottom ice chlorophyll *a* (chl *a*) biomass, snow depth (H_S) and PAR integrated transmittance (T_{PAR}) for transects sampled from 29 April to 11 June. Chl *a* biomass was calculated using the normalized difference index (see section 2.2 for details). Note that chl *a*- T_{PAR} and chl *a*- H_S relationships were based on sites with $H_S < 30$ cm. Solid circle indicates significant correlation ($p < 0.05$). 96

LIST OF COPYRIGHTED MATERIAL

Figure 2.1. Horner, R., 1985. Sea Ice Biota, CRC Press Inc., Florida. pp.45. Copyright (2012) Taylor & Francis Group LLC - Books.....	7
Figure 2.2. Light, B., Maykut, G., Grenfell, T.C., 2003. Effects of temperature on the microstructure of first-year Arctic sea ice, J. Geophys. Res. 108, 3051. Copyright (2012) American Geophysical Union.....	8
Figure 2.3. Grenfell, T., Perovich, K., 1984. Spectral albedos of sea ice and incident solar irradiance in the Southern Beaufort Sea. J. Geophys. Res. 89, 3573-3580. Copyright (2012) American Geophysical Union.....	12
Figure 2.4. Ehn, J.K, Papakyriakou, T., Barber, D.G, 2008. Inference of optical properties from radiation profiles within melting landfast sea ice. J. Geophys. Res. 113, C09024. Copyright (2012) American Geophysical Union.....	14
Figure 2.6. Arrigo, K.R., Mock, T., Lizotte, M., 2010. Primary Producers and Sea Ice, in: Thomas, D.N., Dieckmann, G.S. (Eds.), Sea Ice, second edition, Wiley Blackwell Publishing, Malaysia, pp.283-325. Copyright (2012) John Wiley and Sons.....	20
Figure 2.7. Legendre, L., Gosselin, M., 1991. In situ spectroradiometric estimation of microalgal biomass in first-year sea ice. Polar Biol. 11, 113-115. Copyright (2012) Springer Science.....	29
Figure 2.8. Mundy, C.J., Ehn, J.K, Barber, D.G., 2007. Influence of snow cover and algae on the spectral dependence of transmitted irradiance through Arctic landfast first-year sea ice. J. Geophys. Res. 112, C03007. Copyright (2012) American Geophysical Union.....	30

CHAPTER ONE: INTRODUCTION

1. Rationale and Context

The 8.8 million km² of annually forming sea ice (referred to as first-year ice; FYI) in the Northern Hemisphere is used by communities of algae as a growth substratum (*Richter-Menge et al.*, 2006). During the spring these organisms, referred to as ice algae, experience a bloom that significantly contributes to total production in the Arctic Ocean (*Legendre et al.*, 1992). Despite their importance in the Arctic marine ecosystem, the future status of these populations is uncertain as Arctic sea ice, and therefore ice algae habitat, continues to change at rates exceeding modelled predictions because of climate warming (*Stroeve et al.*, 2007).

Anticipating the response of sea ice primary producers to climate change begins with understanding the bio-physical relationships between algae and their environment. At present, a number of environmental factors associated with the atmosphere, sea ice, and ocean are known to directly and indirectly contribute to biomass variability and ultimately bloom termination. The full extent of these influences on algal spatial and temporal variability, and ultimately the end of the ice algal bloom, however, are not yet fully understood. Also, our current ability to efficiently monitor ice algae biomass is restricted, as representative time series and large spatial scales often cannot be feasibly sampled (*Mundy et al.*, 2007). It follows that development of a non-invasive and efficient sampling technique could improve biomass measurements, and permit a greater scope of sampling across the Arctic.

2. Thesis Objectives

The overarching goal of this research is to efficiently monitor ice algae biomass across time and space, and to assess the physical influences on its variability. To address this goal a non-invasive and portable sampling technique was used. Specifically, the method developed by *Mundy et al.* (2007), which uses normalized difference indices (NDIs) calculated from transmitted irradiance measurements, was applied to estimate algal biomass. Populations were sampled coincident with recording of environmental data over the melt period at point locations, and across the first-year sea ice (FYI) of Allen Bay, Nunavut in 2011. The result is a comprehensive study of ice algae *in situ*. Overall the goal of my research is divided into 2 sub-objectives:

- 1) To validate transmitted irradiance based estimates of chlorophyll *a* (chl *a*) concentration against core based sampling.
- 2) To examine the bio-physical processes influencing ice algal biomass over the spring melt period.

3.0 Thesis Structure

In addition to this introductory section, five other chapters are presented. Firstly, chapter two provides a review of the structure of sea ice and the resultant optical properties over the spring melt season. The optical characteristics of sea ice are highly influential on biomass variability, and along with the absorption characteristics of particles entrained within the ice, are central to the use of the transmitted irradiance technique. Ice algae and the bio-physical relationships contributing to biomass variability and bloom termination are also discussed. Finally, approaches to biomass sampling are reviewed, illustrating the need in the scientific community for non-destructive sampling,

as well as providing information on techniques that may be used to make non-destructive biomass estimates.

The content of chapter three addresses thesis objective 1 where transmitted irradiance is calibrated to core-based chl *a*. The second objective is also discussed as a number of physical variables are analysed for their respective influences on irradiance derived biomass measured at one location over time. This work was compiled into a manuscript and submitted to the *Journal of Marine Systems*:

Campbell, K., Mundy, C.J., Barber, D., Gosselin, M. Time series measurements of ice algae biomass using transmitted irradiance and assessment of influential physical variables over the spring melt period. *J. Mar. Sys.* (in review).

Chapter 4 focuses on one of the most important bio-physical relationships pertaining to the second objective of this document, the nature of the association between algal biomass and snow depth over the spring melt period. The method developed in objective 1 was again used to calculate irradiance derived biomass at time series sites, as well as along transects, and at locations cleared of snow. A second manuscript is currently in preparation for submission to *Polar Biology*:

Campbell, K., Mundy, C.J., Barber, D., Gosselin, M. Characterizing the ice algae biomass-snow depth relationship over spring melt using transmitted irradiance. *Polar Biol.* (in preparation).

Background on the study location and sampling methods are provided within each manuscript respectively, and reference to literature is appended as the final pages of each chapter. A summary of thesis conclusions and potential future works is provided in Chapter 5. Appendix A lists abbreviations used throughout this document.

Literature Cited

- Legendre, L., Ackley, S., Dieckmann, G., Gullikson, B., Horner, R., Hoshiai, T., Melnikov, I., Reeburgh, W., Spindler M., Sullivan, C., 1992. Ecology of sea ice biota 2. *Polar Biol.* 12, 429-444.
- Mundy, C.J., Barber, D.G., Michel, C., Marsden, R.F., 2007. Linking ice structure and microscale variability of algal biomass in Arctic first-year sea ice using an in situ photographic technique. *Polar Biol.* 30, 1099-1114.
- Richter-Menge, J., Overland, J., Proshutinsky, A., Romanovsky, V., Bengtsson, L., Brigham, L., Dyurgerov, M., Gascard, J.C., Gerland, S., Graversen, R., Haas, C., Karcher, M., Kuhry, P., Maslanik, J., Melling, H., Maslowski, W., Morison, J., Perovich, D., Przybylak, R., Rachold, V., Rigor, I., Shiklomanov, A., Stroeve, J., Walker, D., Walsh, J., 2006. State of the Arctic Report, NOAA OAR Special Report. NOAA/OAR/PMEL, Washington.
- Stroeve, J., Holland, M., Meier, W., Scambos, T., Serreze, M., 2007. Arctic sea ice decline: Faster than forecast. *Geophys. Res. Lett.* 34, L09501, doi: 10.1029/2007GL029703.

CHAPTER 2: BACKGROUND

1. *Introduction*

The unique structural characteristics of sea ice, dependent on the processes of ice formation, growth, and decay, are important aspects of ice algae habitat as they control ice optical properties that influence light transmission, as well as the quality of substrate for cell attachment. It follows that changes to sea ice structure, especially over the melt period, directly contribute to biomass variability and bloom termination. Other important considerations pertaining to algal biomass are the presence of snow on sea ice, the primary variable controlling light transmission and air-ice heat fluxes, as well as nutrient, temperature, and salinity levels of the marine environment. Background on these topics is provided in this chapter, beginning with the physical and optical nature of sea ice, followed by a review of ice algae as part of their cryo-habitat, as well as discussion on the main controls on their biomass. Finally, information pertaining to algal sampling, in particular, the development of the transmitted irradiance technique used in this research, is presented.

2. *Sea Ice Formation, Growth, and Decay*

2.1 *Sea Ice Formation*

Seasonal decline in atmospheric temperature cools the ocean surface and triggers convective mixing, a process enhanced by surface wind and wave activity (*Horner, 1985*). Disc-shaped ice crystals, approximately 2 to 3 mm in size, termed frazil ice, develop once surface waters have reached the approximate freezing point of sea water at

-1.84°C, after which the crystals form a matrix before breaking into various shapes (Wadhams, 2000; Petrich and Eicken, 2010). Frazil ice, characterized by random crystal alignment and variability in ice crystal shape, eventually consolidates into solid sheets, resulting in the first stage of sea ice cover (Wadhams, 2000).

2.2 Sea Ice Growth

After consolidation of the frazil ice layer, vertical thermodynamic growth at the bottom ice surface takes place at a rate proportional to heat conduction between the ice and atmosphere (Horner, 1985). Growth rates, therefore, vary in response to the factors influencing heat exchange between the ice and atmosphere, such as presence of surface winds, snow depth, as well as ice thickness itself (Horner, 1985).

2.2.1 Crystal Growth

The orientation of sea ice crystals formed during this phase of growth is described by the axis which runs parallel to the crystal's hexagonal edges, referred to as the c-axis (Figure 2.1). This is important to note as crystals with c-axes aligned parallel to the ice subsurface are favoured for growth through geometric selection (Horner, 1985). As a result, a greater proportion of crystals with c-axes aligned in the horizontal direction is found with increasing distance from the consolidated frazil ice. The specific transition from random to horizontal c-axis alignment is generally located between 5 and 20 cm depth below the air-ice surface (Horner, 1985; Wadhams, 2000). This point in the vertical ice profile marks the beginning of congelation ice characterized by a columnar structure of thin and elongated (10 to 40 cm and up) crystals (Anderson and Weeks, 1958).

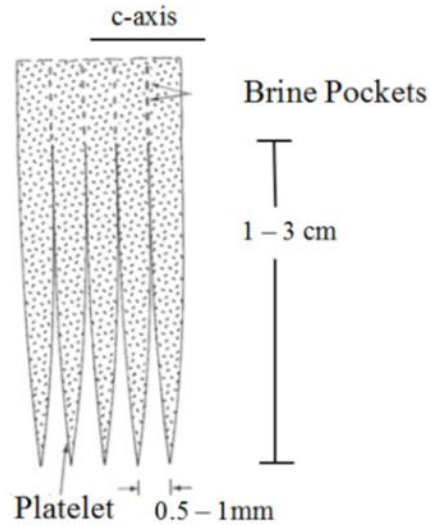


Figure 2.1. Close-up of the sea ice skeletal layer at the growth interface where ice crystals develop by production of platelet extensions. From Horner (1985). Copyright (2012) Taylor & Francis Group LLC - Books.

On a fine scale, vertical growth of congelation ice occurs via the production of platelet crystals that grow parallel to one another and perpendicular to their c-axes (Figure 2.1; Horner, 1985). These extensions of ice represent the skeletal layer of sea ice, widening as they grow to eventually connect with one another (Wadhams, 2000). The unique properties of sea ice are greatly dependent on this growth process because with the formation of skeletal ice crystals, rejected salts are concentrated into a brine solution that becomes trapped in the ice along with air bubbles (Light *et al.*, 2003). Brine may also become entrained within the ice when lower salinity ocean water flows between the platelets and freezes. In both cases the resulting lamellae of brine and ice are approximately 0.3 to 0.5 mm apart (Petrich and Eicken, 2010), with the density of brine inclusions increasing with the rate of ice growth (Horner, 1985).

2.2.2 Brine Inclusions and Drainage

The nature of brine inclusions is not static, instead their characteristics change in response to ice temperature. For example, lowering ice temperature decreases brine inclusion size, especially diameter, as the freshwater component of brine freezes to pocket walls (Figure 2.2; *Light et al.*, 2003). Another important feature of brine inclusions is their ability to house salt precipitates. Mirabilite crystals ($\text{Na}_2\text{SO}_4 \cdot 10\text{H}_2\text{O}$) precipitate at -8.2°C and represent the most abundant salts in sea ice, followed by hydrahalite crystals ($\text{NaCl} \cdot 2\text{H}_2\text{O}$) which precipitate at -22.9°C . These salt crystals occur primarily at the base of elongated brine pockets (brine tubes) and may contribute to increasing their length (*Light et al.*, 2003).

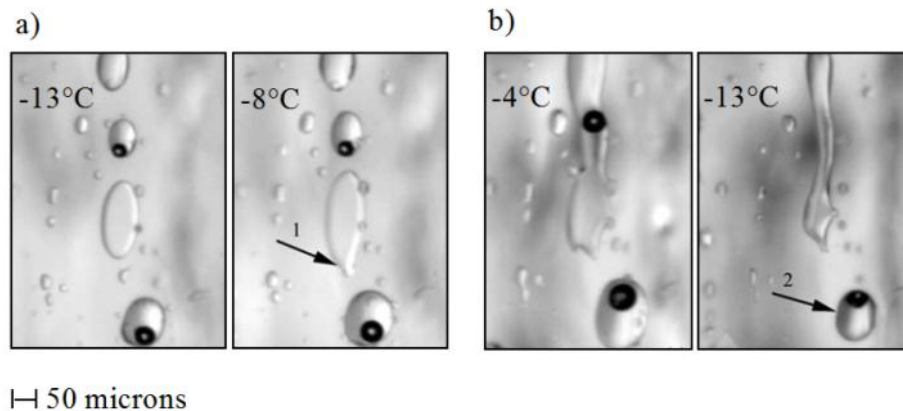


Figure 2.2. (a) Enlargement and (b) shrinkage of brine pockets in sea ice during an experimental warming and cooling sequence highlighted by arrows 1 and 2, respectively. From *Light et al.*(2003). Copyright (2012) American Geophysical Union.

As defined by Wadhams (2000), brine is predominantly drained from inclusions via three methods during the period of ice growth; brine cell migration, brine expulsion, and gravity drainage. Brine cells move, or migrate, towards the ocean because of the vertical temperature gradient in sea ice created by cool ice nearest to the atmosphere that warms

towards the ocean. As a result of this gradient, freezing can occur in the upper portion of brine inclusions as melting ensues at the bottom. This potentially causes the pockets to move downwards through the ice until brine is expelled at the ice-ocean surface. The two remaining methods of drainage rely on the high degree of brine pocket connectivity as well as gravity. As the name suggests, gravity drainage is the movement of brine through the irregular brine channel network down to the ocean. Although this method of brine movement is very similar to brine cell migration, it is largely restricted to the region of ice that is above 5% brine volume content. Brine expulsion occurs as a function of decreasing temperature, where brine pockets "cut-off" from channels build up pressure as they become increasingly smaller with freezing, until pressure and brine are released through the formation of micro-fissures. This mechanism is thought to only be a light influence on desalination. An additional mechanism of brine drainage occurs during advanced melt and is discussed in section 2.4.

2.3 Snow on Sea Ice

Snow accumulation on sea ice occurs once an ice thickness of 0.1 meters has been reached (*Ehn, 2006*). After deposition, its distribution on smooth FYI exhibits snow drift periodicity (*Iacozza and Barber, 1999*) and has a tendency to form barchann dunes (*Massom et al., 2001*). The spatial variability of snow on sea ice creates an environment of horizontally variable thermodynamic properties and transmitted irradiance (*Iacozza and Barber, 1999*).

The physical properties of snow change soon after deposition from the influences of gravity, weather conditions, and ice floe dynamics. For example, the low density of fresh

snow increases over time as gravity aided by surface winds compact snow grains and decrease the proportion of air spaces. Newly deposited snow grains also change size and shape as water and brine is wicked upwards through the profile, an effect especially notable in the bottom hoar layer where grains become the largest as a result of this process (*Colbeck, 1986*). Over the melt period, the majority of snow changes from dry crystals of approximately 0.5 mm diameter, to wet snow 3 to 10 mm across (*Perovich et al., 1998*), with the exception of the bottom hoar layer which can actually decrease in size (*Mundy et al., 2005*). Characteristics of the snowpack on sea ice are also subject to other environmental changes such as rain events which increase grain size (*Perovich et al., 2002*) and melt-freeze cycles that can form ice lenses (*Iacozza pers. comm., 2011*).

2.4 Sea Ice Melt and Decay

The effects of seasonal warming occur primarily at the ice surface as downwelling irradiance is absorbed (*Melnikov, 1997*). Surface radiation is therefore seen as the driver of FYI melt, which can be summarized based on the surface and geophysical conditions of the ice: winter ice (January to March), snow melt (mid-May to late June), melt pond formation (late June), pond drainage (July), and rotten ice once the drainage is finished (*De Abreau et al., 2001*).

Snowmelt in spring takes as little as 2 to 3 weeks from the onset of 0°C (*Horner, 1985*) and results in the formation of melt ponds that deepen and thin the ice at the expense of ice thickness, as they continually absorb radiant energy (*Wadhams, 2000*). The initial location of melt ponds is dependent on snow distribution during the cold period, as melt water collects between snow drifts (*Iacozza and Barber, 2001*). Surface

melt water, including melt ponds, partially drains through the ice the via brine network, seal holes, and flaws in the sea ice. This process flushes brine and represents the largest contributor to, and fastest means of, brine drainage (*Wadhams, 2000*). The size and extent of the drainage network increases with rising temperatures as brine inclusions enlarge and join (Figure 2.2; *Light et al., 2003*). Once the majority of brine is drained and ice temperature is relatively isothermal, the highly porous ice will melt back into the liquid ocean until the next cycle of formation begins (*Timco et al., 2001*).

3. Radiative Transfer

Radiant energy interacting with sea ice can be (i) reflected or absorbed at the surface, (ii) attenuated while travelling through the snow and ice, or (iii) absorbed by biological and non-biological materials. These interactions have different consequences for light reaching algae in the bottom ice. Most notably, the magnitude of light reaching algae is primarily a function of scatter that occurs in the snowpack, and, to a much smaller extent sea ice, while the optical profile of transmitted irradiance is largely dependent on particulate absorption by biological materials (*Perovich, 1996*). Based on the geophysical characteristics of FYI reviewed in section 2, photosynthetically active radiation (PAR; 400-700 nm) light attenuation in the snow-sea ice environment is discussed in this section.

3.1 Albedo

The proportion of electromagnetic radiation reflected or backscattered to the atmosphere in relation to the amount incident on a surface is referred to as albedo. Sea ice

albedo is not constant over time or space; instead it is dependent on the surface characteristics of scatter and absorption (Figure 2.3).

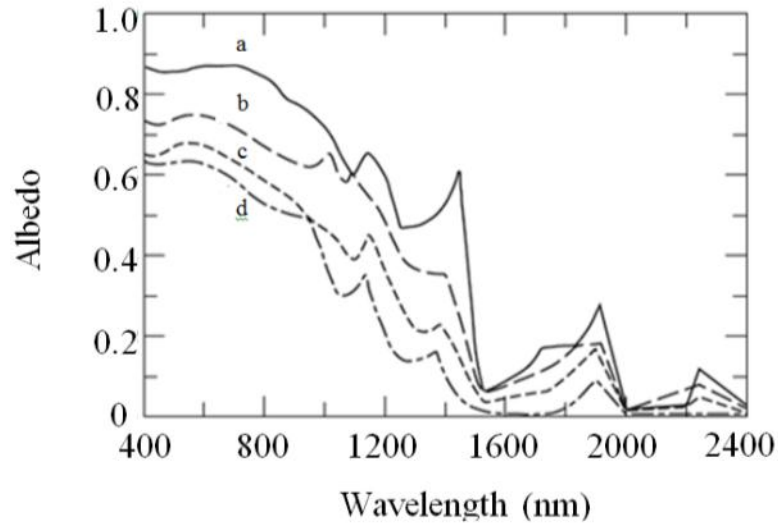


Figure 2.3. Albedo decline as a function of wavelength with melt season progression on first-year ice: (a) dry snow over ice, (b) melting snow over ice, (c) bare ice, and (d) melting ice. From Grenfell and Perovich (1984). Copyright (2012) American Geophysical Union.

With an albedo of over 0.8 for shortwave radiation, dry snow is an efficient reflector of PAR (Ehn *et al.*, 2008). The high albedo of snow at visible wavelengths has many important implications for sea ice, for example by contributing to the postponement of ice ablation in the spring (Iacozza and Barber, 1999). The transition from dry snow to bare and melting ice over the spring results in a decline in albedo value however, the spectral distribution of light remains largely the same (Figure 2.3; Grenfell and Perovich, 1984). This supports the observation that changes to the amount of snow and ice scatter affect the magnitude of light transmitted into and through the ice, but not the type of wavelengths transmitted.

Albedo increases with ice thickness as more scatter-generating inclusions are encountered (*Maykut, 1982; Sturm and Masson, 2010*). This relationship stands until a depth of 0.8 m at which point no significant change in albedo is measured because the path length of backscattered light is too great for wavelengths to reach the surface. Albedo signatures in late spring continue to represent the backscattering properties of sea ice, despite the presence of surface meltwater as it is relatively transparent to short wavelengths (*Perovich, 1996*). Sea ice albedo is also dependent on the scattering characteristics of inclusions (sections 1.2 and 1.4), where inclusions that improve ice backscatter will result in a greater albedo value.

3.2 Sea Ice Attenuation

3.2.1 Vertical Attenuation Profile

Based on the presence and characteristics of inclusions within different parts of the vertical ice profile, Ehn et al. (2008) list four optical regions of FYI: (1) surface layer which includes snow, superimposed and granular ice, (2) the internal homogeneous ice, (3) a detritus layer, and (4) the algal layer (Figure 2.4). The attenuation characteristics of the first three regions are discussed in this section. Algal attenuation of region 4 is to follow in section 4.3.

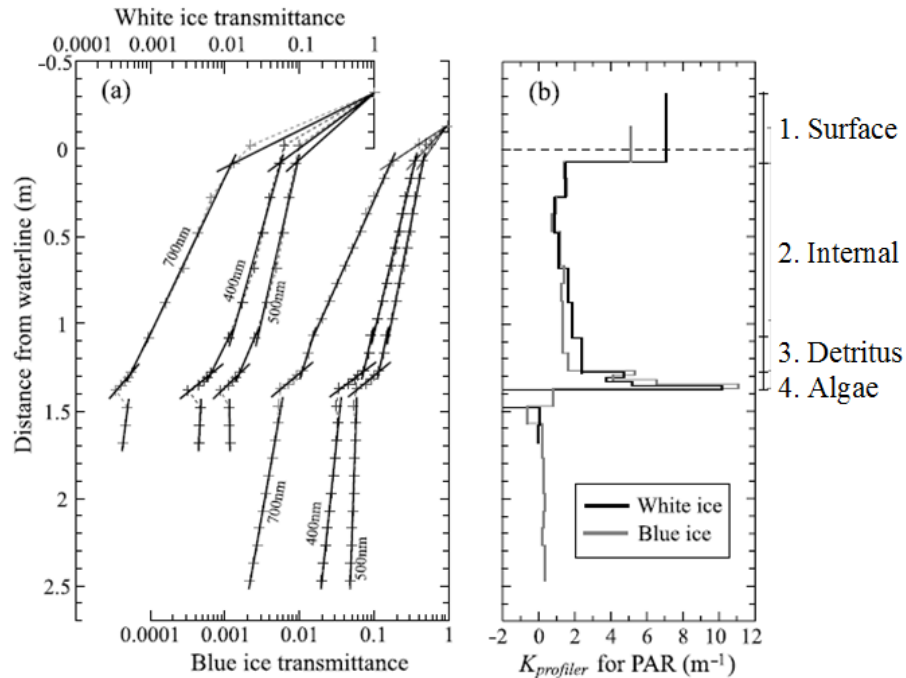


Figure 2.4. (a) Transmittance and (b) spectral diffuse attenuation coefficient ($K_{profiler}$) of photosynthetically active radiation (PAR) through first-year ice. The vertical profile is divided into optically unique 1. Surface, 2. Internal, 3. Detritus, and 4. Algal regions. From Ehn et al. (2008). Copyright (2012) American Geophysical Union.

3.2.2 Surface Layer: Snowpack Attenuation

Light crossing between two mediums of different densities will change direction. In such instances light is effectively scattered or refracted, the extent of which is dependent on the difference in magnitude of refractive index (Perovich, 1996). Light travelling through the snowpack moves primarily between ice and air which have considerably different refractive indices, approximately 1.0 for air, and 1.3 for ice (Arrigo et al., 1991). Light is therefore bent to a high degree when moving between them, with the refraction being wavelength-independent due to the large size of ice-snow grains relative to wavelength size.

Environmental factors that alter snow grain size and snowpack density are highly influential on the magnitude of transmittance, such that decreasing the radius and increasing the density of crystals intensifies scatter (*Mundy et al.*, 2005). It follows, for example, that scatter decreases over time as the snowpack ages and snow grains increase in size. Overall, the combined effect of snow's large surface albedo (Figure 2.3) and high degree of internal scatter relative to sea ice is a negative association between the magnitude of transmitted irradiance measured beneath the sea ice and overlying snow depth (*Perovich et al.*, 1998).

To a much lesser extent than magnitude, snow also has the potential to alter the spectral distribution of light. Introduced materials such as brine, wicked into the snowpack upon deposition (*Sturm and Massom*, 2010), black carbon, sediments, and brown organic carbon (*Doherty et al.*, 2010) absorb wavelengths and cause a spectral shift in light transmitted. The influence of sediments may be particularly important to consider in coastal regions.

3.2.3 Surface Layer: Sea Ice Attenuation

Like snow, sea ice is a scatter-dominated medium which deflects light at all wavelengths equally (*Perovich*, 1996). Light within sea ice may be attenuated by inclusions of brine channels or pockets, air bubbles and potentially salt crystals, which have different refractive indices: brine (1.341-1.397) (*Maykut and Light*, 1995) and salt crystals (1.5) (*Perovich*, 1996) in addition to air and ice mentioned above. Similar to transmission through the snowpack, light is bent when moving between these mediums, the degree of which is proportional to the differences in index value (*Perovich*, 1996). It

then follows, for example, that light travelling between air and ice will be refracted to a greater extent than light moving between ice and brine pockets (*Perovich, 2003*).

Drained ice, known as white ice, typically accounts for approximately 10% of total ice thickness (*Perovich, 2003*). The strong light attenuation in this region is responsible for decreasing PAR transmittance through sea ice to as low as 5 to 16% (*Ehn et al., 2011*). The higher scatter of this region, in comparison to ice more central in the vertical profile (Figure 2.4), may be a result of the greater difference in refractive indices between drained brine inclusions (air) and ice associated with white ice, than between the liquid brine and ice inclusions of the region below. Increased scatter in this region can also be attributed to the granular structure (*Perovich et al., 1998*) and random crystal alignment created during initial formation and consolidation of frazil ice (*Pegeau and Zaneveld, 2000*).

3.2.4 Central Ice Attenuation

The central region of sea ice has relatively constant optical properties (*Ehn et al., 2008*). The majority of attenuation here arises from the presence of large quantities of liquid brine which contribute more to sea ice attenuation than any other naturally occurring component (*Perovich, 2003*). The refractive index of brine is not constant, but is instead controlled by its temperature-dependent density. *Maykut and Light (1995)* documented an increase in index value with density, 1.341 to 1.397, as temperatures declined from -2 to -32°C. The extent to which changes in refractive index will affect scatter is dependent on whether refractive indices between brine and other inclusions become more alike or dissimilar. For example, salt crystal scatter will be greatest in

regions of ice where the difference in brine and crystal refractive index values is greatest. This corresponds to where brine is warmest while still permitting the formation of salt crystals (*Maykut and Light, 1995; Perovich, 2003*).

The structure of columnar ice in this region favours a downward vertical movement of light 50 times greater than any other direction (*Perovich, 1996*). This may arise because light will encounter fewer attenuating crystal edges and brine pocket walls (*Pegeau and Zaneveld, 2000*). The result is little backscatter to the air-ice surface (*Ehn et al., 2008*) and enhanced transmission of light to the bottom ice algae.

3.2.5 Detritus and Other Absorption

Non-algal particles (NAP, e.g. detritus) and coloured dissolved organic matter (CDOM) produced from the decay of organic material by microbial processes, have a marked effect on attenuation (Figure 2.5). Their spectral absorption which declines exponentially with wavelength, is different from that of algae as it is much lower in magnitude and does not display characteristic absorption peaks associated with the chl *a* pigment (*Ehn et al., 2008*). As a result of these material's high affinities for PAR (Figure 2.5), if NAP and CDOM are present in significant quantities, PAR availability to photosynthetic organisms may be affected (*Eurico et al., 1999*).

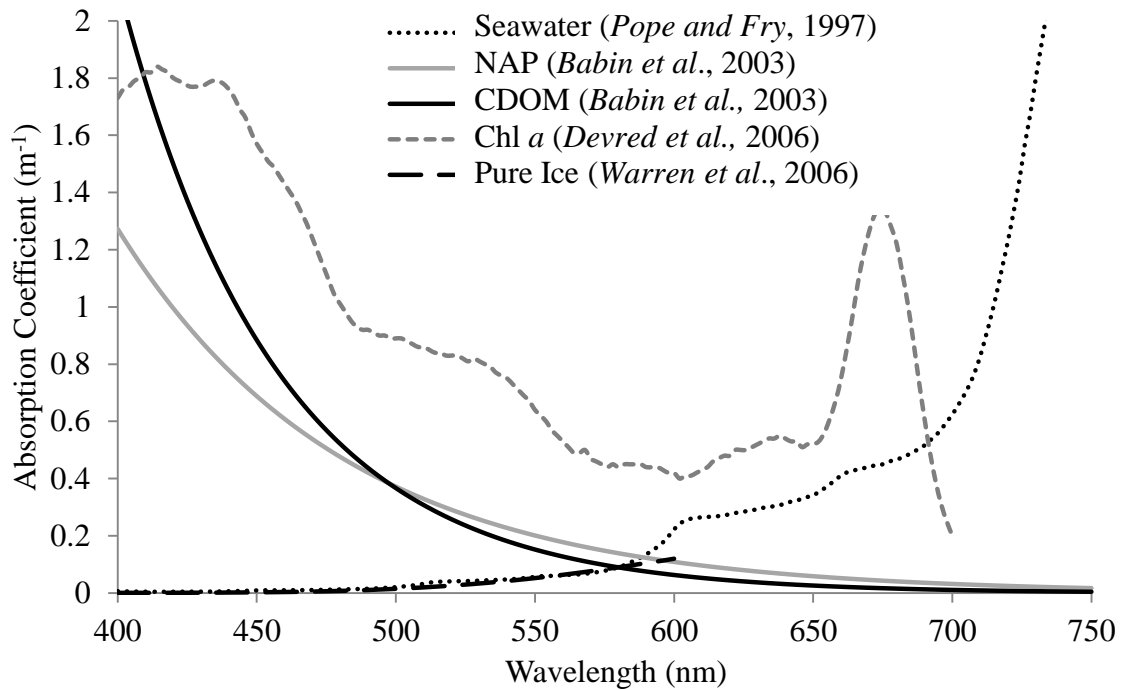


Figure 2.5. Absorption coefficients for pure ice and seawater, chlorophyll a (chl a) calculated for a concentration of 100 mg m^{-3} as well as non-algal particles (NAP) and coloured dissolved organic matter (CDOM) using exponential slopes of -0.0123 and -0.0176 , respectively. Modified from Ehn (2006).

Entrainment of CDOM and NAPs in sea ice may result in layers of concentrated particles, for example, the trapping of sediments during seawater advection (Pegeau and Zanefeld, 2000) or following atmospheric deposition. These layers create localized regions of high and low absorption in the vertical ice profile (Perovich et al., 1998) and can decrease transmittance as a whole (Ehn et al., 2008). Populations of bacteria which have a spectral signature similar to detritus (Arrigo et al., 1991) can also be found in sea ice. Bacteria, however, account for less than 1% of bottom ice carbon; their spectral impact is, therefore, relatively insignificant (Kottmeier et al., 1987).

3.3 Seasonal Changes in Attenuation

The seasonal changes in sea ice radiative transfer can be inferred based on the structurally driven attenuation characteristics discussed in section 3.2. During the early spring when ice temperatures are low, the presence of salt precipitates and abundance of individual brine inclusions results in high scatter and low transmittance. As spring progresses, a number of changes in the sea ice occur simultaneously, resulting in competing optical influences (*Light et al.*, 2003). For example, brine drainage temporarily increases scatter by creating air pockets, while brine channel connectivity decreases the amount of scatter (*Perovich et al.*, 1998). During advanced melt, transmittance below the sea ice increases in response to lower backscatter from thinning sea ice (*Perovich*, 2003), coupled with melt pond formation which permits large quantities of short wavelength transmission (*Perovich*, 1996). Horizontal scatter may become an important consideration during this time, as transmittance of PAR measured under-ice adjacent to melt ponds has been found to be uncharacteristically high as a result (*Ehn et al.*, 2011).

4. Ice Algae

4.1 Habitat

Sea ice can support a number of algae communities in different parts of the vertical ice profile; in melt ponds, at the ice surface, within the interior, as well as at the bottom and immediately below the ice (*Horner et al.*, 1992). The types of assemblages present are dependent on the mechanism of ice formation which greatly influence ice structure. The majority of algae in Arctic sea ice is pennate diatom species living within the skeletal layer and bottommost columnar or congelation ice (Figure 2.6) (*Arrigo et al.*, 2010).

Location in this region optimizes algal growth as cells are positioned to receive maximum downwelling irradiance (DW), as well as nutrients from the ocean water. The spaces between ice crystals at the growth interface (Figure 2.1) also provides ample room for algal colonization, a process aided by slower rates of ice growth (*Legendre et al.*, 1991). The specific mechanism of algal incorporation into the bottom ice is actively discussed in the literature (e.g. *Ackley et al.*, 1987; *Spindler*, 1994) however, it is widely accepted that sticky exopolymeric substances (EPS) produced by algae aid attachment to the ice (*Krembs et al.*, 2002). Ice algae bloom during the spring (from May to June) when light, nutrient, and ice conditions are optimal. The bloom ends with snow and ice melt which causes biomass loss from the sea ice (*Lavoie et al.*, 2005).

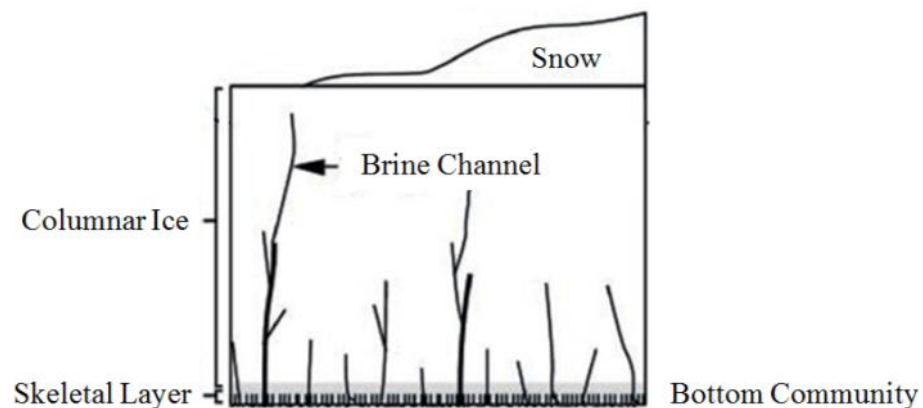


Figure 2.6. Location of bottom ice algal community in a landfast first-year ice ecosystem. Adapted from Arrigo et al., 2010. Copyright (2012) John Wiley and Sons.

4.2 Algae Attenuation Properties

The greatest contributor to attenuation in sea ice is the wavelength-dependent absorption by biological material, including ice algae, in the bottommost centimeters of the profile (Figure 2.4). As photosynthetic organisms, algae use primarily the chl *a* pigment to harvest light, which preferentially absorbs blue light around 440 nm and to a

lesser extent red light around 665-675 nm (Figure 2.5; *Legendre and Gosselin, 1991*). A potential consequence of algal pigment absorption is the shading of cells lower in the ice column (*Robinson et al., 1995*). In response, algae located in the bottommost ice layers may produce accessory pigments to absorb more strongly at wavelengths not preferentially taken up by chl *a*. The accessory pigment fucoxanthin, which has an affinity for the 450-550 nm spectral region (Figure 2.5; *SooHoo et al., 1987*), is a good example. Absorption shifts through increased production of accessory pigments can also occur in response to greater total irradiance, such as the increase in DW PAR over spring melt (*Cota and Smith, 1991; Perovich et al., 1998*). Because of these known absorption characteristics, algal attenuation alters light conditions in the surrounding ice, as well as the water column below the sea ice (*Arrigo et al., 1991; Ehn et al., 2008*) in a predictable manner. For example, with higher biomass, one can expect lower transmission of light at wavelengths 440 and 665-675 nm.

4.3 Influential Factors on Growth

Physical variables contributing to biomass variability and bloom termination include: sub-ice structure (*Eicken, 1992*), ice growth rate (*Legendre et al., 1991*), and brine flushing (*Mundy et al., 2007a*), among others. The most prominent environmental factors affecting biomass, including those listed here, are reviewed in this section. This is with the exception of transmitted irradiance as its influence on ice algal biomass is described in detail in chapters three and four to follow.

4.3.1 Nutrients

Ice algae growth is often limited by nutrients during the latter part of the spring bloom (*Gosselin et al.*, 1990; *Cota et al.*, 1991; *Lavoie et al.*, 2005) as the demand by growing populations outweighs supply. Phosphate (PO_4^{3-}), nitrate (NO_3^-), and silicic acid (Si(OH)_4) are the potential limiting macronutrients of ice algae growth, although which one is most significant varies; PO_4^{3-} may be the limiting nutrient in river plumes (*Gagnon et al.*, 2005), whereas NO_3^- or Si(OH)_4 may limit ice algal growth in more saline waters (*Maestrini et al.*, 1986; *Cota et al.*, 1987; *Gosselin et al.*, 1990; *Smith et al.*, 1997).

The nutrient pool required to support an ice algal bloom resides primarily within the water column (*Cota et al.*, 1990), and nutrient availability is largely controlled by physical rather than biological mechanisms (*Harrison and Cota*, 1990). The main physical mechanisms supplying new nutrients to the bottom ice algae are brine drainage (*Cota et al.*, 1991), tidal mixing (*Cota et al.*, 1987) and water column instability (*Cota et al.*, 1990). These processes rely on ocean turbulence below the sea ice to force ocean water which carries nutrients into the ice (*Cota et al.*, 1991), for example, by the drainage of brine during ice growth or melt which creates small eddies, or during periods of strong tides which causes increased friction between the water-ice interface. In the algal layer, nutrients are also regenerated by biological means (e.g. bacterial and protozoan activities). However, this process is relatively minor in its contribution to nutrient supply compared to the other physical processes mentioned (*Cota et al.*, 1991).

Ice algae take up and store nutrients from their environment. This often results in a decrease in nutrient concentration with depth from the sea ice, as ice algae remove the

nutrients from the water closest to them and store them in their cells (*Cota et al.*, 1990). This gradient intensifies as algae populations increase with accompanying nutrient demand. A potential consequence of nutrient availability is its contribution to algae stratification within the bottom-most layers of sea ice. Algae lower in the ice with better access to nutrient-carrying ocean water may experience less nutrient-based growth limitation than cells higher up, although a trade-off between this and self-shading may arise (*Cota et al.*, 1991).

4.3.2 Salinity and Temperature

Salinity and temperature directly affect the ‘physiological activity’ of ice algae, although their effects are considered independent from one another (*Arrigo and Sullivan*, 1992). Susceptibility of algae to changes in salinity may be species-specific, where a study by Sjøgaard et al. (2011) found that diatoms had a higher tolerance than chlorophytes. Photosynthetic rates have also been documented as salinity-dependent, optimized, for example, between salinities of 30 and 50 ppt (*Arrigo and Sullivan*, 1992). Productivity at salinities exclusive of this range may be hindered as electron transport in photosynthetic pathways is disrupted (*Ralph et al.*, 2007). Physiological acclimation by algae to changing salinities is possible (*Ryan et al.*, 2004), and is a requirement of cells to survive the salinity fluctuations associated with ice growth and melt.

Ice algae also exhibit a preferred range of temperature for photosynthesis, Kottmeirer and Sullivan (1988) determined temperatures between 4 and 14°C were ideal. Most often, however, temperature at the ice bottom remains below zero as a result of freezing point depression, indicating that algal productivity is highly restricted because of

their extreme environment. Another consequence of a low temperature ice environment is the need for cryoprotection. Ice algae have developed cell defenses in response, such as the production of EPS (*Krembs et al.*, 2002), ice binding proteins (*Janech et al.*, 2006), as well as increasing intracellular concentrations of dimethylsulfoniopropionate (DMSP) and dimethylsulfoxide (DMSO; *Lee et al.*, 2001). Lastly, similar to salinity, algae exhibit a high level of adaptability to changing temperatures (*Moch and Hoch*, 2005).

Indirectly, salinity and temperature affect algae through their combined influence on bottom ice structure, as salinity controls sea ice melt and freezing temperatures. Examples include the studies by Gosselin et al. (1986) and Granskog et al. (2005) who attributed biomass variability to salinity's effect on bottom ice porosity. In these instances algal attachment to the ice substrate was hindered by structure loss associated with ice melt. The removal of substrate entirely by bottom ice melt is a primary factor in causing biomass loss (*Krembs et al.*, 2001) and ultimately the termination of the ice algae bloom in the late spring (*Lavoie et al.*, 2005).

4.3.3 Tide and Brine

As discussed in section 4.3.1 tides can positively influence biomass through nutrient supply. Sub-ice current velocities, however, can also decrease chl *a* by physically removing cells (*Mundy et al.*, 2007a) and by increasing ice melt (*Lavoie et al.*, 2005). In addition, another means of mechanical removal of biomass occurs during melt when brine drains from the ice via channels. At these point locations ice melt is enhanced and cells are eroded (*Mundy et al.*, 2007a). Decreases in biomass associated with brine

drainage are especially important to note during advanced stages of the spring when meltwater drains from this network as well.

5. Biomass Sampling Techniques

5.1 Traditional Methodology

Biomass is a measure of the dry weight of organisms present in a volume or area of sample. For ice algae this requires cell counts and volume estimates (*Lalli and Parsons, 1993*). More commonly however, chl *a* concentration is used to estimate ice algae biomass as it is easier to measure. The method of quantifying chl *a* concentration is largely shared amongst researchers; however, the means of obtaining algae samples on which to perform it can vary greatly.

5.1.1 Algal Sample Collection

Until the mid-1900s ice algae were observed and sampled from inverted or broken sea ice. In 1974, *Alexander et al.* used the Snow, Ice, and Permafrost Research Establishment (SIPRE) corer to collect samples for assessment of species composition and algal standing crop (*Hsaio, 1980*). This apparatus, and similar corers like those developed by Kovacs, have since become the standard for ice algae sampling (*Welch et al., 1988*). Efficiency in algae collections using the coring method may decrease to only 10% by June because of weakened algae attachment to the melting ice subsurface, resulting in sample loss during core extraction (*Welch et al., 1988*). Scientists may thus switch to alternative methods, especially during the advanced melt period when the bottom-most ice is quite fragile, in an effort to obtain more accurate biomass estimates.

The primary alternative to SIPRE or Kovacs coring is collection of algae from the ice-ocean interface by divers with handheld corers (*Welch et al.*, 1988) or variations of this, e.g. large syringes referred to as ‘slurp guns’ that collect algae floating at the ice-water interface (*Gosselin et al.*, 1990) and modified drill systems to cut and collect algae debris from the ice subsurface (*Welch et al.*, 1988). Care to preserve the skeletal layer, such as carefully hand chiselling the bottom-most centimeters in place of coring the full sample, can also improve efficiency (*Cota and Horne*, 1989).

5.1.2 *Chl a Processing*

Following the collection methods discussed, samples must be diluted with filtered sea water to avoid cellular osmotic stress during melt (*Garrison and Buck*, 1986; *Cota and Horne*, 1989). Algae are then filtered from the melted samples and pigments are extracted by placement in acetone (e.g. *Mundy et al.*, 2007b) or methanol (e.g. *Gosselin et al.*, 1986). After 24 hours, chl *a* content is estimated using the spectrophotometric (e.g. *Hsaio*, 1980; *Rysgaard et al.*, 2001) or fluorometric (e.g. *Gosselin et al.*, 1990; *Mundy et al.*, 2007b) method. To prevent photo stress on the algae and pigment degradation, samples must remain in the dark during all preparations and measurements. An overview of the methodology and theory for these techniques is provided below; for specific protocols see *Parsons et al.* (1984).

5.1.3 *Spectrophotometry*

The measure of light extinction as a result of absorption during transmission through a pigment sample is the basis of spectrophotometry. Specifically, a spectrophotometer exposes the samples with a known path length between cuvette and

sensor (l) to wavelengths of 665 and 750 nm, and records absorbance of light by the solution before and after acidification with, most often, hydrochloric acid (HCl). Chl a (mg m^{-3}) is then derived using equation (2.2):

$$\text{chl } a = [26.7(665_o - 665_a) \times v] / [V \times l] \quad (2.2)$$

where the reading at 750 nm has been subtracted from absorbance measurements at 665 nm both without (665_o) and with acid (665_a) added, 26.7 is an instrument calibration factor, v is the volume of acetone (ml), and V is the volume of sea water that was filtered (L). An additional calculation can also be done to determine the concentration (mg m^{-3}) of non-photosynthetic (phaeo-) pigments, which contribute to total sample absorption, and can therefore be important to quantify (*Parsons et al.*, 1984).

5.1.4 Fluorometry

Upon exposure to light, isolated chlorophyll pigments re-emit a large portion of the energy as photons (*Campbell and Reece*, 2005). The resulting fluorescence of the algal pigment sample can be quantitatively measured with a fluorometer and converted to chl a concentration by calculation. The fluorometric method is 5 to 10 times more sensitive than the spectrophotometer approach and is, therefore, more commonly used. Duplicate fluorometer measurements are, however, necessary because this technique can compromise accuracy as a result of its indirect nature; induced fluorescence is followed by measurement instead of a direct absorption measurement on the sample as done with spectrophotometry.

Fluorometric readings are taken on the same extracted pigment solutions used in spectrophotometry, both before and after the addition of HCl. Fluorometric readings,

volume and instrument calibration measurements are all variables in determining chlorophyll concentration (mg m^{-3}):

$$\text{chl} = [Fd (\tau/(\tau-1)) \times (Rb-Ra) \times (v/Fw)] \times V \quad (2.3)$$

where Fd is the Fluorometer Calibration (mg m^{-3}),

Rb is the Fluorescence before acidification,

Ra is the Fluorescence after acidification,

τ is the ratio of Ra to Rb for a pure chl a sample,

Fw is the ml volume of sample filtered, and

Fd is the slope of a linear regression between chl a concentration and fluorescence

(Parsons *et al.*, 1984).

5.2 Developing Methodology

Removal of ice algae from their natural environment for sampling is destructive. A truly representative time series with traditional methods therefore cannot be achieved as different algal populations are actually sampled over time. Spatial sampling to capture the variable distribution of ice algae along the sea ice bottom using traditional techniques is also restricted as core collection and laboratory analysis is time-intensive. Developing techniques that use transmitted irradiance to estimate biomass may improve on these spatial and or temporal sampling requirements. This sampling approach is based on the influence ice algae pigment absorption has on the spectral distribution of transmitted irradiance measured below the sea ice. The development of biomass sampling using transmitted irradiance is reviewed below.

5.2.1 Biomass Estimates Using Ratios of Transmitted Irradiance

The influence of ice algae on the distribution of light measured immediately beneath the ice subsurface was first used by Legendre and Gosselin (1991) as means of biomass estimation. In this study, chl *a* sampled from ice cores was used to calibrate transmitted irradiance measurements from a stationary spectroradiometer beneath the sea ice. Biomass was characterized using a ratio of transmitted irradiance at wavelengths where i) maximum under-ice irradiance is measured (low chl *a* absorption) and where ii) minimum under-ice irradiance occurs (high chl *a* absorption; Figure 2.7). The ratio using wavelengths 540 and 671 nm was found to best represent the above criteria and accounted for 55% of core derived chl *a* variability. The linear relationship between irradiance ratio and chl *a*, however, was greatly dependent on snow, ice, and water depth above the radiometer. Therefore, inter-comparisons of irradiance ratios were done between sites with these factors accounted for (Legendre and Gosselin, 1991).

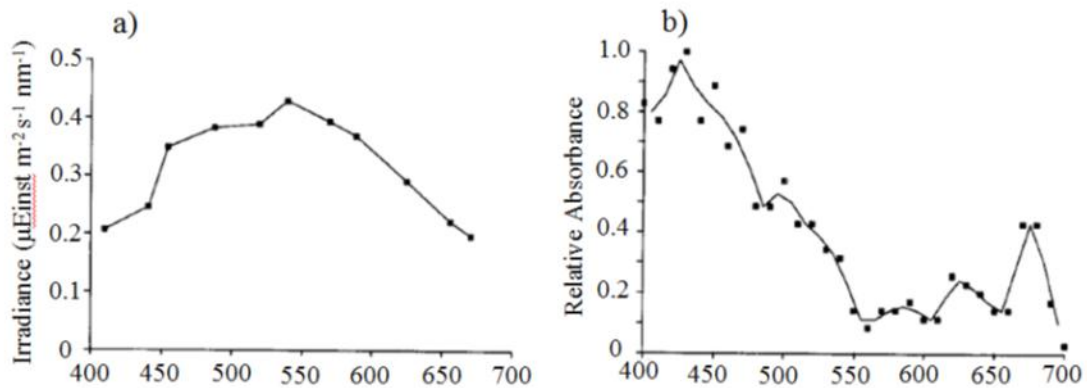


Figure 2.7. (a) Sub-ice irradiance from algae free surface and (b) relative absorbance by a suspension of ice algae across photosynthetically active radiation (PAR) wavelengths. From Legendre and Gosselin (1991). Copyright (2012) Springer Science.

5.2.2 Biomass Estimates Using Normalized Difference Indices (NDIs)

Chl *a* – transmitted irradiance relationships have also been summarized by calculation of normalized difference indices (NDIs):

$$\text{NDI} = [\text{T}(\lambda_1) - \text{T}(\lambda_2)] / [\text{T}(\lambda_1) + \text{T}(\lambda_2)] \quad (2.4)$$

where transmitted irradiance between two different wavelengths ($\text{T}(\lambda_x)$) is compared.

The use of NDIs makes comparison of site values easier than using irradiance ratios as NDI values range between -1 and +1. Mundy *et al.* (2007b) determined that an NDI using wavelengths 485 and 472 nm was optimal to represent algal biomass as it was highly correlated with fluorometrically determined chl *a* and accounted for 89% of its variation (Figure 2.8). This study also represented an improvement of sampling efficiency as sub-ice irradiances were obtained from a mobile spectroradiometer deployed via mechanical arm.

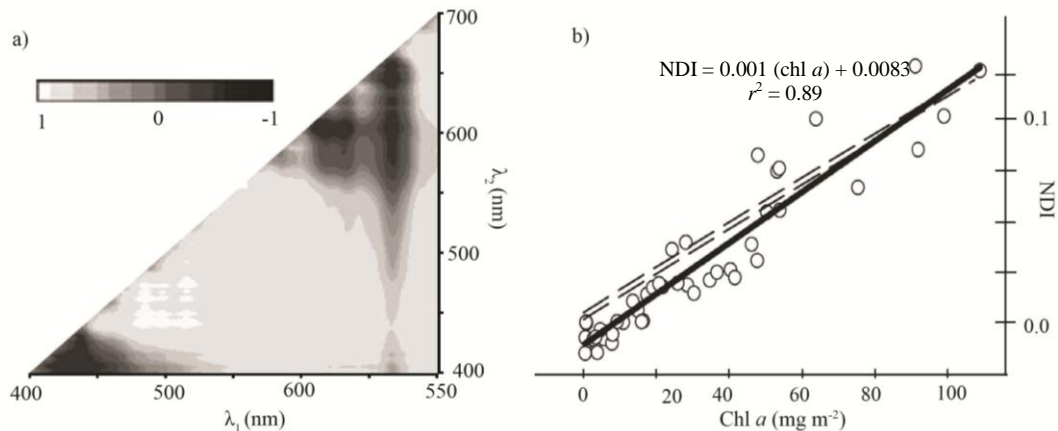


Figure 2.8. (a) Correlation surface between core based chl *a* and all possible NDI wavelength (λ) combinations and (b) regression of NDI calculated for wavelengths 485 and 472 with core derived biomass, dashed lines represent model output and circles observed values. From Mundy *et al.* (2007b). Copyright (2012) American Geophysical Union.

Literature Cited

- Ackley, S.F., Dieckmann, G.S., Shen, H., 1987. Algal and foram incorporation into new sea ice. *EOS Trans. Am. Geophys. Union* 68, 1736.
- Anderson, D.L., Weeks, W.F., 1958. A theoretical analysis of sea ice strength, *Trans. Am. Geophys. Union* 39, 632-640.
- Arrigo, K.R., Sullivan, C.W., 1992. The influence of salinity and temperature covariation on the photophysiological characteristics of Antarctic sea ice microalgae. *J. Phycol.* 28, 746-756.
- Arrigo, K.R., Sullivan, C., Kremer, J., 1991. A bio-optical model of Antarctic sea ice. *J. Geophys. Res.* 96, 10581-10592, doi:10.1029/91JC00455.
- Arrigo, K.R., Mock, T., Lizotte, M., 2010. Primary Producers and Sea Ice, in: Thomas D.N., Dieckmann G.S. (Eds.), *Sea Ice*, second edition. Wiley Blackwell Publishing, Malaysia, pp. 283-325.
- Babin, M., Stramski, D., Ferrari, G.M., Claustre, H., Bricaud, A., Obolensky, G., Hoepffner, N., 2003. Variations in the light absorption coefficients of phytoplankton, nonalgal particles, and dissolved organic matter in coastal, waters around Europe. *J. Geophys. Res.* 108, 3211, doi:10.1029/2001JC000882.
- Campbell, N.A., Reece, J., 2005. Chapter 10: Photosynthesis, in: *Biology*, seventh edition. Pearson Education Inc., San Francisco, pp. 181-198.
- Colbeck, S.C., 1986. Statistics of coarsening in water-saturated snow. *Acta Metallurg.* 34, 347-352.
- Cota, G., Horne, E., 1989. Physical control of arctic ice algal production. *Mar. Ecol. Prog. Ser.* 52, 111-121.
- Cota, G., Legendre, L., Gosselin, M., Ingram, R.G., 1991. Ecology of bottom ice algae: I. Environmental controls and variability. *J. Mar. Syst.* 2, 257-277.
- Cota, G., Smith, R., 1991. Ecology of bottom ice algae: III. Comparative physiology. *J. Mar. Syst.* 2, 297-315.
- Cota, G., Prinsenberg, S., Bennett, E., Loder, J., Lewis, M., Anning, J., Watson, N., Harris, L., 1987. Nutrient fluxes during extended blooms of Arctic ice algae. *J. Geophys. Res.* 92, 1951-1962, doi:10.1029/JC092iC02p01951.
- Cota, G., Anning, J., Harris, L., Harrison, W., Smith, R.E.H., 1990. Impact of ice algae on inorganic nutrients in seawater and sea ice in Barrow Strait, NWT, during spring. *Can. J. Fish. Aquat. Sci.* 47, 1402-1415.

- De Abreau, R., Arkette, M., Yackel, J., Barber, D., 2001. Operational satellite sensing of Arctic first year sea ice melt. *Can. J. Rem. Sens.* 27, 487-501.
- Devred, E., Sathyendranth, S., Stuart, V., Maass, H., Ulloa, O., Platt, T., 2006. A two-component model of phytoplankton absorption in the open ocean: Theory and applications. *J. Geophys. Res.* 111, C03011, doi:10.1029/2005JC002880.
- Doherty, S.J., Warren, S.G., Grenfell, T.C., Clarke, A.D., Brandt, R.E., 2010. Light-absorbing impurities in Arctic snow. *Atm. Chem. and Phys. Disc.* 10, 18807-18878.
- Ehn, J., 2006. Light Transport in the Arctic Sea Ice Environment. Ph.D. Dissertation, University of Manitoba.
- Ehn, J., Papakyriakou, T., Barber, D., 2008. Inference of optical properties from radiation profiles within melting landfast sea ice. *J. Geophys. Res.* 113, C09024, doi:10.1029/2007JC004656.
- Ehn, J., Mundy, C.J., Barber, D., Hop, H., Rossnagel, A., 2011. Impact of horizontal spreading on light propagation in melt pond covered seasonal sea ice in the Canadian Arctic. *J. Geophys. Res.* 116, C00G02, doi: 10.1029/2010JC006908.
- Eicken, H., 1992. The role of sea ice in structuring Antarctic ecosystems. *Polar Biol.* 12, 3-13.
- Eurico, J.D., Steward, R.G., Vodacek, A., Blough, N.V., Phinney, D., 1999. Determining optical absorption of colored dissolved organic matter in seawater with a liquid capillary. *Limnol. Oceanogr.* 44, 1142-1148.
- Gagnon, R., Levasseur, M., Weise, A.M., Fauchot, J., Campbell, P.G.C., Weissenboeck, B.J., Merzouk, A., Gosselin, M., Vigneault, B., 2005. Growth stimulation of *Alexandrium tamarense* (dinophyceae) by humic substances from the Manicougan river (Eastern Canada). *J. Phycol.* 41, 489-497.
- Garrison, D.L., Buck, K.R., 1986. Organism losses during ice melting: A serious bias in sea ice community studies. *Polar Biol.* 6, 237-239.
- Gosselin, M., Legendre, L., Therriault, J.-C., Demers, S., Rochet, M., 1986. Physical control of the horizontal patchiness of sea-ice microalgae. *Mar. Ecol. Prog. Ser.* 29, 289-298.
- Gosselin, M., Legendre, L., Therriault, J.-C., Demers, S., 1990. Light and nutrient limitation of sea-ice microalgae (Hudson Bay, Canadian Arctic). *J. Phycol.* 26, 220-232.

- Granskog, M.A., Kaartokallio, H., Kuosa, H., Thomas, D.N., Ehn, J., Sonninen, E., 2005. Scales of horizontal patchiness in chlorophyll *a*, chemical and physical properties of landfast sea ice in the Gulf of Finland (Baltic Sea). *Polar Biol.* 28, 276-283.
- Grenfell, T., Perovich, K., 1984. Spectral albedos of sea ice and incident solar irradiance in the Southern Beaufort Sea. *J. Geophys. Res.* 89, 3573-3580, doi:10.1029/JC089iC03p03573.
- Harrison, W., Cota, G., 1990. Primary production in polar waters: relation to nutrient availability. *Polar Res.* 10, 87-104.
- Horner, R.A., 1985. *Sea Ice Biota*. CRC Press Inc., Florida.
- Horner, R., Ackley, S.F., Dieckmann, G.S., Gulliksen, B., Hoshiai, T., Legendre, L., Melnikov, I.A., Reeburgh, W.S., Spindler, C.W., Sullivan, C.W., 1992. Ecology of sea ice biota I. Habitat, terminology, and methodology. *Polar Biol.* 12, 417-427.
- Hsaio, S.I.C., 1980. Quantitative composition, distribution, community structure and standing stock of sea ice microalgae in the Canadian Arctic. *Arctic* 33, 768-793.
- Hsaio, S.I.C., 1992. Dynamics of ice algae and phytoplankton in Frobisher Bay. *Polar Biol.* 12, 645-651.
- Iacoza, J., Barber, D.G., 1999. An examination of the distribution of snow on sea ice. *Atmos. Ocean.* 37, 21-51.
- Iacoza, J., Barber, D.G., 2001. Ablation patterns of snow cover over smooth first-year sea ice in the Canadian Arctic. *Hydrol. Proc.* 15, 3559-3569.
- Janech, M.G., Krell, A., Mock, T., Kang, J.S., Raymond, J.A., 2006. Ice-binding proteins from sea ice diatoms (*Bacillariophyceae*). *J. Phycol.* 42, 410-416.
- Kottmeier, S.T., Grossi, S.M., Sullivan, C.W., 1987. Sea ice microbial communities, VIII, Bacterial production in annual sea ice of McMurdo Sound, Antarctica. *Mar. Ecol. Prog. Ser.* 35, 175-186.
- Kottmeier, S.T., Sullivan, C.W., 1988. Sea ice microbial communities. IX. Effects of temperature and salinity on metabolism and growth of autotrophs and heterotrophs. *Polar Biol.* 8, 293-304.
- Krembs, C., Mock, T., Gradinger, R., 2001. A mesocosm study of physical-biological interactions in artificial sea ice: effects of brine channel surface evolution and brine movement on algal biomass. *Polar Biol.* 24, 356-364.
- Krembs, C., Eicken, H., Junge, K., Deming, J., 2002. High concentrations of expolymeric substances in Arctic winter sea ice: implications for the polar

- ocean carbon cycle and cryoprotection of diatoms. *Deep-Sea Res. I* 49, 2163-2181.
- Lalli, C.M., Parsons, T.R., 1993. *Biological Oceanography: An Introduction*. Pergmon Press, New York.
- Lavoie, D., Denman, K., Michel, C., 2005. Modeling ice algal growth and decline in a seasonally ice-covered region of the Arctic (Resolute Passage, Canadian Archipelago). *J. Geophys. Res.* 110, C11009, doi:10.1029/2005JC002922.
- Lee, P.A., Mora, S.J., Gosselin, M., 2001. Particulate dimethylsulfoxide in Arctic sea-ice algal communities: the cryoprotectant hypothesis revisited. *J. Phycol.* 37, 488-499.
- Legendre, L., Gosselin, M., 1991. In situ spectroradiometric estimation of microalgal biomass in first-year sea ice. *Polar Biol.* 11, 113-115.
- Legendre, L., Aota, M., Shirasawa, K., Martineau, M.J., Ishikawa, M., 1991. Crystallographic structure of sea ice along a salinity gradient and environmental control of microalgae in the brine cells. *J. Mar. Syst.* 2, 347-357.
- Light, B., Maykut, G., Grenfell, T.C., 2003. Effects of temperature on the microstructure of first-year Arctic sea ice. *J. Geophys. Res.* 108, 3051, doi:10.1029/2001JC000887.
- Maestrini, S.Y., Rochet, M., Legendre, L., Demers, S., 1986. Nutrient limitation of the bottom-ice microalgal biomass (southeastern Hudson Bay, Canadian Arctic). *Limnol. Oceanogr.* 31, 969-982.
- Massom, R.A., Eicken, H., Haas, C., Jeffries, M.O., Drinkwater, M.R., Sturm, M., Worhy, A.P., Wu, X., Lytle, V.I., Ushio, S., Morris, K., Reid, P.A., Warren, S.G., Allison, I., 2001. Snow on Antarctic sea ice. *Rev. Geophys.* 39, 413-445.
- Maykut, G.A., 1982. Large-scale heat exchange and ice production in the central Arctic. *J. Geophys. Res.* 87, 7971-7984, doi:10.1029/JC087iC10p07971.
- Maykut, G., Light, B., 1995. Refractive-index measurements in freezing sea-ice and sodium chloride brines. *Appl. Optics* 34, 950-961.
- Melnikov, I.A., 1997. *The Arctic Sea Ice Ecosystem*. Cambridge University Press, Amsterdam.
- Moch, T., Hoch, N., 2005. Long-term temperature acclimation of photosynthesis in steady-state cultures of the polar diatom *Fragilariopsis cylindrus*. *Photosyn. Res.* 85, 307-317.

- Mundy, C.J., Barber, D.G., Michel, C., 2005. Variability of snow and ice thermal, physical and optical properties pertinent to sea ice biomass during spring. *J. Mar. Syst.* 58, 107-120.
- Mundy, C.J., Barber, D.G., Michel, C., Marsden, R.F., 2007a. Linking ice structure and microscale variability of algal biomass in Arctic first-year sea ice using an in situ photographic technique. *Polar Biol.* 30, 1099-1114.
- Mundy, C.J., Ehn, J.K., Barber, D.G., Michel, C., 2007b. Influence of snow cover and algae on the spectral dependence of transmitted irradiance through Arctic landfast first-year sea ice. *J. Geophys. Res.* 112, C03007, doi:10.1029/2006JC003683.
- Mundy, C. J., Gosselin, M., Gratton, Y., Brown, K., Galindo, V., Campbell, K., Levasseur, M., Barber, D., Papakyriakou, T., ms. The role of environmental factors on under-ice phytoplankton bloom initiation: A case study on landfast sea ice in Resolute Passage, Canada. *J. Limnol. Oceanogr.*
- Parsons, T.R., Maita, Y., Lalli, C.M., 1984. *Manual of Chemical and Biological Methods for Seawater Analysis*. Pergamon Press, New York.
- Pegeau, S., Zaneveld, J., 2000. Field Measurements of in-ice radiance. *Cold Reg. Technol.* 31, 33-46.
- Perovich, D., 1996. *The Optical Properties of Sea Ice*. US Army Corps of Engineers. Cold Research and Engineering Laboratory, Monograph 96-1 1-23.
- Perovich, D., 2003. Complex yet translucent: the optical properties of sea ice, *Physica B.* 338, 107-114.
- Perovich, D., Roesler, C., Pegau, W., 1998. Variability in Arctic sea ice optical properties. *J. Geophys. Res.* 103, 1193-1208, doi:10.1029/97JC01614.
- Perovich, D.K., Grenfell, T.C., Light, B. and, Hobbs, P.V., 2002. The seasonal evolution of Arctic sea ice albedo of multiyear sea ice. *J. Geophys. Res.* 107, 8044, doi:10.1029/2000JC000438.
- Petrich, C., Eicken, H., 2010. Growth, Structure and Properties of Sea Ice, in: Thomas D.N., Dieckmann G.S. (Eds.), *Sea Ice*, second edition. Wiley Blackwell Publishing, Malaysia, pp. 23-27.
- Pope, R.M., Fry, E.S., 1997. Absorption spectrum (380-700 nm) of pure water. II. Integrating cavity measurements. *Appl. Optics* 36, 8710-8723.
- Ralph, P.J., Ryan, K.G., Martin, A., Fenton, G., 2007. Melting out of sea ice causes greater photosynthetic stress in algae than freezing in. *J. Phycol.* 43, 948-956.

- Robinson, D., Arrigo, K., Iturriaga, R., Sullivan, C., 1995. Microalgal light-harvesting in extreme low-light environments in McMurdo Sound, Antarctica. *J. Phycol.* 31, 508-520.
- Ryan, K.G., Ralph, P., McMinn, A., 2004. Acclimation of Antarctic bottom-ice algal communities to lowered salinities during melting. *Polar Biol.* 27, 679-686.
- Rysgaard, S., Kuhl, M., Hansen, J.W., 2001. Biomass, production and horizontal patchiness of sea ice microalgae in a high-Arctic fjord (Young Sound, NE Greenland). *Mar. Ecol. Prog. Ser.* 223, 15-26.
- Smith, R.E.H., Gosselin, M., Taguchi, S., 1997. The influence of major inorganic nutrients on the growth and physiology of high arctic ice algae. *J. Mar. Syst.* 11, 63-70.
- Søgaard, D.H., Hansen, P.J., Rysgaard, S., Glud, R.N., 2011. Growth limitation of three Arctic sea ice algal species: effects of salinity, pH, and inorganic carbon availability. *Polar Biol.* 34, 1157-1165.
- SooHoo, J., Palmisano, A., Kottmeier, S., Lizotte, M., SooHoo, S., Sullivan, C., 1987. Spectral light absorption and quantum yield of photosynthesis in sea ice microalgae and a bloom of *Phaeocystis pouchetii* from McMurdo Sound, Antarctica. *Mar. Ecol. Prog. Ser.* 39, 175-189.
- Spindler, M., 1994. Notes on the biology of sea ice in the Arctic and Antarctic. *Polar Biol.* 14, 319-324.
- Sturm, M., Massom, R.A., 2010. Snow and Sea Ice, in: Thomas D.N., Dieckmann G.S. (Eds.), *Sea Ice*, second edition. Wiley Blackwell Publishing, Malaysia, pp. 154-204.
- Timco, G., Johnston, M., Kabut, I., 2001. Ice Decay and the Ice Regime System, Technical Report HYD-TR-070. NRC Publications Archive.
- Wadhams, P., 2000. Chapter 2, in: *Ice in the Ocean*. Gordon and Breach Science Publishers, London, pp. 37-80.
- Warren, S.G., Brandt, R.R., Grenfell, T.C., 2006. Visible and near-ultraviolet absorption spectrum of ice from transmission of solar radiation into snow. *Appl. Optics* 45, 5320-5334.
- Welch, H., Bergmann, M., Jorgenson, J.K., Burton, W., 1988. A subice suction corer for sampling epontic ice algae. *Can. J. Fish. Aquat. Sci.* 45, 562-568.

CHAPTER THREE: TIME SERIES MEASUREMENTS OF ICE ALGAE BIOMASS USING TRANSMITTED IRRADIANCE AND ASSESSMENT OF INFLUENTIAL PHYSICAL VARIABLES OVER THE SPRING MELT PERIOD

This paper has been prepared and submitted for peer review in the Journal of Marine Systems. The work represents a core chapter of my thesis and this work was all conceived, conducted, analyzed and reported by me as the first author.

Campbell, K., Mundy, C.J., Barber, D., Gosselin, M. Time series measurements of ice algae biomass using transmitted irradiance and assessment of influential physical variables over the spring melt period. J. Mar. Syst. (in review).

Abstract

Collection of a representative time series of ice algal biomass has been impeded by traditional destructive core extraction sampling techniques. In this study, we support previous work showing that a normalized difference index (NDI) using 2 spectral bands of transmitted irradiance (478 and 490 nm) can be used as a precise and non-invasive method to estimate sea ice chlorophyll *a* (chl *a*) following a simple calibration to the local region. Application of this method over the spring melt period, 9 May to 26 June, 2011, provided the first representative time series dataset collected to monitor changes in bottom ice chl *a* at a single point location. The dataset was collected on landfast first-year sea ice of Allen Bay, Nunavut. Physical variables were measured coincident with transmitted irradiance at the site to assess processes affecting chl *a* accumulation and loss at the ice bottom. The ice temperature gradient over the lower half of the ice was a dominant factor, positively associated with chl *a* prior to 25 May, and negatively thereafter, indicating a potential threshold of optimal gradient. The increasing gradient

associated with rising internal ice temperatures likely contributed to loss of chl *a* through its positive influence on brine drainage and ice melt, whereas its contribution via brine flushing, that which is aided by a meltwater hydrostatic head, did not. Chl *a* was also negatively associated with a large increase in transmitted irradiance of photosynthetically active radiation (400-700 nm) following a 10 June storm event that caused extensive surface melt, as well as with current velocity measured below the ice which followed a bi-weekly tidal cycle.

Keywords: Ice algae; Biomass; Sea ice; Transmitted irradiance; Arctic zone; Algal blooms

1. Introduction

Ice algae are an important feature of the Arctic marine ecosystem, contributing between one and two thirds of total primary production in some regions (*Horner and Schrader, 1982; Legendre et al., 1992*) with chlorophyll *a* (chl *a*) concentrations ranging from 1 to 340 mg m⁻² (*Arrigo et al., 2010*). Their biomass provides a concentrated food resource for sea ice and pelagic grazers in early spring. They also extend biological production in polar waters by approximately one to three months (*Cota et al., 1991*).

Algae using sea ice as a growth substrate are concentrated largely in the bottom 10 cm (*Smith et al., 1990*) because it maintains cells in an optimal position to receive maximum irradiance from above as well as the bulk supply of nutrients in the ocean water below. Ice algae growth commences once a minimum irradiance threshold for photosynthesis has been reached around the months of February to March (*Gosselin et al., 1985; Cota and Horne, 1989; Welch and Bergmann, 1989; Smith et al., 1990*). After

this point, algae grow exponentially until a potential plateau as they transition from light to nutrient limitation (*Gosselin et al.*, 1990; *Lavoie et al.*, 2005). The bloom ends with the onset of sea ice melt (*Lavoie et al.*, 2005), however, the primary physical mechanisms contributing to biomass variability and especially loss from the ice remain points of debate. Potential mechanisms include: influences of sub-ice structure (*Eicken*, 1992), ice growth rate (*Legendre et al.*, 1991), brine drainage (*Mundy et al.*, 2007a), ice melt and warming rate, snow depth, light transmission, heat release by algal cells following transmitted irradiance (T_{λ}) absorption (biological melt; *Lavoie et al.*, 2005), and photoinhibition (*Rintala et al.*, 2006).

The concentration of the chl *a* pigment in sea ice is often used as an index of ice algal biomass because of the reliable positive relationship between the variables (*Hsaio*, 1992). Collection of chl *a* samples is primarily accomplished by ice core extraction followed by lab analysis from subsamples taken after the ice core has melted. The use of core-based estimates may result in the underestimate of ice algal biomass in some cases, however, because of sample loss during core extraction to the surface (*Welch et al.*, 1988). This may be especially problematic when the algae are not strongly attached to the ice during advanced stages of melt. Furthermore, due to the destructive nature of ice core extraction, a representative time series of ice algal biomass at a single point location cannot be collected.

The photosynthetic and accessory pigments found in ice algae preferentially absorb light at particular wavelengths, most notably with chl *a* at 440 and 665-675 nm (*Bricaud et al.*, 1988; *Legendre and Gosselin*, 1991). As a result, ice algae alter the spectral distribution of the light environment below the sub-ice surface in a way that has been

statistically associated with their biomass. The use of T_λ to assess biomass was first examined by Legendre and Gosselin (1991) and later improved upon by Mundy et al. (2007b) who accounted for 89% of biomass variability using a normalized difference index (NDI) of wavelengths 485 and 472 nm.

High-resolution time series observations are necessary to understand the ecosystems associated with sea ice (*Cota and Smith, 1991*). This study addresses such a need by using the standardised T_λ method developed by *Mundy et al. (2007b)* to estimate biomass of a single population over the whole spring melt period, 9 May to 26 June, on landfast first-year sea ice (FYI) of Allen Bay, Nunavut. Coincident physical variables were sampled to determine the bio-physical processes affecting algal biomass accumulation and loss over this period. This paper presents a comprehensive study of the ice algae spring bloom, a necessary step in anticipating responses of the Arctic marine system to changes in climate.

2. *Materials and Methods*

2.1 *Study Site*

Measurements were taken in the area surrounding an ice camp that was established as part of the Arctic-ICE (Arctic-Ice Covered Ecosystem) initiative. The sampling region of smooth ice 1.3-1.7 m thick overlay a water depth of ~60 m in the bay. During the sampling period air temperature ranged from -28.5 to 6.6°C and the sea ice surface evolved from snow depths ranging from 5.5 to 50 cm in early spring to white ice (*Maykut and Grenfell, 1975*) and melt pond cover towards the end of the study.

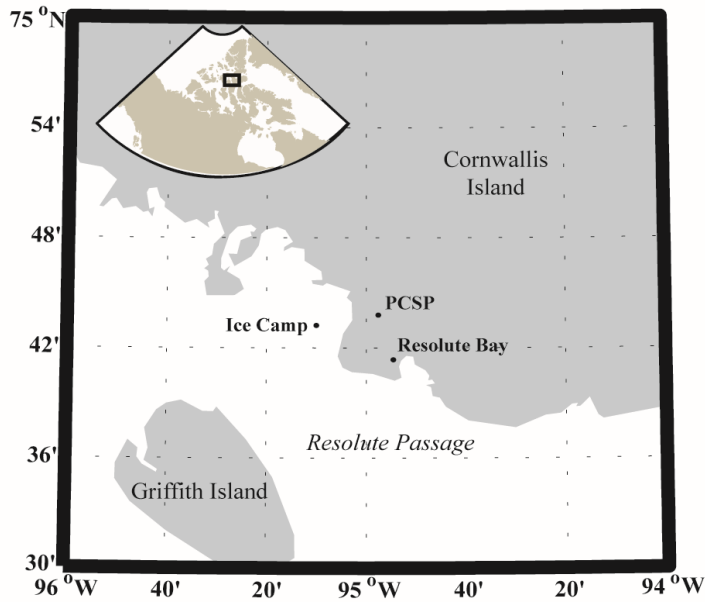


Figure 3.1. Location of 2011 Arctic-ICE Allen Bay camp ($74^{\circ} 43.165' N$; $95^{\circ} 10.099' W$).

2.2 Transmitted Irradiance Measurements

From 9 May to 24 June, the spectral composition of the incident downwelling (DW) and T_{λ} , approximately 15 cm beneath the ice-water interface, was measured daily at one location ($74^{\circ} 43.110' N$; $95^{\circ} 10.077' W$). A dual head VIS-NIR spectrometer (Analytical Spectral Devices Inc.©) with reverse cosine receptor (RCR; 180° field of view) that measured wavelengths from 350 to 1050 nm with a 1.4 nm band width was used to record all DW and T_{λ} measurements. Deployment of the under-ice RCR largely followed that described by *Mundy et al.* (2007b) where the sensor head was fixed to an underwater arm and positioned 1.5 m south of the auger hole created for deployment, as well as perpendicular to the ice surface. An opaque foam cover was placed within the auger hole during and between measurements to minimize light contamination. During the first half of the study, a surface layer of ice would form overnight and thus the hole

had to be re-excavated upon the next visit. Caution was taken when operating the auger so as to not flood or have ice shavings fall on the time series site.

The reference RCR was positioned approximately 1 m above the snow surface to take spectral DW readings simultaneously with under-ice measurements. This set-up was arranged on a sled for ease of mobility between different site locations. Spectra recorded using the underwater calibrated sensor were integrated over 4.35 seconds and surface values over 17 ms to avoid saturation. A total of five spectra were recorded per measurement and dark currents were subtracted intermittently during sampling to remove instrument noise. Spectrometer and cable calibrations were completed prior to the field so irradiance (in W m^{-2}) was recorded automatically. An average of 5 snow depths was recorded 1 m east of the irradiance sampling area on a snow cover similar to the time series site.

2.3 Deriving Time Series Chl a from T_λ

2.3.1 Core Sampling

Every fourth day, new sample locations were established to represent each of the surface conditions present; three snow depth categories of low (L; < 10 cm), medium (M; 10 to 18 cm), and high (H; > 18 cm) during the early spring or, in advanced melt, each of the two surface types present; melt ponds (L) and snow or drained white ice (H). Measurements at melt ponds were considered extensions of the L snow depth category into the late spring because ponds are predisposed to form between drifts at low snow depth sites (*Iacoza and Barber, 2001*). Similarly, the persistence of snow or white ice was assumed to be prior locations of H snow depths. At these locations T_λ was measured

according to the method described in section 2.2 followed by the extraction of two ice cores using a 9 cm Mark II Kovacs coring system.

The bottom 10 cm of each site's cores were combined with filtered sea water (FSW) at a ratio of 3 parts FSW to 1 part ice core volume, then melted slowly in the dark to minimize osmotic and optical stress (*Garrison and Buck, 1986*). Once melted (after approximately 18 to 24 hours), pseudo-replicate subsamples were filtered onto Whatman GF/F filters. The filters were placed in 10 ml of 90% acetone for 18 to 24 hours followed by a fluorometric measurement of chl *a* using a Turner Designs Fluorometer 10-005R before and after acidification with 5% HCl (*Parsons et al., 1984*). Areal chl *a* concentration was calculated based on these measurements and the equations of Holm-Hansen et al. (1965).

2.3.2 Calculation of Time Series Biomass

Following Mundy et al. (2007b), Pearson correlation surfaces were determined for all possible NDIs (3.1):

$$\text{NDI} = [T_{\lambda_1} - T_{\lambda_2}] / [T_{\lambda_1} + T_{\lambda_2}] \quad (3.1)$$

and therefore, all wavelength band combinations of transmitted irradiance and core based chl *a* data. Correlation values calculated from wavelengths greater than 700 nm were noisy and therefore, only wavelengths of photosynthetically active radiation (PAR; wavelengths 400-700 nm) were used. Chl *a* concentrations (in mg m⁻²) at the time series site were calculated using a linear least squares regression fit of the core based chl *a* concentrations versus the highest correlated NDI.

2.4 Physical Sampling

In addition to snow depth, a number of potential environmental influences on ice algae biomass were investigated. PAR integrated transmittance (T_{PAR} ; 400-700 nm) was determined directly from T_λ and DW measurements made at the time series site. The meteorological tower maintained near the ice camp (74° 42.850' N, 95° 11.980' W) recorded variables such as upwelling (UW) and downwelling (DW) PAR (Wm^{-2} ; Kipp & Zonen PAR-Lite; 1 second sampling interval), air temperature (Vaisala HMP45C212; 1 second sampling interval), wind speed (RM Young 05103 anemometer; 2 second sampling interval), and ice temperature (Type T thermocouples; 2 second sampling interval) by data logger (Campbell Scientific CR23X) that recorded minute averages. Surface DW values, measured at the meteorological site, were averaged daily and integrated over PAR wavelengths, represented hereafter as S_{PAR} . In addition, a bottom ice temperature gradient (TG; $^{\circ}C m^{-1}$) was calculated by subtraction of ice temperature measured at 0.6 m depth below the air-ice interface from 1.2 depth, and dividing by 0.6 m. It follows that greater TG values represent warming of the bottom ice and overall a more isothermal sea ice environment. Ice temperature values prior to 24 May were linearly corrected for instrument error. Albedo was also calculated using the UW and DW measurements collected at the meteorological station.

Alongside coring for chl *a* analysis an additional core was taken at the M class (H class during the melt period) site to measure temperature (Testo 720 probe) at 10 cm intervals and salinity (WTW 330i conductivity meter) for 10 cm sections. These values were later used to calculate percent brine volume following the equations of Cox and

Weeks (1983). As a consequence of sampling time restrictions, these core based values were made only every 4 days.

Lastly, an ice tether with an ALEC Infinity-EM current sensor monitored current velocity (cm s^{-1}) at 2.5 m below the air-ice surface at a nearby site ($74^{\circ} 43.103' \text{ N}$; $95^{\circ} 10.031' \text{ W}$). Current velocities were averaged over 24 hour periods to obtain a variable of mean daily current velocity (hereafter MDV).

2.5 Principal Component Analysis

A principal component analysis (PCA) (Pielou, 1984; Gotelli and Ellison, 2004) was performed, using JMP statistical software, to explore the relationships between environmental factors (snow depth (H_S), S_{PAR} , T_{PAR} , TG, and MDV) and NDI estimated chl *a* throughout the study period.

3. Results and Discussion

3.1 Site Conditions

Air temperature remained below 0°C , warming from -28.5 to -0.3°C , from 9 May to 6 June. During this period, H_S at the time series site ranged between 10.8 and 20.4 cm and averaged 16.2 cm depth. The characteristics of the sea ice surface quickly transitioned during a storm weather event on 10 June which brought strong northeastern winds, increasing to 17.5 m s^{-1} , and rainfall. Following the storm, site conditions were characterized by low H_S and eventually white ice with melt water of no more than 0.5 cm depth. A rapid decrease in H_S corresponded to a rise in T_{PAR} at the time series site (Figure 3.2) as well as an albedo decline from on average 0.83 (10 June and earlier) to 0.41 (11

June and later) at the nearby meteorological tower (data not presented). Over the course of 10 June alone, albedo changed from 0.66 to 0.40. These large differences are a consequence of snow melt as larger snow grains, and ultimately the ice surface or melt water, permitted greater transmission of incoming radiation into the ice instead of reflecting it back to the atmosphere (Perovich *et al.*, 1998; Mundy *et al.*, 2005). Lastly, air temperature stayed above 0°C from 14 June to the end of sampling on 26 June.

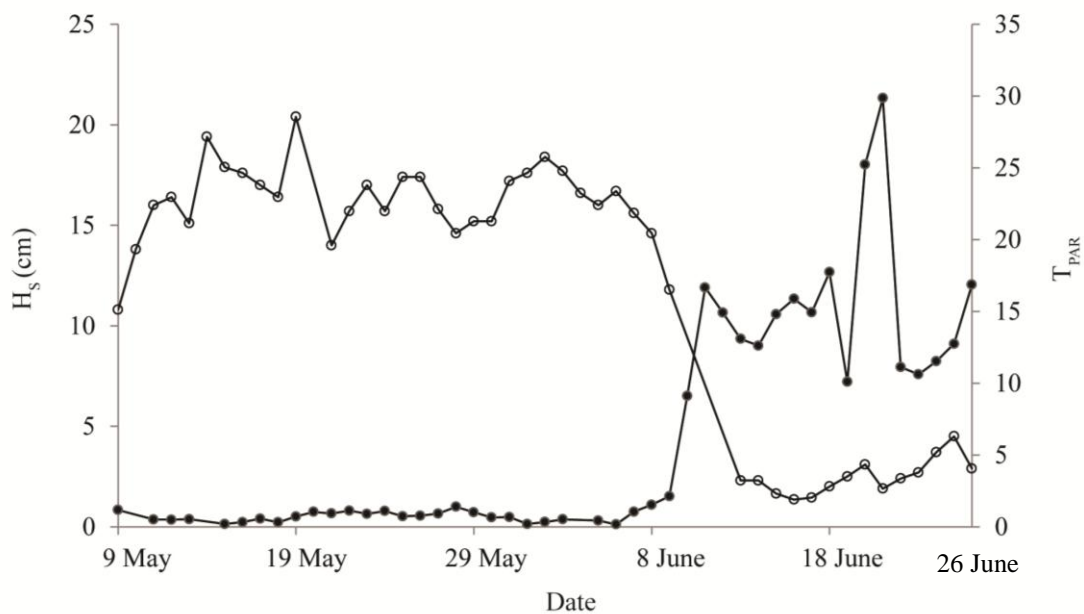


Figure 3.2. Changes in snow depth (H_s , circle) and integrated transmittance of photosynthetically active radiation (T_{PAR} , solid) at the time series site from 9 May to 26 June. H_s values following 9 June are representative of snow or white ice depth.

3.2 Optimal NDI

The correlation analysis between all possible NDI wavelength combinations and ice core chl *a* concentrations measured under high, medium and low snow cover is presented in Figure 3.3. Regression analysis was based on the data from H, M, and L calibration sites grouped together because no significant difference between snow depth categories was found (Chow Test; $p > 0.05$). Similar to the relationships reported by Mundy *et al.*

(2007b), NDIs were strongest using wavelengths less than 570 nm. In this assessment the wavelength combination of 478 and 490 nm (hereafter NDI_x) was chosen as the best representation of algae biomass because it demonstrated the strongest correlation with $r = 0.90$, and accounted for 81% of chl *a* variability following regression analysis. The wavelengths of NDI_x fell between 400-570 nm where, in the absence of introduced particulates which can contribute to absorption, snow has a minimal influence on the spectral distribution of light. In addition, NDIs based on a combination of wavelengths close together, like NDI_x , are more dependent on algae absorption properties than those of snow and ice (Mundy *et al.*, 2007b).

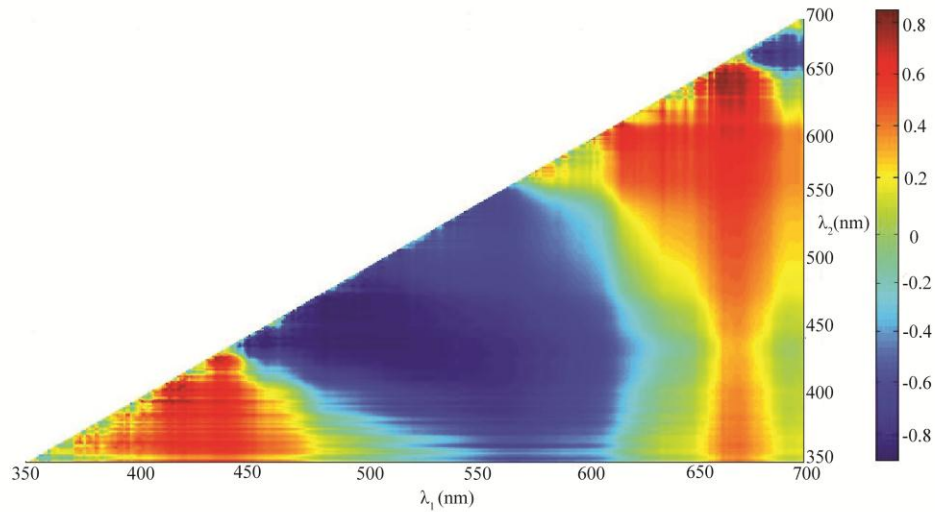


Figure 3.3. Pearson correlation surface of all possible normalized difference indices (NDIs) with core derived chlorophyll *a* (chl *a*) measurements.

3.3 Time Series Chl *a* Calculation

The calculated regression (section 2.3.2) between NDI_x and core based chl *a*

concentration (3.2):

$$\text{chl } a \text{ (mg m}^{-2}\text{)} = (-497.21 \times (\text{NDI}_x) + 15.202) \quad (3.2)$$

was used for all time series chl *a* calculations (Figure 3.4). Resultant values indicated a chl *a* increase to 13 May after which biomass oscillated between 10.3 and 23.9 mg m⁻² until the peak chl *a* concentration on 6 June at 27.6 mg m⁻². Biomass declined sharply thereafter, becoming lower than any prior biomass on 10 June, until reaching -0.91 mg m⁻² on 14 June. The length of the time series therefore resulted in a full description of the ice algae bloom; development, peak biomass, and termination. Subsequent chl *a* concentrations fluctuated between approximately -1.58 and 8 mg m⁻². The negative values highlight a small error associated with the scatter in the calibration relationship. For the purposes of this study, negative NDI biomass estimates were assigned values of 0 mg m⁻² for analyses

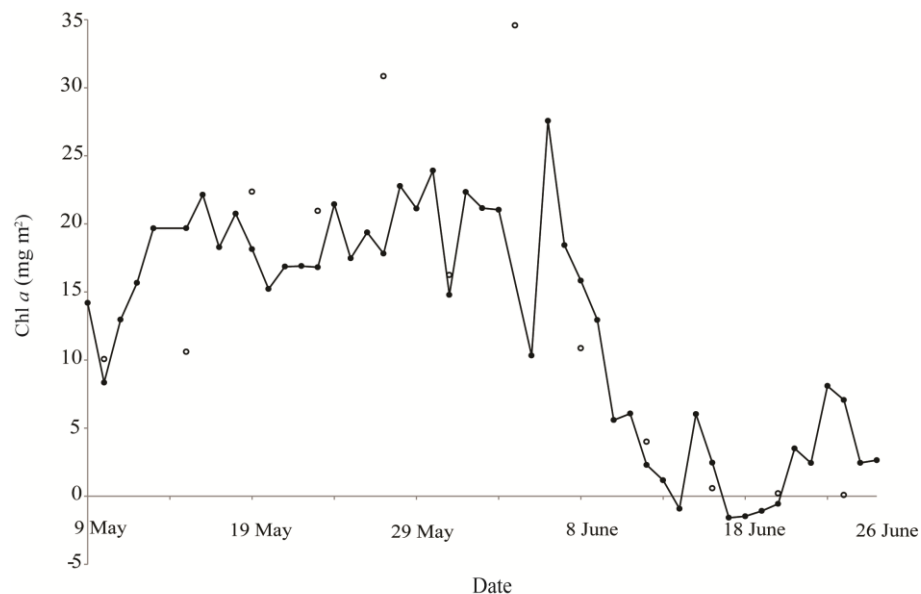


Figure 3.4 Changes in chlorophyll a (chl a) concentration at the time series site (calculated values, solid) and at high snow depth core locations (measured values, circle) from 9 May to 26 June.

With the exception of measurements during the advanced melt period, calculated chl *a* values adhered well to core based estimates under high H_S. Indeed even the perceived sudden changes in time series biomass on 10 and 31 May and on 6 June corresponded to large rises or falls in H_S core based estimates as well (Figure 3.4). The drop in chl *a* on 5 June did not appear to be supported by core based biomass and was believed to be associated with sampling error, for example, the presence of attenuating snow in the connection points between fibre optic cables and the ASD instrument.

The large fluctuations in biomass within short periods of time seen in Figure 3.4 may be attributed to spatial variability. Small scale variability of ice algae biomass, capable of changing within 1-30 mm at the ice-ocean interface, could not be captured with the T_λ methodology used in this study because repositioning of the sampling arm at the exact position between measurements was not possible (Mundy *et al.*, 2007a). Unknowingly placing the sensor under different biomass patches within the same greater sampling region could have caused fluctuations in NDI chl *a* estimates and contributed to the time series biomass variability observed in Figure 3.4. Also, the presence of water column algae, whether phytoplankton or sloughed ice algae, between the sensor and ice interface, would falsely increase biomass estimates of the bottom ice chl *a*.

The presence of algae in the water column can be considered especially high during late stages of melt as ice algae slough off the ice en masse at the end of their bloom and float at the ice-water interface (Campbell and Mundy, pers. obs.), followed by under-ice phytoplankton growth in the water column (Mundy *et al.*, ms). Therefore, the deviation of NDI based chl *a* estimates from the low core based estimates following 14 June was likely a function of spectral absorption by algae in the water column and not bottom ice

algae. Use of the T_λ technique during times when absorption by biological materials immediately below the sea ice is high may therefore be problematic for obtaining accurate biomass estimates unless their origin, ice or water column, can be accounted for. Limitations of the method during advanced melt were also highlighted by the presence of negative biomass values which may further restrict its use and reliability during this period.

3.4 Environmental Influences on Ice Algae Biomass

3.4.1 Principal Component Analysis

The results of the PCA analysis are displayed in Figure 3.5 using components 1 and 2 as ‘x and y axes’, which together accounted for 84.09% of data variability, the majority of which was described by component 1 (eigenvalue (χ) = 4.00, 66.74%). Data points on this figure represent the different days on which data for chl a , T_{PAR} , MDV, TG, S_{PAR} , and H_S variables, depicted as vectors, were collected. Only variables with daily sampling frequency were used in this analysis and therefore BV_{AVG} was not included.

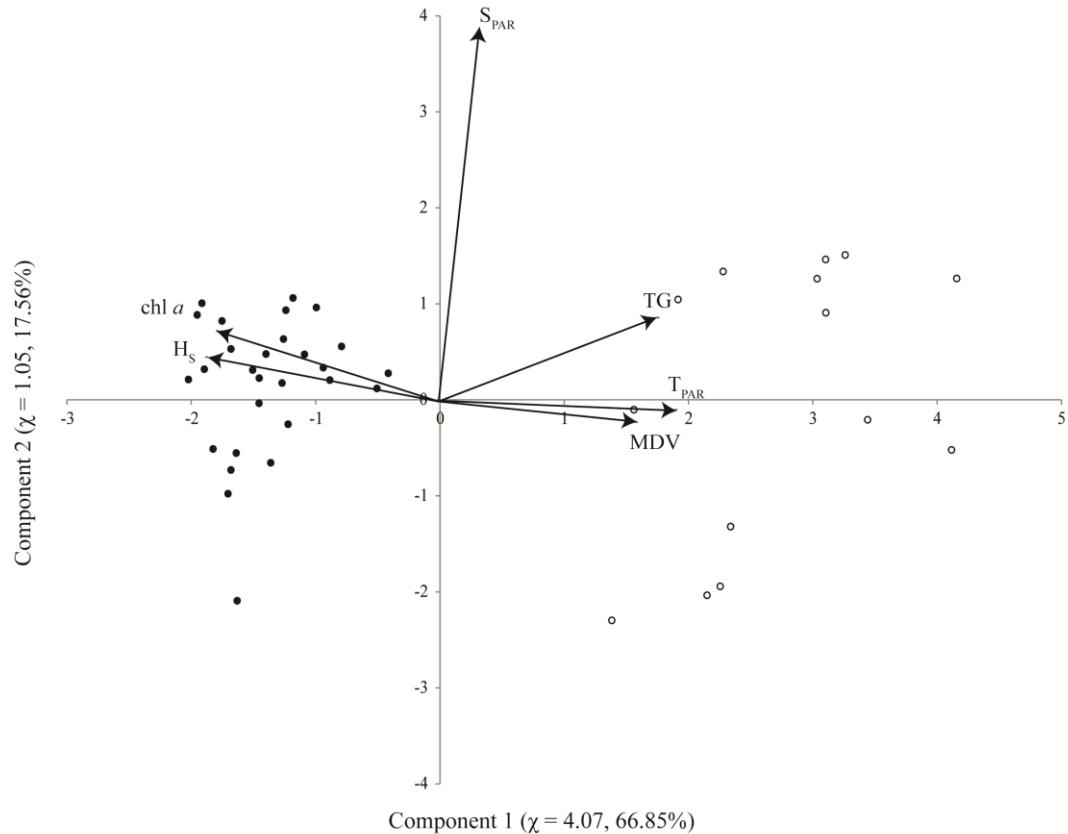


Figure 3.5. Principal component analysis of variables sampled on the landfast ice of Allen Bay (Nunavut) from 9 May to 9 June (solid) and from 10 to 26 June (circle). The environmental and biological variables are: snow depth (H_S), incident downwelling of photosynthetically active radiation (S_{PAR}), PAR integrated transmittance (T_{PAR}), bottom ice temperature gradient (TG), mean daily current velocity at 2.5 m depth beneath the air-ice interface (MDV), and bottom ice chlorophyll a ($chl a$) concentration.

Data points formed 2 distinct groups along the axis of component 1: days prior to the 10 June storm event (on the left hand side) and those after (on the right hand side). Days with missing data for any one of the variables were excluded in the PCA analysis. As a result of missing H_S data, points for 11-13 June are not present in Figure 3.5, a factor which may have contributed to the gap observed between groups. Nevertheless, values of bottom ice $chl a$ concentration and all environmental variables, with the exception of S_{PAR} , changed significantly following the spring storm, an observation

supported by the field observations discussed in section 3.1. Based on the position of sample days relative to vectors, the time series site before 10 June had higher bottom ice chl *a* biomass in a snow covered, low T_{PAR} environment with a steeper bottom ice temperature gradient (lower ice temperatures) and weaker tidal currents while the opposite trend was observed after 10 June. Fortier et al. (2002) observed a rapid loss of algae from the sea ice following rain events and warm spells similar to that observed in our study. Our results agree with these findings, suggesting that single weather events can have large effects on the physical FYI environment and subsequently on ice algae biomass levels.

Based on vector length, the largest contributors to point spread over component 1 were T_{PAR} and H_S , which were negatively associated with each other. These observations demonstrate the strong influence of snow on light transmission. The negative association between H_S and TG also illustrates the thermal influence of snow on the sea ice environment, where, bottom ice temperature was more isothermal (more positive or less negative TG) when lower snow depths were present, as a result of greater conductive heat flux between the ice and atmosphere. The vector of S_{PAR} was nearly parallel with the axis of component 2. Therefore, the broad distribution of points along this axis was a result of variable incident downwelling PAR over the entire sample period. This outcome represents the variability associated with daily changes in cloud cover and weather conditions, and illustrates that S_{PAR} is not a good predictor of the variables assessed, including algal biomass.

3.4.2 Linear Regression Analysis

To further assess bio-physical relationships, linear regressions between environmental variables and associated chl *a* NDI_x estimates at the time series site were performed (Figure 3.6; Table 3.1). This analysis resulted in 2 point clusters for variables H_S and T_{PAR} when plotted against chl *a* which did not permit linear statistical analysis over the entire sample period. Therefore, data were examined as two separate groups based on the division seen in Figure 3.6a, which corresponded the parting noted following PCA analysis: prior to and after 10 June.

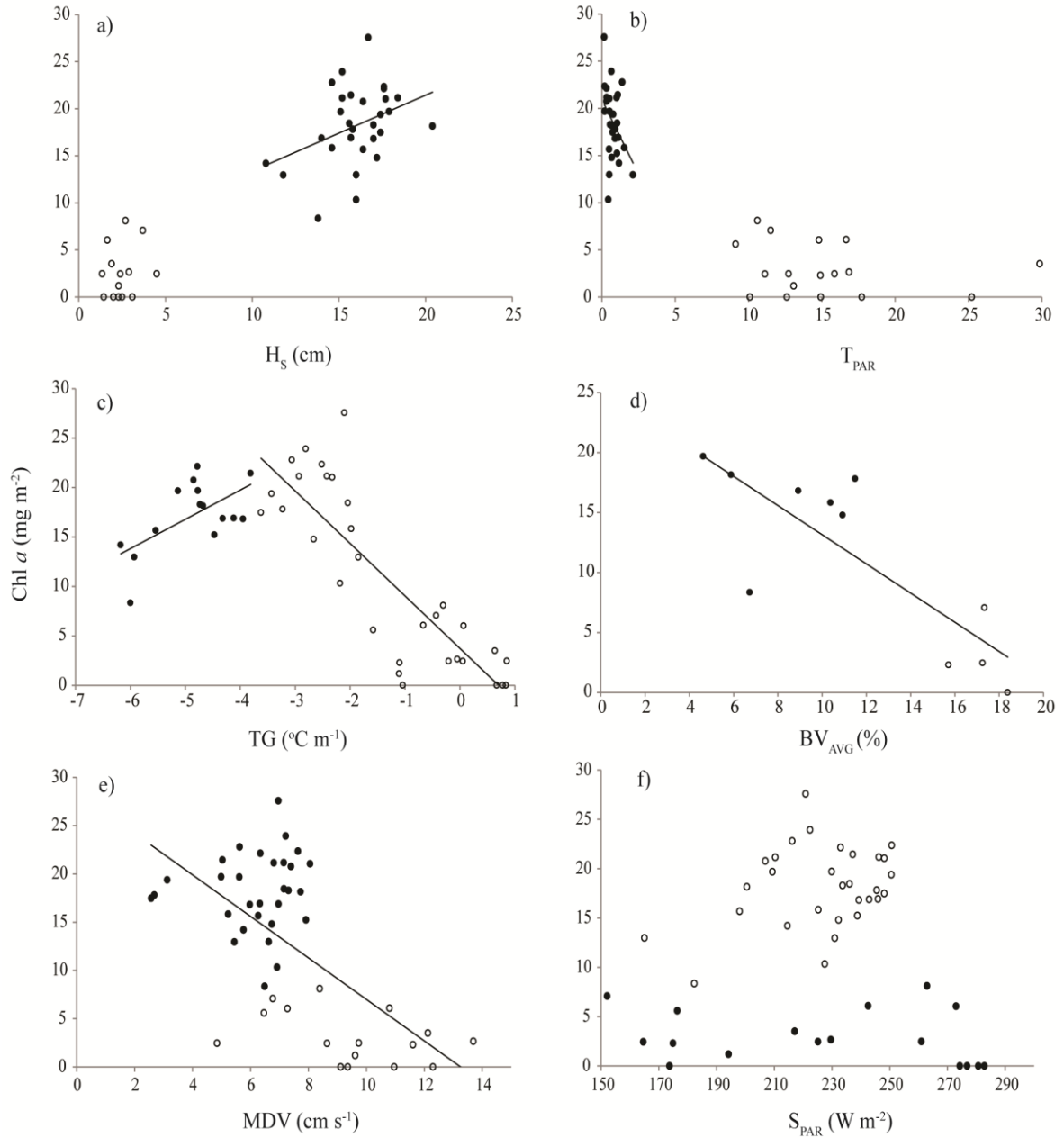


Figure 3.6. Relationships between calculated chlorophyll *a* (chl *a*) concentration and (a) snow depth (H_s), (b) integrated transmittance of photosynthetically active radiation (T_{PAR}), (c) bottom ice temperature gradient (TG), (d) average percent brine volume of total ice thickness (BV_{AVG}), (e) mean daily current velocity at 2.5 m depth below the air-ice interface (MDV), and (f) incident downwelling PAR (S_{PAR}) before (inclusive; solid) and after (circle) 9 June. Note that in (c), the data are presented before (solid) and after (circle) 25 May.

Table 3.1. Coefficients of determination (r^2 values) between calculated chl *a* concentration and environmental variables (snow depth, H_S ; surface PAR, S_{PAR} ; PAR integrated transmittance, T_{PAR} ; average brine volume, BV_{AVG} ; bottom ice temperature gradient, TG ; and mean daily under-ice velocity, MDV) for 3 sampling periods: early spring (9 May to 9 June, but 9 to 24 May for TG), late spring (10 to 26 June, but 25 May to 26 June for TG) and the total sampling period (9 May to 26 June) when point distributions permitted statistical analysis. Bolded values are significant at $p < 0.05$.

Variable	Early Spring		Late Spring		Total Period	
	r^2	n	r^2	n	r^2	n
H_S	0.141	29	0.039	14	-	-
S_{PAR}	0.097	30	0.043	17	0.000	47
T_{PAR}	0.140	29	0.047	17	-	-
BV_{AVG}	0.065	7	0.042	4	0.669	11
TG	0.306	15	0.740	32	-	-
MDV	0.006	30	0.131	17	0.387	47

The strong negative relationship between snow depth and the magnitude of transmitted irradiance through sea ice has been well documented (*Perovich, 1996; Belzile et al., 2001; Mundy et al., 2007b*) and was observed in Figures 3.3 and 3.5. The large division of H_S and T_{PAR} data around the 10 June storm in Figure 3.6a and b illustrates the role snow melt and therefore, an increase in PAR transmittance, has as a principal variable in determining the start of biomass decline and therefore bloom duration (*Gosselin et al., 1986; Lavoie et al., 2005*). This argument is supported by chl *a* dropping below the previous range of variability on 10 June (Figure 3.4). The low (and insignificant associations in the late spring) however, suggest that most of the time series biomass variability could not be explained by H_S or T_{PAR} .

A second order polynomial fit of chl *a* versus TG ($y = -0.9194 x^2 - 7.2193 x + 4.5335$; $r^2 = 0.709$, $p < 0.05$) had an inflection point of $-3.93^\circ\text{C m}^{-1}$ (x at $\frac{\delta y}{\delta x} = 0$) and therefore, for statistical assessment, data were grouped together on either side of this point in time for linear regressions; 9 to 23 May and 24 May to 26 June. During the latter

period a significant negative relationship between biomass and TG was observed such that chl *a* decreased as the ice became increasingly isothermal ($r^2 = 0.740$, $p < 0.05$). Warming of the bottom ice can negatively impact ice algae biomass a) by causing ice ablation, resulting in the melt of algae off into the water column (*Lavoie et al.*, 2005) or b) by brine drainage, where warming ice increases permeability by connecting brine pockets and channels, thereby eroding the ice algal habitat and causing algae to slough, particularly where liquid brine drains from the ice (*Lavoie et al.*, 2005; *Mundy et al.*, 2005; *Juhl and Krembs*, 2010).

Over the sampling period ice thickness decreased at medium snow depth core locations by up to 0.34 m. However, this thinning was not significant over time ($r^2 = 0.267$, $p = 0.085$). As a result, the contribution of ice ablation to the removal of ice algae could not be conclusively deducted in this study because the decrease seen may have simply been a function of spatial variability. Ice thickness at the time series location was not assessed because of complications associated with maintaining a time series; the site could not be disturbed for thickness measurements, and estimates from the maintained auger hole would not have been accurate.

Free movement of brine through sea ice by interconnecting brine pockets and channels has been modelled and observed to occur once the ice reaches near -5°C , which corresponds to approximately 5% brine volume in first-year columnar sea ice (*Golden et al.*, 1998; *Pringle et al.*, 2009). Brine volume averaged over the entire ice thickness was primarily above this 5% threshold for the whole sampling period, remaining within $\pm 1.7\%$ of 5% until 23 May after which, BV_{AVG} then increased to a plateau between 10.4

and 11.5%. A final rise in BV_{AVG} occurred following 8 June peaking at 18.4% (Figure 3.7).

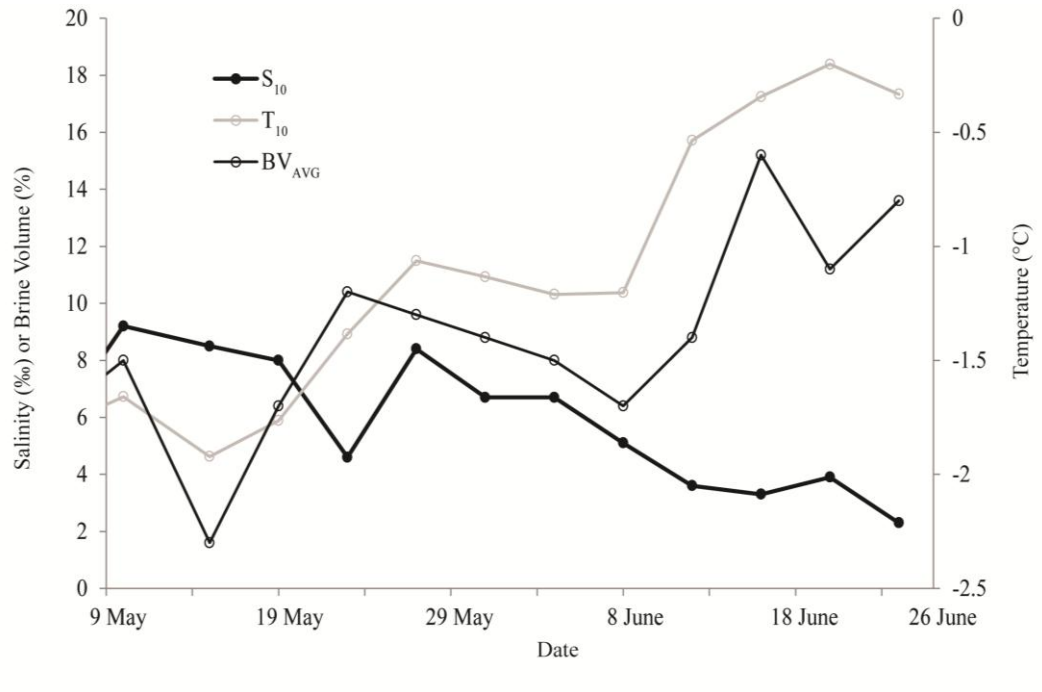


Figure 3.7. Changes in temperature (T_{10}) and salinity (S_{10}) in the bottom 10 cm of sea ice, and average percent brine volume of the entire ice column (BV_{AVG}) from 9 May to 24 June measured at medium snow depth core locations.

The regression of chl *a* versus BV_{AVG} had a distribution of points similar to the plots of chl *a* and H_s , and chl *a* with T_{PAR} , where two groups of data were separated by the 10 June weather event (Figure 3.6). The two BV_{AVG} groups represent; (left) early spring when sea ice held lower volumes of brine and supported a larger ice algal community and, (right) a period in advanced stages of melt when large volumes of brine and low chl *a* was measured in the sea ice. Severe weather events therefore had the capacity to not only rapidly change the surface ice environment, but also the internal characteristics of the sea ice.

The decline in bottom 10 cm ice salinity over time ($r^2 = 0.783$, $p < 0.05$), especially between 4 and 12 June, shows that drainage of brine from the ice and replacement by less saline ocean water, without the aid of a hydrostatic head, likely occurred (Figure 3.7). Theoretically this mechanism of brine drainage, inextricably linked with ice temperature and subsequent density gradients of brine within the ice, could contribute to biomass loss by eroding the interior ice which serves as a growth substrate, or through expansion of the brine network, removing the substrate altogether. The influence of each brine drainage mechanism, erosion and substrate removal, on the removal of algal cells could not be determined. Also, following the initial spring bloom termination, further biomass variability, like that observed after 14 June (Figure 3.3), may be attributed to periods of brine drainage (algae removal) and nutrient flux into the ice (algae growth) because of nutrient rich ocean water replacing the sinking brine (*Lavoie et al.*, 2005). Therefore, brine drainage in addition to the factors discussed in section 3.3 were likely responsible for the fluctuating chl *a* values measured during advanced melt.

Brine flushing, drainage of brine aided by a meltwater hydrostatic head, has been suggested as a greater contributor to biomass loss during advanced stages of the spring bloom than either melt (biological or physical) or nutrient level influences (*Lavoie et al.*, 2005). A drop in salinity throughout the ice column is indicative of flushing events (*Polashenski et al.*, 2012) as brine is replaced by less saline melt and ocean water. Analysis of salinity profiles measured from ice cores over the season did not show a similar result (data not presented), indicating that a brine flushing event did not occur in this study.

The validity of a -5°C brine threshold in FYI described by Golden et al. (1998) was questioned by Polashenski et al. (2012) when they found a 6 week delay between its onset and flushing by meltwater percolation. In their research, a layer of refrozen meltwater within the upper layer of ice persisted beyond the -5°C mark to cause a delay in bulk ice permeability which we hypothesize could translate into postponement in the brine drainage means of algae removal. A similar result to that observed by Polashenski et al. (2012) may thus explain why a brine flushing mechanism was not documented here despite the sea ice's bulk brine volume being equal to or above the 5% brine volume percolation threshold.

These findings illustrate that the mechanism of brine drainage may have contributed to biomass variability, especially late in the spring; however, it was not dominant in causing the bloom decline. Nevertheless, the strong regression between chl *a* versus average brine volume (Table 3.1; Figure 3.6d) suggests instead that brine volume of the ice column as a whole can be used as a predictor of ice algal biomass.

Increasing chl *a* values during the period of lowest ice temperatures (most negative TG) may be a function of time or the physical environment (Table 3.1). Sampling began during the accumulation phase of the ice algae bloom, resulting in biomass increases concurrent with, but not necessarily resulting from, rising ice temperatures. Environmental influences in the early spring positively affecting spring bloom development, such as reaching a minimum T_{PAR} threshold for photosynthesis (*Gosselin et al.*, 1985), could have contributed to the trend by exhibiting a great influence on algal biomass than other factors inhibiting algal growth during this period.

Alternatively, the significant early spring trend may have represented a threshold of ice temperature at which algae found optimal conditions at the ice subsurface. Ice algae are able to thrive at temperatures as cold as -20°C because of physiological adaptations (Morgan-Kiss *et al.*, 2006) and at temperatures much higher than those recorded in this study (Kottmeirer and Sullivan, 1988; Morgan-Kiss *et al.*, 2002). As a result, instead of physiological responses, temperature induced changes to algal habitat would have more likely influenced biomass. For example, ice growth which was still likely occurring during the early spring would increase nutrient supply because of the turbulence created at the ice interface following the movement of brine from the ice (Cota *et al.*, 1991). This positive influence on biomass would have ended when ice growth ceased as a result of warming temperatures.

Fortnightly tidal cycles were observed over the sample period when under-ice current velocity was plotted over time (data not presented). Tides (and therefore current velocities) beneath the ice can have competing influences on ice algal biomass: increases from nutrient supply (Cota *et al.*, 1991), decreases by enhancing bottom ice melt (Lavoie *et al.*, 2005), and through mechanical removal of cells (Mundy *et al.*, 2007a). In this study, the removal of algae by currents was supported as chl *a* was negatively correlated with under-ice current velocity ($r = 0.622$, $p < 0.05$), although the specific mechanism of biomass loss was not addressed in this research.

4. Summary and Conclusions

The difference in NDI selection between Mundy *et al.* (2007b) and this study may represent a limitation in the broader scale applicability of the method, suggesting core

calibration before use of T_λ in biomass estimation is required. Differences in the physical environment and algae populations, such as pigment composition, could be factors in the alternative optimal NDIs between studies. For example, the average chl *a* measured by Mundy et al. in 2003 in the Resolute Bay area was 30.6 mg m^{-2} , reaching concentrations of 109 mg m^{-2} . In contrast, the 2011 biomass was just over half the 2003 average at 16.8 mg m^{-2} and only reached a maximum biomass of 22.1 mg m^{-2} during the same time period. Higher concentrations of chl *a* and therefore algal biomass can lead to shading of algae lower in the ice column (Robinson et al., 1995) resulting in stronger absorption in the 450-550 nm region through enhanced production of the accessory pigment fucoxanthin (Soochoo et al., 1987). This suggests that calibration of T_λ estimates is required especially when measuring algae populations of different relative biomass.

Furthermore, sampling in our study extended longer into the spring melt period by 34 days meaning different environmental conditions were experienced. During later melt stages, ice algae can change their physiological state from shade-acclimation (high photosynthetic carotenoids to chl *a* ratio) to photoprotection (high photoprotective carotenoids to chl *a* ratio) (Alou et al., submitted). A change in these pigment compositions would directly affect the NDI_x wavelength bands used in our study as the most abundant diatom photosynthetic carotenoid, fucoxanthin, has a broad absorption peak from 490 to 515 nm, whereas the important photoprotective carotenoid, diadinoxanthin, has a sharp peak centered at $\sim 490 \text{ nm}$ (Bricaud et al., 2004). Lastly, noise in the data may have been introduced as a result of instrument sensitivity because measurement of longer PAR wavelengths approaches the edge of the spectrometer's measurement capacity.

Despite these complications the sampling method applied in this research permitted true time series measurements of ice algae biomass. This work illustrates for the first time the influence of many environmental variables on a single ice algae population over an extended spring melt sampling period. Applying this method of ice algae observation to remotely operated and automated underwater vehicles (ROVs and AUVs) as suggested by Mundy et al. (2007b), definitely has promise for future large spatial scale assessments of ice algae biomass. The potential also exists for automated time series over even larger temporal scales if a radiometer were to be frozen into the ice to record transmitted irradiance.

No single environmental parameter fully explained variability in algal biomass. However, the majority of it was accounted for by a combination of the variables examined. Most notable was the ice temperature gradient, which did not likely contribute to large biomass losses via brine flushing events; rather localized brine drainage was an important mechanism in causing loss of algal biomass from the ice. Although it could not be determined statistically in this study, loss of algae by physical ablation was likely a factor. Assessment of ice temperature also revealed that an optimal threshold for algal habitation of the bottom ice may exist. By whichever mechanism, the significance of the chl *a* versus the ice temperature gradient relationship raises concerns regarding the potential impact of warming ice from rising air (*Graversen et al., 2008; Jones et al., 2012*) and ocean water temperatures in parts of the Arctic as a result of climate change (*Steele et al., 2010*).

The quick and, as suggested in this research, precise measurements prior to bloom termination of algal biomass obtained using transmitted irradiance will permit efficient

monitoring of ice algae chl *a* in response to climate warming in the future. An assessment of this method's efficiency in comparison to core estimates would be beneficial in further development of the technique. Analysis of the wide range of ice algae bio-physical relationships reviewed in this study illustrate the need for additional integrated studies combined with modeling sensitivity analysis to make definitive conclusions on ice algal environmental controls. A study examining the contribution of nutrients in addition to the influences reviewed would especially help further assessments. While nutrients were not part of our assessment, the decrease in biomass measured with increasing under-ice velocity indicates biomass loss by tides outweighed their positive influence of nutrient supply that is often reported (*Cota et al.*, 1987).

Acknowledgements

This research was supported through a Northern Scientific Training Program (NSTP) grant to K. Campbell as well as funding from the Natural Sciences and Engineering Research Council of Canada (NSERC), Canada Research Chairs program (CRC), Polar Continental Shelf Program (PCSP) of Natural Resources Canada, and the Centre for Earth Observation Science (CEOS) at the University of Manitoba. We would also like to thank Kristy Hugill, Wayne Chan, Lauren Candlish, and Matt Gale for their contributions.

Literature Cited

- Alou, E., Mundy, C.J., Roy, S., Gosselin, M., Agusti, S., 2012. Ice algae pigment composition in the Canadian Beaufort Sea during spring. Submitted March 2012 to *Mar. Ecol. Prog. Ser.*
- Arrigo, K.R., Mock, T., Lizotte, M., 2010. Primary Producers and Sea Ice, in: Thomas, D.N., Dieckmann, G.S. (Eds.), *Sea Ice*, second edition. Wiley Blackwell Publishing, Malaysia, pp. 283-325.
- Belzile, C., Vincent, W., Gibson, J., Hove, P., 2001. Bio-optical characteristics of the snow, ice, and water column of a perennially ice-covered lake in the High Arctic. *Can. J. Fish. Aquat. Sci.* 58, 2405-2418.
- Bricaud, A., Bedhomme, A.L., Morel, A., 1988. Optical properties of diverse phytoplanktonic species: experimental results and theoretical interpretation. *J. Plankton Res.* 10, 851-873.
- Bricaud, A., Claustre, H., Ras, J., Oubelkheir, K., 2004. Natural variability of phytoplanktonic absorption in oceanic waters: Influence of the size structure of algal populations. *J. Geophys. Res.* 109, C11010, doi:10.1029/2004JC002419.
- Cota, G., Horne, E., 1989. Physical control of arctic ice algal production. *Mar. Ecol. Prog. Ser.* 52, 111-121.
- Cota, G., Smith, R., 1991. Ecology of bottom ice algae: III. Comparative physiology. *J. Mar. Syst.* 2, 297-315.
- Cota, G., Prinsenberg, S., Bennett, E., Loder, J., Lewis, M., Anning, J., Watson, N., Harris, L., 1987. Nutrient Fluxes During Extended Blooms of Arctic Ice Algae. *J. Geophys. Res.* 92, 1951-1962, doi:10.1029/JC092iC02p01951.
- Cota, G.F., Legendre, L., Gosselin, M., Ingram R. G., 1991. Ecology of bottom ice algae: 1. Environmental controls and variability. *J. Mar. Syst.* 2, 257-277.
- Cox, G.F.N, Weeks, W.F., 1983. Equations for determining the gas and brine volumes of in sea-ice samples. *J. Glaciol.* 29, 306-316.
- Eicken, H., 1992. The role of sea ice in structuring Antarctic ecosystems. *Polar Biol.* 12, 3-13.
- Fortier, M., Fortier, L., Michel, C., Legendre, L., 2002. Climatic and biological forcing of the vertical flux of biogenic particles under seasonal Arctic sea ice. *Mar. Ecol. Prog. Ser.* 225, 1-16.

- Garrison, D.L., Buck, K.R., 1986. Organism losses during ice melting: A serious bias in sea ice community studies. *Polar Biol.* 6, 237-239.
- Golden, K.M., Ackley, S.F., Lytle, V.I., 1998. The percolation phase transition in sea ice. *Science* 282, 2238-2241.
- Gosselin, M., Legendre, L., Demers, S., Ingram, R.G., 1985. Responses of sea-ice microalgae to climatic and fortnightly tidal energy inputs (Manitounuk Sound, Hudson Bay). *Can. J. Fish. Aquat. Sci.* 42, 999-1006.
- Gosselin, M., Legendre, L., Therriault, J.C., Demers, S., Rochet, M., 1986. Physical control of the horizontal patchiness of sea-ice microalgae. *Mar. Ecol. Prog. Ser.* 29, 289-298.
- Gosselin, M., Legendre, L., Therriault, J.C., Demers, S., 1990. Light and nutrient limitation of sea-ice microalgae (Hudson Bay, Canadian Arctic). *J. Phycol.* 26, 220-232.
- Gotelli, N.J., Ellison, A.M., 2004. *A Primer of Ecological Statistics*. Sinauer, Sunderland.
- Graversen, R.G., Mauritsen, T., Tjernstrom, M., Kallen, E., Svensson, G., 2008. Vertical structure of recent Arctic warming. *Nature* 451, 53-57.
- Holm-Hansen, O., Lorenzen, J., Holmes, R.W., Strickland, J.D., 1965. Fluorometric determination of chlorophyll. *ICES J. Mar. Sci.* 30, 3-15.
- Horner, R., Schrader, G.C., 1982. Relative contributions of ice algae, phytoplankton, and benthic microalgae to primary production in nearshore regions of the Beaufort Sea. *Arctic* 35, 485-503.
- Hsaio, S.I.C., 1992. Dynamics of ice algae and phytoplankton in Frobisher Bay. *Polar Biol.* 12, 645-651.
- Iacozza, J., Barber, D.G., 2001. Ablation patterns of snow cover over smooth first-year sea ice in the Canadian Arctic. *Hydrol. Proc.* 15, 3559-3569.
- Jones, P.D., Lister, D.H., Osborn, T.J., Harpham, C., Salmon, M., Morice, C.P., 2012. Hemispheric and large-scale land-surface air temperature variations: An extensive revision and an update to 2010. *J. Geophys. Res.* 117, D05127, doi:10.1029/2011JD017139.
- Juhl, A., Krembs, C., 2010. Effects of snow removal and algal photoacclimation on growth and export of ice algae. *Polar Biol.* 33, 1057-1065.
- Kottmeier, S.T., Sullivan, C.W., 1988. Sea ice microbial communities. IX. Effects of temperature and salinity on metabolism and growth of autotrophs and heterotrophs. *Polar Biol.* 8, 293-304.

- Lavoie, D., Denman, K., Michel, C., 2005. Modeling ice algal growth and decline in a seasonally ice-covered region of the Arctic (Resolute Passage, Canadian Archipelago). *J. Geophys. Res.* 110, C11009, doi:10.1029/2005JC002922.
- Legendre, L., Gosselin, M., 1991. In situ spectroradiometric estimation of microalgal biomass in first-year sea ice. *Polar Biol.* 11, 113-115.
- Legendre, L., Aota, M., Shirasawa, K., Martineau, M.J., Ishikawa, M., 1991. Crystallographic structure of sea ice along a salinity gradient and environmental control of microalgae in the brine cells. *J. Mar. Syst.* 2, 347-357.
- Legendre, L., Ackley, S., Dieckmann, G., Gullikson, B., Horner, R., Hoshiai, T., Melnikov, I., Reeburgh, W., Spindler, M., Sullivan, C., 1992. Ecology of sea ice biota II. Global significance. *Polar Biol.* 12, 429-444.
- Maykut, G.A., Grenfell, T.C., 1975. The spectral distribution of light beneath first-year sea ice in the Arctic Ocean. *Limnol. Oceanogr.* 20, 554-563.
- Morgan-Kiss, R., Ivanov, A.G., Williams, J., Mobashsher, K., Huner, N.P., 2002. Differential thermal effects on the energy distribution between photosystem II and photosystem I in thylakoid membranes of a psychrophilic and mesophilic alga. *Biochim. Biophys. Acta.* 1561, 252-265.
- Morgan-Kiss, R., Priscu, J.C., Pockock, T., Gudynaite-Savitch, L., Huner, N.P.A., 2006. Adaptation and acclimation of photosynthetic microorganisms to permanently cold environments. *Microbiol. Mol. Biol. Rev.* 70, 222-252.
- Mundy, C.J., Barber, D.G., Michel, C., 2005. Variability of snow and ice thermal, physical and optical properties pertinent to sea ice biomass during spring. *J. Mar. Syst.*, 58, 107-120.
- Mundy, C.J., Barber, D.G., Michel, C., Marsden, R.F., 2007a. Linking ice structure and microscale variability of algal biomass in Arctic first-year sea ice using an in situ photographic technique. *Polar Biol.* 30, 1099-1114.
- Mundy, C.J., Ehn, J.K., Barber, D.G., Michel, C., 2007b. Influence on snow cover and algae on the spectral dependence of transmitted irradiance through Arctic landfast first-year sea ice. *J. Geophys. Res.* 112, C03007, doi:10.1029/2006JC003683.
- Parsons, T.R., Maita, Y., Lalli, C.M., 1984. *Manual of Chemical and Biological Methods for Seawater Analysis*. Pergamon Press, New York.
- Perovich, D., 1996. The optical properties of sea ice. Monograph 96-1, US Army Corps of Engineers, Cold Research and Engineering Laboratory, 1-23.

- Perovich, D., Roesler, C., Pegau, W., 1998. Variability in Arctic sea ice optical properties. *J. Geophys. Res.* 103, 1193-1208, doi:10.1029/97JC01614.
- Pielou, E.C., 1984. *The Interpretation of Ecological Data: A Primer on Classification and Ordination.* Wiley, New York.
- Polashenski, C., Perovich, D., Courville, Z., 2012. The mechanisms of sea ice melt pond formation and evolution. *J. Geophys. Res.* 117, C01001, doi:10.1029/2011JC007231.
- Pringle, D.J., Miner, J.E., Eicken, H., Golden, K.M., 2009. Pore space percolation in sea ice single crystals. *J. Geophys. Res.* 117, C12017, doi:10.1029/2008JC005145.
- Rintala, J.M., Piiparinen, J., Ehn, J., Autio, R., Kuosa, H., 2006. Changes in phytoplankton biomass and nutrient quantities in sea ice as responses to light/dark manipulations during different phases on the Baltic winter 2003. *Hydrobiologia* 554, 11-24.
- Robinson, D., Arrigo, K., Iturriaga, R., Sullivan, C., 1995. Microalgal light-harvesting in extreme low-light environments in McMurdo Sound, Antarctica. *J. Phycol.* 31, 508-520.
- Smith, R.E.H., Harrison, W.G., Harris, L.R., Herman, A.W., 1990. Vertical fine structure of particulate matter and nutrients in sea ice of the High Arctic. *Can. J. Fish. Aquat. Sci.* 47, 1348-1355.
- SooHoo, J., Palmisano, A., Kottmeier, S., Lizotte, M., SooHoo, S., Sullivan, C., 1987. Spectral light absorption and quantum yield of photosynthesis in sea ice microalgae and a bloom of *Phaeocystis pouchetii* from McMurdo Sound, Antarctica. *Mar. Ecol. Prog. Ser.* 39, 175-189.
- Steele, M., Zhang, J., Ermold, W., 2010. Mechanisms of summertime upper Arctic Ocean warming and the effect on sea ice melt. *J. Geophys. Res.* 115, C11004, doi:10.1029/2009JC005849.
- Welch, H., Bergmann, M.A., 1989. Seasonal development of ice algae and its prediction from environmental factors near Resolute, N.W.T., Canada. *Can. J. Fish Aquat. Sci.* 46, 1793-1804.
- Welch, H.E., Bergmann, M.A., Jorgenson, J.K., Burton, W., 1988. A subice suction corer for sampling epontic ice algae. *Can. J. Fish Aquat. Sci.* 45, 562-568.

CHAPTER FOUR: CHARACTERIZING THE ICE ALGAE BIOMASS – SNOW DEPTH RELATIONSHIP OVER SPRING MELT USING TRANSMITTED IRRADIANCE

This paper has been prepared for submission to the Journal of Polar Biology. The work represents a core chapter of my thesis and this work was all conceived, conducted, analysed, and reported by me as the first author.

Campbell, K., Mundy, C.J., Barber, D., Gosselin, M. Characterizing the ice algae biomass-snow depth relationship over spring melt using transmitted irradiance. Polar Biol. (in preparation).

Abstract

The nature of the ice algae chlorophyll *a* (chl *a*) - snow depth (H_S) relationship was investigated on first-year sea ice in Allen Bay, Nunavut, from 27 April to 13 June 2011. A transmitted irradiance technique was used to estimate ice algae chl *a* throughout the period at time series locations under a snow cleared site, and under a low, medium, and high snow depth cover. Furthermore, chl *a* was estimated along transects perpendicular to dominant snow drift orientation, and at short term snow clear experimental sites. The association between chl *a* and H_S was characterized by four phases over the spring bloom period; light limitation (characterized by a strong negative relationship), a transitional period (no relationship), limitation driven by excess irradiance (strong positive relationship), and snow independent limitation (no relationship). These periods held true for low, medium, and the majority of high snow depths, but algae under H_S greater than 30 cm did not follow these trends and were likely light limited throughout the spring. Algal biomass under areas cleared of snow was lower and experienced earlier termination

(reaching zero biomass) than snow-covered control sites. Rates of biomass decline were also greater at snow free locations, especially towards the end of the spring period. Results indicated that bottom ice temperature and the magnitude of photosynthetically active radiation incident at the ice surface (S_{PAR}) were the most important factors driving biomass loss from snow free areas, most likely due to minor ice melt and accompanying changes in ice structure. From these results we conclude that rain and warm weather events which serve to rapidly melt the snowpack and increase the level of S_{PAR} transmitted through the ice, predicted to become increasingly common in the Arctic, could cause significant depletion of algal biomass and possibly early termination of the bloom if they occur late in the spring. However, the occurrence of such events early in the season, when the ice temperatures are sufficiently low, would likely not have the same impact.

Keywords: Ice Algae, Spring Bloom, Snow, Transmitted Irradiance

1. Introduction

Accessibility of light to sea ice primary producers during the spring bloom is largely dependent on radiative transfer through the snow and sea ice cover. Absorption and scattering of photons within the sea ice matrix, composed of ice, brine, air, and sometimes salts, efficiently attenuates light, resulting in an exponential decline of photosynthetically active radiation transmittance (T_{PAR}) with ice thickness (*Perovich, 1996; Ehn et al., 2008*). Despite the attenuation properties and thickness of sea ice, it is actually the much thinner layer of overlying snow that primarily controls the magnitude of bottom ice PAR because of its high albedo and greater capacity to scatter light. In

addition, snow also affects bottom ice temperature, and therefore bottom ice ablation, insulating it from the warming atmosphere during the spring (*Sturm and Massom, 2010*). As a result of these characteristics, the uneven distribution of snow on sea ice from wind forced displacement of drifts creates a non-uniform light and thermal environment at the ice bottom that translates to a spatially variable distribution of ice algae biomass on the order of 100 meters (*Gosselin et al., 1986*). Biomass further varies at the microscale because of ice substructure and brine hole spacing (*Mundy et al., 2007a*), as well as at much larger scales (kilometers) due to the influences of ocean water salinity, ice thickness, and nutrient availability (*Gosselin et al., 1986; Robineau et al., 1997; Granskog et al., 2005*).

The manner in which snow depth (H_S) influences algal biomass can change as the melt season evolves. During early melt, when the ice surface is dominated by a relatively thick snow cover (i.e. in late winter or early spring), ice algae are often negatively associated with H_S as the energy required for photosynthesis is greatly restricted by a drop in transmitted radiation below snow drifts. During this period of the bloom, algae adapt to the low irradiance by decreasing their maximum photosynthetic rate (*Robinson et al., 1995*), and by producing accessory pigments to enhance light harvesting (*Arrigo et al., 2010*), but positive net photosynthesis cannot begin until a minimum level of irradiance, on the order of $7.6 \mu\text{mol photons m}^{-2} \text{s}^{-1}$, is reached (*Gosselin et al., 1985*).

Later in the spring, snow melt from rising air temperatures permits an increase in the amount of radiation entering the sea ice. The resultant change in light environment at the bottom ice causes algae to transition from shade to light adaptation (*Gosselin et al., 1985*). Despite the adaptability of the algae to the changed light conditions, increased

levels of irradiance can have negative physiological effects such as photoinhibition (Robinson *et al.*, 1995). For this reason, along with the thermal influence of snow as it buffers the sea ice from warming atmospheric temperatures, thereby reducing bottom ice ablation, the negative association between biomass and H_S may switch to a positive relationship (Gosselin *et al.*, 1986; Sturm and Massom, 2010). During this latter period of the spring, algae are also limited by depleted nutrient resources due to algal consumption and may experience a form of light limitation as cells higher in the ice column absorb preferred wavelengths. Over the course of the bloom, ice algae populations can thus shift from a phase characterized by light limitation to that of nutrient limitation, self-shading induced light limitation, photoinhibition, and, or ice ablation (i.e., habitat erosion; Gosselin *et al.*, 1990; Cota *et al.*, 1991; Lavoie *et al.*, 2005). The bloom ends in the late spring with the release of ice algae into the water column following snow and ice melt.

Spring melt in the Arctic is anticipated to occur quicker and earlier due to the warming climate (ACIA, 2005). Understanding the potential response of ice algae to rapid decreases in snow and, therefore, increasing light conditions at different times during the spring is necessary for predicting the timing and extent of the sea ice bloom. This is important as changes in overall productivity or the timing of bloom termination could have critical implications for the Arctic ice-covered ecosystem (Leu *et al.*, 2011).

A study by Juhl and Krembs (2010) concluded that ice algal response to rapid increases in light may be attributed to the magnitude of change in irradiance, as well as the photophysiology of cells. Furthermore, their observations suggest ice algae may therefore have the capacity to acclimate to increased light levels given sufficient time. However, algal exposure to sudden increases in irradiance levels without adequate

response time to acclimate will likely result in a decline in biomass (*Fortier et al.*, 2002; *Juhl and Krembs*, 2010).

The objectives of our study were to document the relationship between biomass and H_S , and to examine the effects rapidly changing snow depths have on algal biomass across the spring bloom period. The study used a transmitted irradiance technique (*Campbell et al.*, ms; see Chapter three) to estimate chl *a* concentrations at time series sites, along transects, and at locations cleared of snow in Allen Bay, Nunavut, in spring 2011. By meeting the objectives, we will provide new information on potential ice algal responses to abrupt warming events expected to occur in the Arctic associated with a warming climate.

2. Materials and Methods

2.1 Study Site

Data were collected between 27 April and 13 June 2011, in Allen Bay, Nunavut (Figure 4.1). The region was characterized by smooth landfast first-year sea ice (FYI) approximately 1.3-1.7 m thick overlying a 60 m water depth. For sampling purposes snow depths were categorized as low (L; <10 cm), medium (M; 10 to 18 cm), or high (H; >18 cm) in the early spring. During advanced melt, areas of low H_S are predisposed to form ponds (*Iacozza and Barber*, 2001); therefore, melt ponds in this study were considered extensions of the low snow depth category, and snow or white ice cover persisting into late stages of spring were categorized as high. Meteorological variables including air temperature (Vaisala HMP 45C212), wind speed-direction (RM Young 05103), downwelling surface PAR (S_{PAR} ; Kipp & Zonen PAR-Lite), and surface

upwelling (UW) and downwelling (DW) shortwave radiation from wavelengths 305 to 2800 nm (Kipp & Zonen CNR1) were recorded every minute at a weather station installed on the ice surface throughout the entire research period. Albedo was calculated using the UW and DW measurements from this location to provide a descriptor of surface change over time. All variables from this meteorological site were averaged on a daily basis.

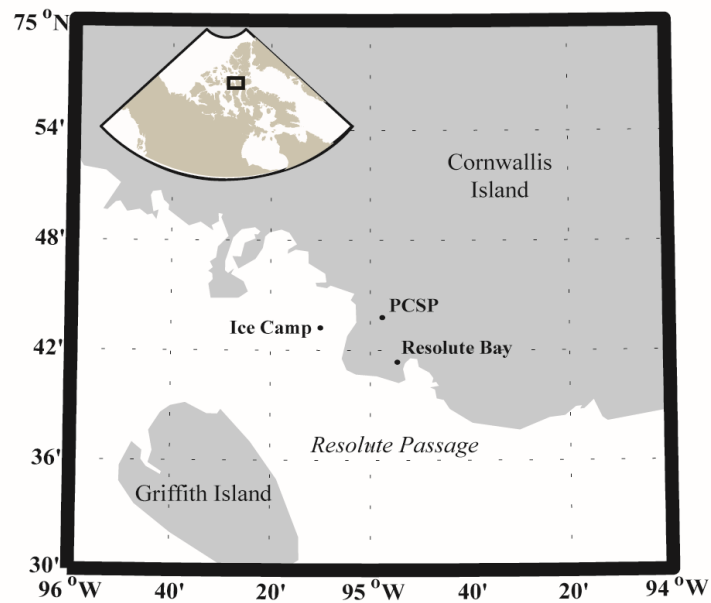


Figure 4.1. Location of 2011 ice camp in Allen Bay, Nunavut, Canada ($74^{\circ} 43.165' N$; $95^{\circ} 10.099' W$).

2.2 Determining Biomass from Transmitted Irradiance

Ice algae biomass was estimated in this study using the transmitted irradiance technique described by Mundy et al. (2007b) and presented in Campbell et al. (ms; see Chapter three). The method requires calibration of transmitted irradiance (T_{λ}) to core based chl *a* estimates, establishment of an optimal wavelength combination to represent chl *a* in the form of a normalized difference index (NDI):

$$\text{NDI} = [T_{\lambda_1} - T_{\lambda_2}] / [T_{\lambda_1} + T_{\lambda_2}], \quad (4.1)$$

and the calculation of biomass from T_{λ} measurements using the relationship between core chl a and the best NDI wavelength combination (NDI_x).

2.2.1 Measurement of T_{λ}

T_{λ} was measured approximately 0.15 m beneath the sea ice at core locations for NDI calibration (see section 2.3), along transects, and at snow clear sites. This was achieved using a dual head visible-near infrared spectrometer (Analytical Spectral Devices Inc.©; hereafter ASD) with reverse cosine receptor (RCR; 180° field of view) that measured spectral irradiance (W m^{-2}) over wavelengths from 350 to 1050 nm at a 1.4 nm bandwidth. The underwater sensor was positioned beneath the ice by attachment to a mechanical arm, deployed through a 9 inch auger hole, which positioned the sensor 1.5 m south of the hole. Underwater spectra were integrated over 4.35 s. While the instrument recorded irradiance, a solid foam device covered the hole to minimize light contamination on the measurement. Coincident with all T_{λ} measurements, surface spectral irradiance was also recorded using the reference ASD sensor and was integrated over 17 ms. The transmittance of PAR integrated wavelengths (T_{PAR}) was calculated from these measurements by summing the magnitude of radiation at PAR wavelengths beneath the ice divided from PAR irradiance incident at the surface (*Campbell et al.*, ms; see Chapter three).

2.2.2 T_{λ} Calibration

Cores from high, medium, and low sites in the early spring, or high and low during advanced melt, were taken, using a 9 cm Mark II Kovacs core barrel, at new locations

every four days following T_λ measurement around 10:00 h central daylight time. The bottom 10 cm of each core was collected and melted over a period of 18 to 24 hours in 0.2 μm filtered sea water that was added at a ratio of 3:1. Samples for fluorometric analysis were obtained from filtration of the melted cores (Whatman GF/F filters) followed by extraction of pigments by placement of the filter in 10 ml of 90% acetone at 5°C for approximately 24 hours. Fluorometric measurements (Turner Designs Fluorometer 10-005R) were then taken on replicate pigment samples before and after acidifying the solution with 5% HCl (*Parsons et al.*, 1984). Areal chl *a* concentration was calculated based on these measurements and the equations of Holm-Hansen et al. (1965).

2.2.3 Normalized Difference Index (NDI) and Biomass Calculation

No significant difference in the relationship between core chl *a* versus NDI was observed between snow depths (Chow Test; $p > 0.05$) and therefore, NDI analysis was accomplished with all high, medium, and low data pooled together. To determine NDI_x , a Pearson correlation matrix of core chl *a* against all possible NDI wavelength combinations was calculated (*Campbell et al.*, ms; see Chapter three). The NDI using wavelengths 478 and 490 nm was the highest correlated ($r = 0.90$) and met other desirable criteria listed by Mundy et al. (2007b) such as: NDIs with wavelengths close together increases its dependence on algal absorption rather than that of snow or ice. The regression between core chl *a* and NDI_x :

$$\text{chl } a \text{ (mg m}^{-2}\text{)} = (-497.21 \times \text{NDI}_x) + 15.202, \quad (4.2)$$

accounted for 81% of chl *a* variability and was used to calculate biomass at all locations where T_λ alone was measured. Due to error associated with the data spread in the calibration, the technique resulted in slightly negative biomass estimates during the

advanced melt period (*Campbell et al.*, ms; see Chapter three). An assumption that negative values represented zero algal biomass was accepted for this research as negative estimates were only 6.7% of the entire range observed during the study.

2.3 Snow Clear Experimentation

Snow cover on patches of sea ice was removed to assess the response of algal biomass to rapid increases in transmitted irradiance over the spring. Sampling of these experiments began with the measurement of T_λ for one day under sites of undisturbed medium snow cover, with the exception of one low H_S site. An area of 9 m² immediately south of the hole augered for deployment of the radiometer was then marked, sampled for average H_S , and cleared that evening. This area was deemed sufficiently large to exclude any influence of horizontal scattering from neighboring snow covered ice, comparable to areas used in similar experiments such as 10 m² by Gradinger et al. (1991). A total of six snow cleared regions were created, all of which were kept free of snow for a period of approximately 10 days, apart from the first location (site A) which was maintained over the entire sampling period as a time series site (see section 2.4). T_λ was sampled daily between 09:00 and 11:00 h at the snow cleared sites, immediately after clearing the surface, while ensuring the underwater sensor was centered under the cleared area. These experimental treatments were created until the onset of melt ponds, which corresponded to the disappearance of most snow from the ice surface.

2.4 Time Series

Three sites representing each of the snow depth categories were selected as locations for measurement of a single algal population's *in situ* biomass over the spring.

Following the method outlined above, T_{λ} was recorded daily at each site followed by measurement and averaging of five snow depths on a nearby surface comparable to the sample location. Precautions were taken in an effort to maintain the natural integrity of the snow surfaces, such as careful re-excavation of the auger hole during the cold period when ice would reform between measurements, and no traffic was permitted on the sample area. On 19 May these time series were contaminated by soot fallout from the ice camp furnaces upwind and therefore, three new sites of the same characteristics were selected approximately 50 m away (at locations out of the contaminated area). For the purposes of analysis, the new high, medium, and low sites were loosely considered extensions of the previous locations where the two sampled areas of each snow depth category were treated as one continuous time series.

The first snow clear experimental site established was maintained as a time series from 27 April to 2 June to observe long term biomass response to increased light transmittance. Sampling followed the procedure outline in the section above with daily clearing of snow and sampling of T_{λ} . A consequence of snow removal over time was the creation of a snow mound immediately north of the site. Periodically this snow was relocated to avoid shadowing of the site; however, complete removal was not achieved and some shading of this time series may have occurred when the sun was in a northern position.

2.5 Transect Sampling

Transects running in the East-West direction, perpendicular to snow drift orientation, were randomly constructed approximately every 4 days (Table 4.1). This directionality was chosen to capture the potential influence of snow depth on ice algae

chl *a* (Gosselin *et al.*, 1986). Holes for operating the mechanical arm were made at two meter intervals along each transect, followed by recording of T_{λ} measurements between 14:00 and 16:30 h. Snow or melt pond depth was then measured every meter at the approximate location T_{λ} was sampled (1.5 m south of hole). Transect length was a function of time, such that T_{λ} measurements had to be completed before the sun was in a far west position, and DW surface irradiance became too low for optimal T_{λ} sampling. As a result of weather and equipment failures affecting sampling time, half of all transects sampled were approximately 30 m in length, while the remainder were 60 m.

*Table 4.1. Summary of transect measurements including sample date, transect length and number of chlorophyll *a* (chl *a*) biomass, snow depth (H_S) and PAR integrated transmittance (T_{PAR}) observations.*

Transect	Date	Distance (m)	Observations (n)	
			chl <i>a</i> - T_{PAR}	H_S
1	29 April	24	13	25
2	3 May	30	16	31
3	9 May	24	13	26
4	13 May	60	31	61
5	17 May	28	15	61
6	21 May	30	16	31
7	25 May	60	31	61
8	29 May	60	31	61
9	3 June	60	31	61
10	6 June	60	31	61
11	11 June	30	16	31

2.6 Sampling End Date

The use of transmitted irradiance to estimate algal biomass during the late spring can result in falsely high chl *a* values because of absorption by algal derived particulate and dissolved material in the water column between the sensor and ice subsurface (Campbell *et al.*, ms; see Chapter three). To prevent falsely high biomass estimates from

absorption by these materials, measurements at time series and snow cleared sites were ceased once zero biomass was reached. Zero biomass was not reached during the first 10 days of snow clear experiments A, B and C therefore measurements for the desired 10 day length of sampling were used. Sample days used in analysis of sites D and E however are less than the desired 10 days as biomass declined to zero on sample day 6 and 3, respectively. In addition, based on the 13 June date at which snow covered time series reached zero biomass (see section 3.2), no measurement at any sampling location was used past this date, serving to shorten snow clear site F to 8 days total.

3. Results

3.1 Site Characteristics

Daily averaged surface air temperature increased approximately linearly over the sampling period from a minimum of $-21.8 \pm 3.3^{\circ}\text{C}$ on 27 April to a maximum of $1.4 \pm 0.6^{\circ}\text{C}$ on 10 June, with intensifying S_{PAR} (Figure 4.2a, c). This increase was associated with a transition of sea ice from an average snow cover depth of about 14 cm, and a maximum of 66 cm, to a mixed surface comprising of melt ponds, snow mounds, and white ice. Albedo remained relatively constant around 0.84 until 10 June, after which values declined sharply to a low of 0.30 ± 0.02 on 13 June (Figure 2b). The rapid change in albedo and thus surface conditions was a result of a storm event on 10 June that brought strong winds and rain. Bottom ice temperature and under-ice current velocities, which followed a bi-weekly tidal cycle, also increased as the spring progressed (Campbell *et al.*, ms; see Chapter three).

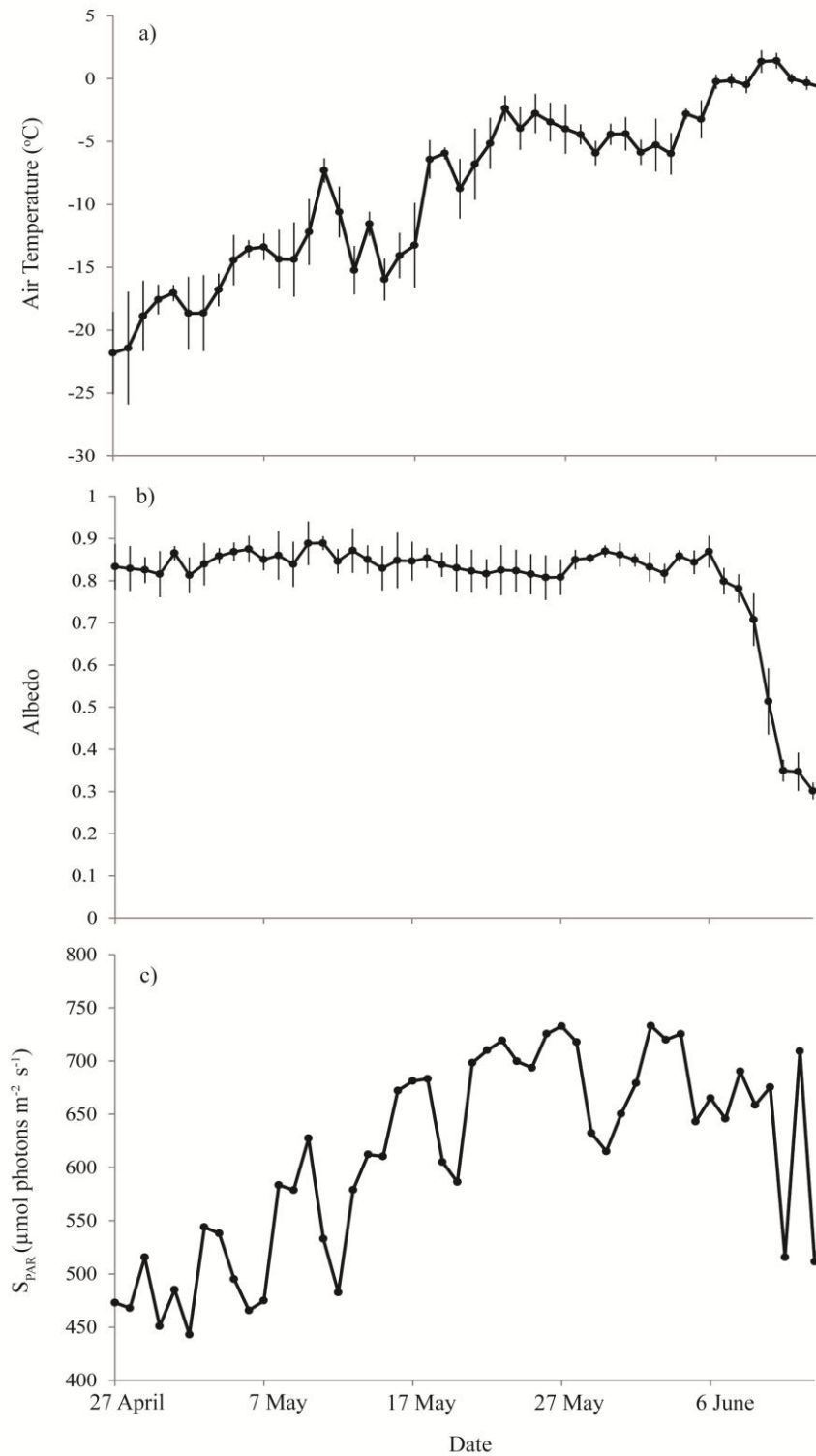


Figure 4.2. Daily average values of (a) air temperature, (b) albedo and (c) surface photosynthetically active radiation (S_{PAR}) measured at the meteorological station over the sample period. In (a) and (b), bars represent the standard deviation.

3.2 Time Series Analysis

Data for biomass growth and loss at each of the four time series: snow clear site A, and high, medium, and low snow depth locations, are presented in Figure 4.3.

Demonstrating distinct stages of accumulation and loss of ice algal biomass over the time series, each site exhibited a significant second order polynomial distribution with inflections of 14 May at the snow clear experimental site ($y = -0.245x^2 + 6.5861x - 433.97$; $r^2 = 0.746$), 25 May under high snow ($y = -0.0231x^2 + 6.7237x - 469$; $r^2 = 0.475$), 19 May under medium ($-0.0198x^2 + 5.5384x - 368.21$; $r^2 = 0.580$), and 15 May under low snow depths ($y = -0.0138x^2 + 3.7417x - 237.22$; $r^2 = 0.600$). The increasingly later date of inflection point with deeper snow covers indicated that under deeper snow, algal populations were able to maintain a biomass accumulation phase longer into spring. However, this trend did not translate to greater total biomass accumulation over the spring, as daily chl *a* values averaged over the entire sampling period at high, medium, and low time series were nearly equivalent at 12.25, 12.04, and 12.09 mg m⁻², respectively. These values are exclusive of the biomass maximums at the medium site at 35.5 mg m⁻² and under high H_S at 49.7 mg m⁻² as they were uncharacteristic of the overall trend, potentially representing error associated with water column algae affecting our sampling late in the period.

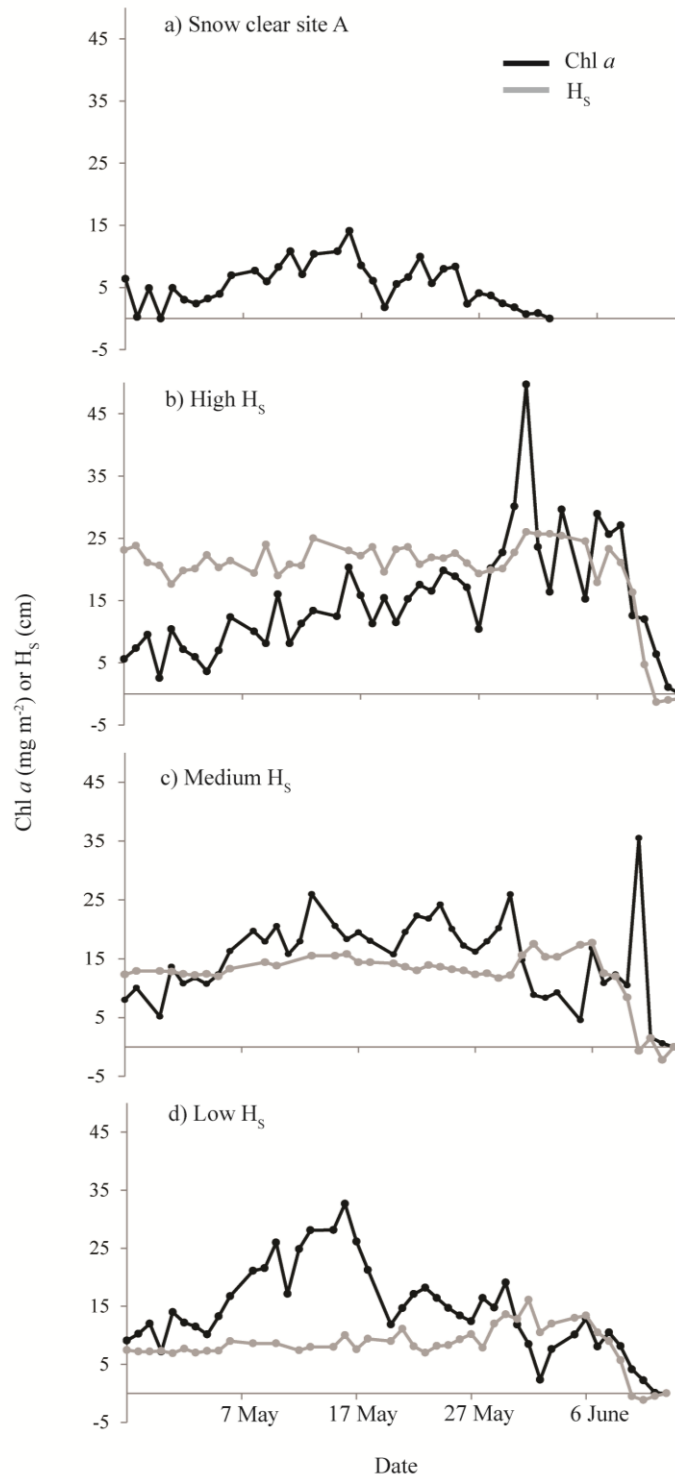


Figure 4.3. Time series of bottom ice chlorophyll *a* (*chl a*) biomass and snow depth (H_s) at (a) the snow clear site A and (b) under high, (c) medium and (d) low snow cover sites. *Chl a* biomass was calculated using the normalized difference index (see section 2.2 for details).

Accumulation of biomass during the beginning of the sampling period was quickest under low snow, followed by medium, and was slowest under high snow. The opposite was observed for declines in biomass associated with bloom termination at these sites where the decrease appeared to be most gradual under low, followed by medium and high snow sites, respectively. The algal biomass trend over the spring therefore differs with snow depth category, such that ice algae experience periods of rapid and gradual change under high and low snow cover while they were relatively more constant under medium snow over the spring bloom. Despite these differences in biomass response over the bloom, all snow covered locations terminated (reaching zero biomass) on 13 June.

The snow clear time series (site A) was classified as a medium site prior to the removal of snow therefore, the medium snow site was treated as a control for this experiment (Figure 4.3a, c). Significant differences in the magnitude of chl *a* between curves (ANOVA, $p < 0.05$) indicates that throughout the experiment, biomass accumulation was suppressed at the snow clear location (average $5.21 \text{ mg chl } a \text{ m}^{-2}$) compared to the control (average $13.66 \text{ mg chl } a \text{ m}^{-2}$) over the same time period. In addition, the snow clear site reached zero biomass nearly 2 weeks earlier than all other time series (Figure 4.3). The experimental site also did not share the same timing of trend inflection as the medium site. Instead, it was relatively similar to the low snow site, suggesting that the snow clear and low snow sites had corresponding biomass accumulation phases.

3.3 Snow Clear Experimentation

Biomass (B) was calculated using the normalized difference index (section 2.2) at the snow clear experimental sites for sample day 1 (snow covered) through n (day 2

onwards; snow cleared). The change in biomass between all consecutive sample days ($B_n - B_{n-1}$) were then calculated and summed, after which they were averaged over each snow clear site's duration in days (N) (see section 2.6, the first ten days were used for site A). These average rates of biomass change following snow removal (R_X):

$$R_X = \frac{\sum_2^n (B_n - B_{n-1})}{N} \quad (4.3)$$

for sites A through F ranged between $0.06 \pm 3.90 \text{ mg m}^{-2} \text{ d}^{-1}$ on 27 April at site A, and $-6.35 \pm 6.27 \text{ mg m}^{-2} \text{ d}^{-1}$ on 31 May at site E (Figure 4.4). Overall, R_X became increasingly negative for experiments done progressively later in the spring, with site E having an uncharacteristically large negative response in relation to the overall trend.

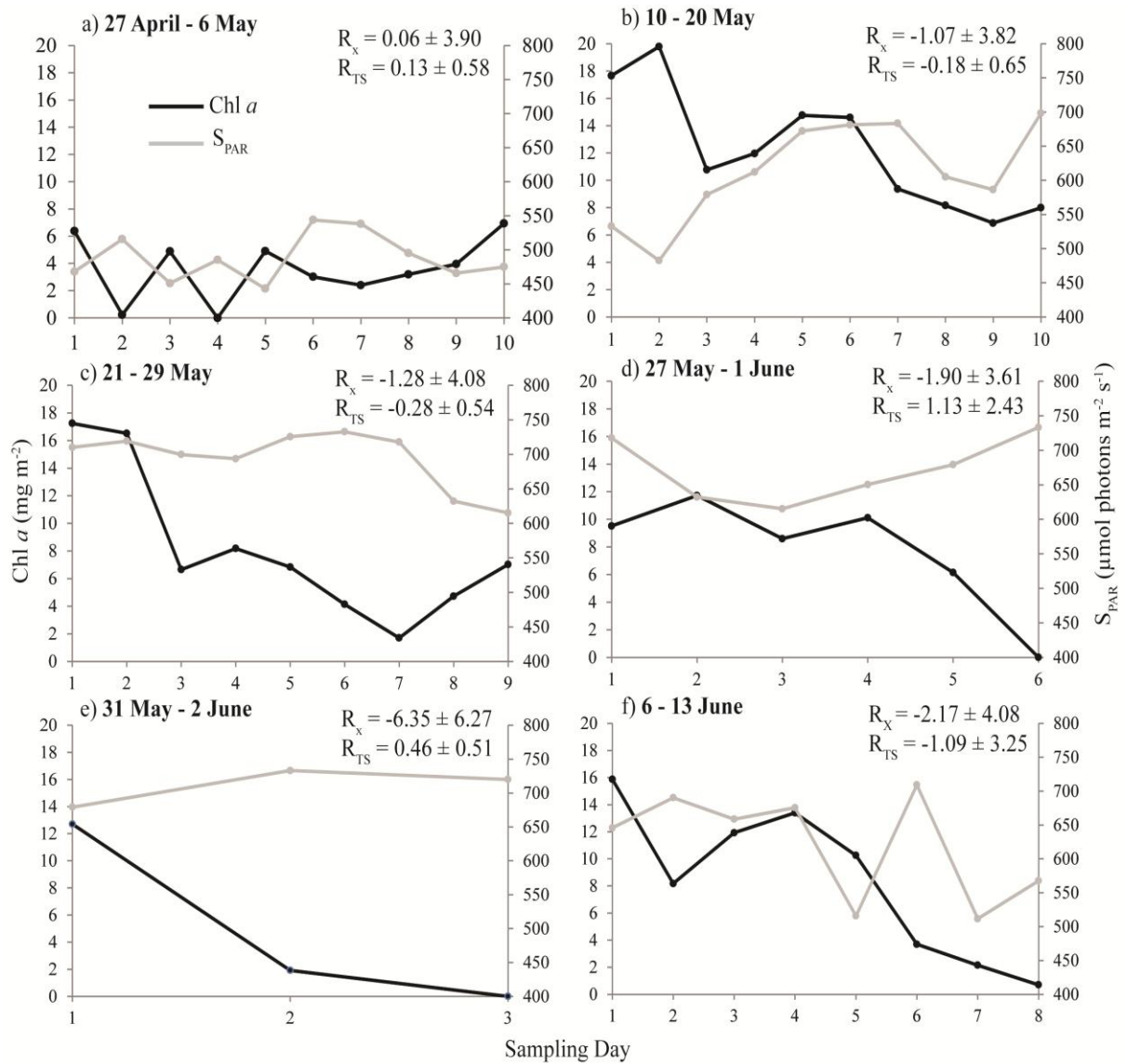


Figure 4.4. Temporal changes in bottom ice chlorophyll *a* (*chl a*) biomass and daily average surface photosynthetically active radiation (S_{PAR}) at snow clear sites (a) A, (b) B (c) C, (d) D, (e) E and (f) F. Sample day one is snow covered, sample day 2 and onwards represent measurements following snow removal. Chl *a* biomass was calculated using the normalized difference index (see section 2.2 for details). The rate of change of *chl a* biomass at each site (R_X) and for the same period at the time series site under medium snow cover (R_{TS}) was determined following equation (4.3), with the exception of site D where R_{TS} was calculated from the time series site under low snow cover. Standard deviations of daily R_X and R_{TS} values about the mean are also provided.

The daily change in *chl a* at the medium time series site (Figure 4.3) was also calculated and averaged for the sampling period of each snow clear experiment (R_{TS}).

This was with the exception of site D, where the low snow depth time series was used instead. The resultant rates of change at snow covered sites, during the same dates as snow clear experiments, were used as controls to which the snow clear sites could be compared. Comparison of biomass changes under snow covered and cleared sites indicated that algal response under snow free areas were less positive at site A, and more negative at sites B through F. Similar to the assessment of snow clear site A time series, the removal of snow was therefore again seen to hinder the accumulation of bottom ice algal biomass.

Daily averaged albedo on sample day 1 of each snow clear experiment did not change over the sample period ($r^2 = 0.004$, $p = 0.909$) as all snow clear experiments were carried out prior to ponding (Figure 4.2). However, the average magnitude of S_{PAR} on sample day 1 of each site increased significantly over the sampling period ($r^2 = 0.678$, $p < 0.05$). This indicated that the magnitude of radiation entering the sea ice increased over the melt period as solar insolation rose. Unfortunately surface irradiance values at each snow free site were not accurately recorded so T_{PAR} for snow cleared sites could not be calculated to support this. Nevertheless, it can be concluded that as the spring progressed, algae populations were exposed to continually greater changes in irradiance upon snow removal.

Based on the 14 May inflection point calculated for snow clear site A (Figure 4.3a), experiments prior to this date were expected to be in a positive accumulation phase, while those following should have experienced a negative one marked by biomass decline. This hypothesis is supported by the clear snow sites experiments, which show a change in R_X from a positive value during the growth phase (Figure 4.4a) and to negative values during

the decline phase (Figure 4.4c-f), with the exception of site B potentially as a result of its position at the boundary between the two phases (Figure 4.4b).

Lastly, the biomass response following removal of low snow depths at site D is important to note as it did not deviate from the trend of declining R_X value with time. This indicates that algae under low H_S had a similar response to snow removal than algae associated with medium depths.

3.4 Transect Analysis

3.4.1 Seasonal Trends

The distributions of chl a , H_S , and T_{PAR} along transects sampled over the study are summarized in Figure 4.5. Spatial variability of chl a , indicated by the length of error bar and box plotted, was low during the initial and final transects sampled, implying that small levels of biomass were distributed relatively evenly across the bottom ice during early and late spring (Figure 4.5a). Median transect biomass increased until approximately 21 May and declined thereafter, illustrating the development and ultimate end of the ice algae bloom. This point of transition between rising and decreasing median biomass values fell between the inflection points of the medium and high snow cover series (Figure 4.3b, c). The timing of relative chl a inflection point was likely a consequence of sampling as the majority of snow depths measured along transects fell within medium and high snow classes (38% medium and 40% high). That is, transect chl a was dominated by algal biomass trends characteristic of populations under high and medium snow covers.

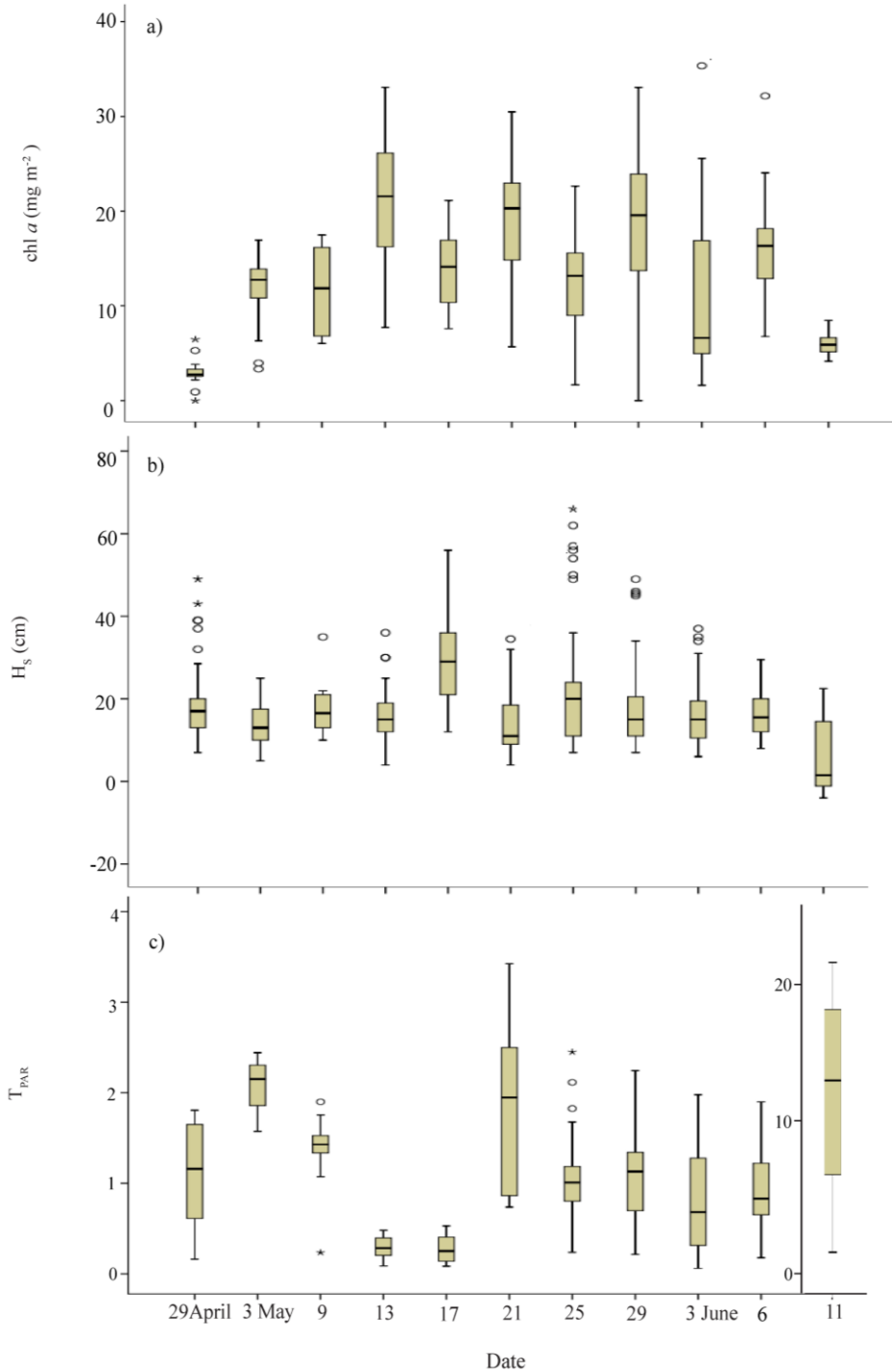


Figure 4.5. Temporal changes and variability in (a) bottom ice chlorophyll a (*chl a*) biomass, (b) snow depth (H_S) and (c) PAR integrated transmittance (T_{PAR}) from 29 April to 11 June along transects. *Chl a* biomass was calculated using the normalized difference index (see section 2.2 for details). Boxes represent the median and interquartile ranges, vertical lines the sample range, and outliers are indicated by circles and stars for extreme cases. In (c), note the change in scale for 11 June.

The transects sampled on 17 May, 25 May, and 3 June appeared to deviate from the general parabolic trend of chl *a* (Figure 4.5a). H_S was positively skewed on 17 May and on 25 May as a number of high snow depth outliers were inadvertently sampled (Figure 4.5b). The uniqueness of these transects could be explained by inadvertent sampling across an area of thick snow cover such as a ridge or patch of rough ice which are known to accumulate deeper snow (*Iacozza and Barber, 1999*). If this occurred, irregular features on FYI, that cause preferential snow drift accumulation could have the potential to negatively affect biomass during the spring bloom. However, the low median chl *a* on 3 June, also documented at medium and low time series sites (Figure 4.3c, d), was not a result of skewed sampling as the range of H_S did not appear to deviate from the average (Figure 4.5a, b). A widespread early sloughing event therefore likely occurred.

In comparison to chl *a*, H_S and T_{PAR} did not exhibit the same parabolic seasonal trend. Instead, median values and spatial variability remained largely consistent over time with the exception of H_S on 17 and 25 May (as described above) and T_{PAR} on 11 June (Figure 4.5b, c). The large increase in T_{PAR} median and range values between 6 and 11 June illustrated the effect the severe weather event, as discussed above, and increasing air temperatures (Figure 4.2a) had on the sea ice light environment, as H_S decreased and ponds formed.

3.4.2 Chl *a* – H_S association

Relationships between transmitted irradiance derived chl *a* and H_S were evaluated for each transect, using linear regression analysis (Figure 4.6). The relationship between chl *a* versus H_S changed from negative to positive between 29 May and 3 June (Figure 4.6h, i). Algal biomass measured under depths of snow greater than 30 cm was

consistently low over the spring despite observed changes in biomass under other snow depths. The low biomass associated with high snow depths was exemplified in transects sampled on 21 May and 3 June where biomass under low snow had begun to decline, resulting in a peak biomass at medium snow depths and overall polynomial distribution (Figure 4.6f, i).

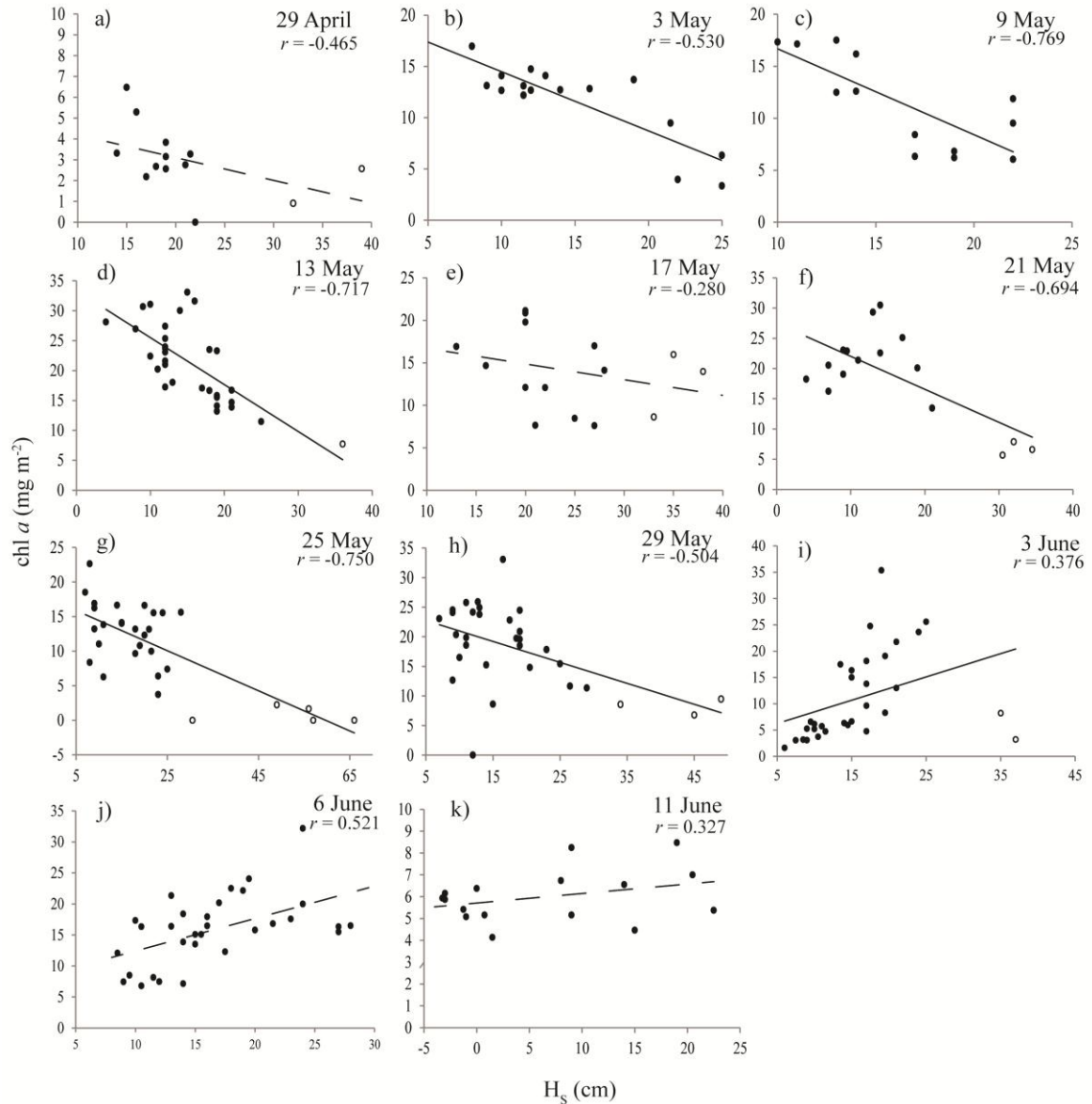


Figure 4.6. Linear regressions between bottom ice chlorophyll a (*chl a*) biomass and snow depth (H_s) for transects sampled from the 29 April to 11 June. Open circles represent sites covered with ≥ 30 cm of snow. *Chl a* biomass was calculated using the normalized difference index (see section 2.2 for details). Solid lines indicate slope significantly different from zero ($p < 0.05$) while dashed lines represent non-significant relationships ($p > 0.05$).

For all transects sampled, biomass under snow covers of ≥ 30 cm averaged 6.12 mg m⁻² and linearly declined with increasing H_s ($r = 0.514$, $p < 0.05$; data not presented).

This value is much lower than *chl a* of populations under snow less than 30 cm at 14.55

mg m⁻² on average (Figure 4.6). Therefore, biomass accumulation under snow covers deeper than 30 cm was likely light limited over the entire spring, the extent of which was dependent on small variations within this category of H_S. However, these deep snow covers only accounted for 0.06% of the total depths sampled, and therefore, the relationship between chl *a* versus H_S below 30 cm was also evaluated (see section 4.2).

4. Discussion

4.1 Biomass Response to Snow Removal

Suppressed biomass and early termination at the snow free time series (Figure 4.3), along with the negative biomass responses documented at other experimental sites (Figure 4.4), indicated a general negative effect of snow removal on biomass accumulation. Clearing of snow cover increases both light transmission into the ice and conductive flux between the atmosphere and sea ice. In turn these changes affect ice algal biomass via photoinhibition, or by ice melt associated with either an enhanced exposure to the warming atmosphere during spring and, or light absorption by sea ice as well as the absorption and conversion of radiation to heat by algal cells, referred to as biological melt (Zeebe *et al.*, 1996; Lavoie *et al.*, 2005; Juhl and Krembs, 2010). Ice melt may also indirectly cause cell removal following enhanced brine drainage (Mundy *et al.*, 2005; Campbell *et al.*, ms; see Chapter three).

Ice algae have the capacity to acclimate to increasing irradiance levels given enough time and permitting the increases occur in small increments (Juhl and Krembs, 2010). It follows then that the gradual rise of S_{PAR} over this study (Figure 4.2) resulted in algal populations later in the spring exhibiting a higher degree of light acclimation than

those early on. It has been found that once ice algae become light-acclimated, exposure to rapid increases in radiation may not result in photoinhibition. Alternatively, biomass of more shade-acclimated populations may decline in part because of photoinhibition when subjected to large jumps in irradiance (*Juhl and Krembs, 2010*). Based on this reasoning, biomass suppression and greater loss rates due to photoinhibition were expected for snow clear experiments conducted in the early spring. However, the less negative responses and biomass levels well above zero documented earlier in the spring (snow clear sites A, B, and C), and more rapid biomass loss often reaching zero later in the season (snow clear sites D, E, and F) suggest other mechanisms influencing ice algal biomass were of greater importance. This is possible as ice algae are capable of acclimating to high light environments such that even in the presence of light saturation, photoinhibition does not necessarily occur (*Rysgaard et al., 2001; McMinin et al., 2007*). The greater changes in irradiance following snow removal as a result of significantly increasing S_{PAR} over the spring may, however, indicate photoinhibition contributed to the severity of response documented later in the spring.

The similarity in biomass response following snow removal at low (light acclimated algae; site D) and medium snow depths (shade acclimated algae; all other snow clear sites) supports the mechanisms independent of algal physiological state as more important in determining ice algal biomass suppression and loss. This result does not support the observations of *Juhl and Krembs (2010)* where exposure of algae associated with different snow depths resulted in differences in biomass response in part due to differences in cell physiology. Specifically in their study, algae under low snow

cover did not experience as large of a decline in chl *a* following snow removal in comparison to algae under greater snow depths.

The removal of snow does not necessarily result in bottom ice ablation unless atmospheric temperatures are high enough to significantly warm the ice (*Juhl and Krembs, 2010*). The cold atmospheric (Figure 4.2a) and bottom ice temperatures (ranging from about -6.2 to -1.85°C; *Campbell et al., ms*; see Chapter three) present during early sampling therefore make unlikely conditions for biomass loss via ablation even following snow removal. However, the strong linear association between R_X (without the site E outlier) and the bottom ice temperature gradient on day 1 of sampling obtained from *Campbell et al. (ms)* ($r^2 = 0.93$, $p < 0.05$), supports that factors associated with ice melt were important controls on biomass. From these results we suggest that the less negative R_X values and presence of biomass recovery during the first three snow clear experiments, when ice ablation was likely not occurring, indicated that exposure of algae to rapid increases of irradiance at a time when cells can maintain attachment to a stable ice matrix permits biomass recovery and does not necessarily result in termination of the spring bloom. The possible negative influence of rapid exposure during the latter part of the spring is shown by the large difference in rates of biomass change between snow cleared (R_X) and snow covered (R_{TS}) sites from 27 May to 2 June (Figure 4.4d, e).

Although insignificant, R_X was also negatively associated with S_{PAR} over the sample period ($r^2 = 0.632$, $p = 0.105$). It is unlikely that increasing S_{PAR} was enough to cause significant bottom ice ablation however, small increases in ice temperature following absorption of radiant energy by the sea ice and algal cells may have still altered bottom ice structure, a factor known to affect algal biomass (*Eicken et al., 1992*).

Changes in ice structure, particularly the connectivity of brine inclusions, are especially important to note at ice temperatures above -5°C (*Light et al.*, 2003). Because bottom ice temperature in this study largely remained at or above this critical value for the duration of sampling (*Campbell et al.*, ms; see Chapter three) biomass loss associated with changing bottom ice structure is plausible, as is loss associated with brine drainage. Assessment of biological melt contributions to biomass loss from sea ice have largely focused on enhanced ice ablation when chl *a* concentrations are high (*Zeebe et al.*, 1996; *Juhl and Krembs*, 2010), therefore further investigations into the influence of biological melt at low biomass and low temperatures is required.

The potential influence of S_{PAR} may have also been a contributing factor to the rapid negative response documented at snow clear experiment E, where biomass reached zero in only 2 days after snow removal (Figure 4.4e). At site E, the average value of S_{PAR} on the first day of snow free sampling (sample day 2) at $733 \mu\text{mol photons m}^{-2} \text{s}^{-1}$ was higher than any other experiment. This was followed by site C at $719 \mu\text{mol photons m}^{-2} \text{s}^{-1}$, which had the second largest negative biomass loss rate (Figure 4.4c, e). In contrast, less negative (or positive) R_X values like those during experiments at sites A and B at the beginning of the spring corresponded to the two lowest day 2 S_{PAR} values of the season (Figure 4.4a, b). The magnitude of S_{PAR} exposure following snow removal therefore appears to have been a factor in biomass response in these experiments. The greater influence of ice temperature and S_{PAR} later in the spring were potentially coincident with the negative effects of nutrient limitation associated with this period, as well as brine drainage which was found to significantly decrease biomass in *Campbell et al.* (ms).

4.2 Seasonality of the Biomass – H_S Relationship

The change in association between chl a and H_S along transects is summarized in Figure 4.7, where the Pearson Correlation statistic (r) determined for locations with H_S less than 30 cm is plotted. The result is an approximately linear and significant increase of r values from -0.855 to 0.761 over time ($r^2 = 0.720$, $p < 0.05$), that can be used to divide the spring into four periods of chl a - H_S association: significant negative (29 April to 13 May), not significant (14 to 29 May), significant positive (30 May to 6 June), and not significant (11 June and later).

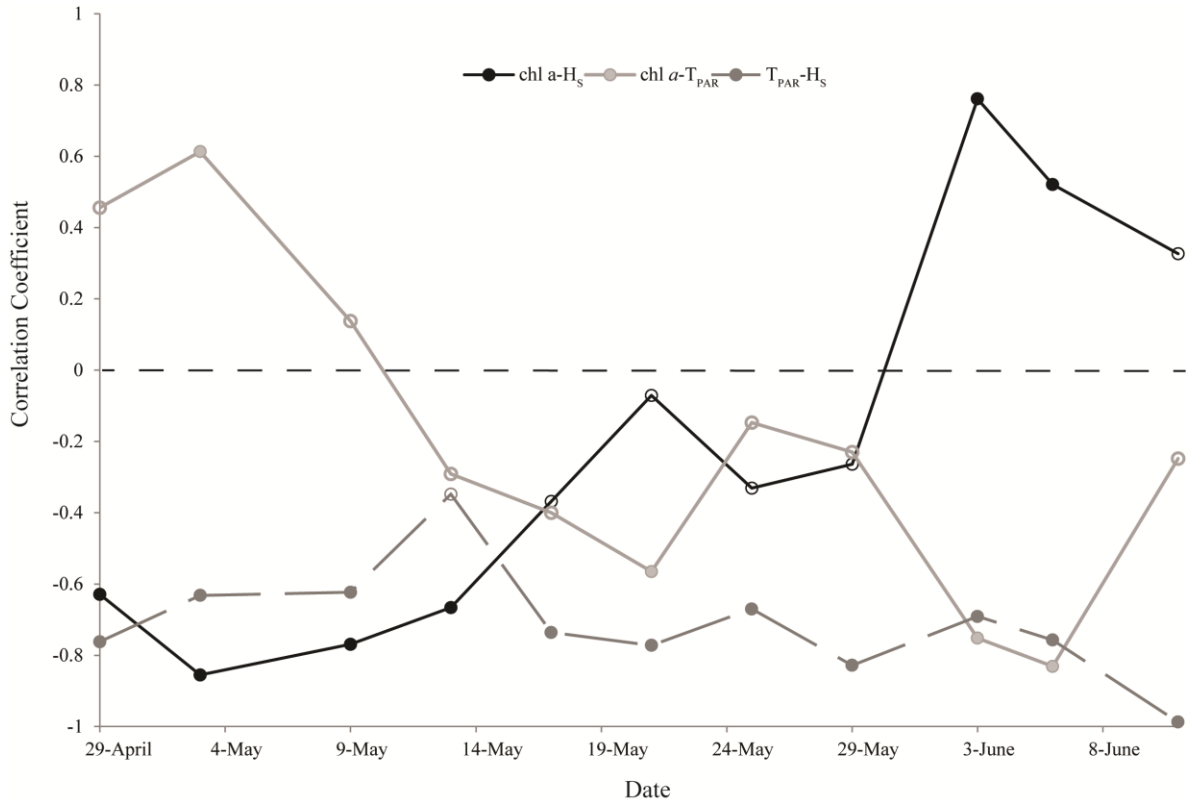


Figure 4.7. Temporal changes in Pearson correlation coefficient (r) between bottom ice chlorophyll a (chl a) biomass, snow depth (H_S) and PAR integrated transmittance (T_{PAR}) for transects sampled from 29 April to 11 June. Chl a biomass was calculated using the normalized difference index (see section 2.2 for details). Note that chl a - T_{PAR} and chl a - H_S relationships were based on sites with $H_S < 30$ cm. Solid circle indicates significant correlation ($p < 0.05$).

Early in the spring (29 April to 13 May), the accumulation of algal biomass was significantly hindered by the presence of snow cover on the sea ice, indicated by an r value of -0.73 on average during this period. The strong negative association between chl a and H_S was likely a result of light limitation caused by low solar insolation (and therefore low S_{PAR} ; Figure 4.2), and the strong attenuating properties of snow which are represented by the largely positive r values describing chl a and T_{PAR} in Figure 4.7. Following this period, a transitional phase (14 to 29 May) between low light and other environmental limitations occurred, represented by the low negative and insignificant correlations of chl a with both H_S and T_{PAR} . In their modeling efforts, Lavoie et al. (2005) documented a similar period of changeover between phases where a low light phase was followed by a period characterized by alternating diurnal light and nutrient limitation, before reaching the final period dominated by low nutrient levels.

During more advanced stages of melt (30 May to 6 June) in this study, algae populations became inhibited by factors related to a thinning snowpack, having a mean positive correlation coefficient of 0.64. The greater loss of biomass associated with greater bottom ice temperatures in snow clear experiments suggested that populations of algae were able to persist late in the spring under higher snow depths as a result of a delay in bottom ice warming, and perhaps melt associated with this. It should be noted that populations may have the potential to revert back to light limitation during this period of the spring, supported by the sloughing event documented at 3 June transects and times series that possibly occurred due to the influence of a storm which increased snow depth on all sites on 30 May and was associated with a drop in S_{PAR} (Figure 4.3). The coupled influence of deeper and newly deposited snow, which has a greater capacity to

scatter light, and low surface irradiance, would have caused a sudden decrease in T_{PAR} to the ice bottom. In addition, high velocities of under-ice currents can contribute to biomass loss from the ice (*Campbell et al.*, ms; see Chapter three) and have even been shown to cause mid-bloom sloughing events in other studies (*Mundy et al.*, 2007a). Strong currents likely contributed to this biomass loss event as daily averaged under-ice velocities, which have a documented significant negative influence on biomass accumulation, reached a maximum in their bi-weekly tidal cycle on 3 June at 8.05 cm s^{-1} (*Campbell et al.*, ms; see Chapter three).

Timing of the transitional period in Figure 4.7 is further reinforced by the inflection points of all time series sites in our study (Figure 4.3), which fell within this phase. The progressively later inflection dates for deeper snow depths can be explained by the rates of biomass accumulation, where faster growth of biomass would have resulted in quicker use of available nutrients leading to earlier nutrient limitation. For example, algae under low snow depths, which experienced lower amounts of light limitation, increased to peak biomass fastest, in turn using up available nutrients sooner. Rózanska et al. (2009) demonstrated that maximum chl *a* in Arctic first-year landfast ice was a function of surface nitrate concentrations. Although nutrients were not specifically sampled in this research, our observations could reflect the significant role they played in regulating biomass throughout the majority of the spring. It also implies that algal populations under different snow depths may simultaneously be experiencing slightly different limitation states.

The shift from a negative to positive relationship between chl *a* and H_S occurred approximately two weeks later in our study than in the Hudson Bay study by Gosselin et

al. (1986). In general, Hudson Bay undergoes melt onset in May, much earlier than the higher latitude location of Resolute Bay in the Canadian Archipelago where ponding does not occur until June (*Fequet et al.*, 2011). This observation, along with the early termination documented at the snow clear time series illustrates that the earlier snow melt occurs, the sooner bloom termination will likely occur. The important role snow serves in delaying the end of the ice algal spring bloom is thus supported (*Lavoie et al.*, 2005).

The fourth and final phase contained the 11 June transect, which had insignificant r values for both chl a - H_S and chl a - T_{PAR} associations. We suggest that ice algae biomass at this date and later were declining as a result of bloom termination independent of any association with H_S or T_{PAR} . That is, any spatial variability present in ice algae was a relic of previous conditions as all populations were subjected to critical levels of widespread ice melt and, or nutrient limitation. It is important to note that the phases discussed above were a function of only those sites where snow depth was 30 cm or less. Ice algae at sites with snow ≥ 30 cm remained within a light limited phase throughout the spring, the extent of which was linearly dependent on small variations in snow depth.

5. Conclusions

The association between ice algae and snow depth was investigated in this study. Analysis of time series revealed that the nature of response and total accumulation of biomass during the spring bloom was dependent on the class of overlying snow depth (none, low, medium, or high). For algae under less than 30 cm the nature of chl a – H_S association can be summarized into four periods; light limitation in the early spring, a transitional period, limitation driven by excess irradiance, and snow independent decline. Algae under snow greater than 30 cm depth remain primarily light limited over the entire

spring bloom. These snow depth dependent trends in biomass accumulation and loss undoubtedly contribute to the bottom-ice spatial distribution of ice algae that is often documented.

Ice temperature, and to a lesser extent S_{PAR} , were especially important factors in causing low biomass in these experiments, likely through their influence on ice structure and melt. The influence of these factors was not as significant earlier in the spring when ice temperatures were still cold enough to essentially lock the algae in the ice matrix. These observations along with previous documentation of an ice temperature threshold by Campbell et al. (ms; see Chapter three) suggest that the severity of algal response to rapid exposure of high irradiance is dependent on the time of spring. It follows that rain events and warm spells which are anticipated to increase in frequency in the Arctic as a result of climate change (*ACIA*, 2005) would have greater negative effects if they were to occur later in the spring. Sooner bloom termination from these events in the early spring is unlikely based on our results as the algae showed the capacity to recuperate during periods of low to zero ice melt.

Acknowledgements

The authors would like to recognize the support provided by the Northern Scientific Training Program grant (NSTP) to K. Campbell, and by the Natural Sciences and Engineering Research Council of Canada (NSERC), the Canada Research Chairs program (CRC), the Polar Continental Shelf Program (PCSP) of Natural Resources Canada, and the Centre for Earth Observation Science (CEOS) at the University of Manitoba. We also wish to thank Kristy Hugill and Matt Gale for their contributions.

Literature Cited

- ACIA, 2005. ACIA, Arctic Climate Impact Assessment. Cambridge University Press, New York.
- Arrigo, K.R., Mock, T., Lizotte, M., 2010. Primary Producers and Sea Ice, in: Thomas D.N., Dieckmann G.S. (Eds.), *Sea Ice*, second edition. Wiley Blackwell Publishing, Malaysia, pp. 283-325.
- Campbell, K., Mundy C.J., Barber D., Gosselin M., ms. Time series measurements of ice algae biomass using transmitted irradiance and assessment of influential physical variables over the spring melt period. *J. Mar. Syst.*
- Cota, G., Smith, R.E.H., 1991. Ecology of bottom ice algae: III. Comparative physiology. *J. Mar. Syst.* 2, 297-315.
- Ehn, J., Papakyriakou, T., Barber, D., 2008. Inference of optical properties from radiation profiles within melting landfast sea ice. *J. Geophys. Res.* 113, C09024, doi:10.1029/2007JC004656
- Eicken, H., 1992. The role of sea ice in structuring Antarctic ecosystems. *Polar Biol.* 12, 3-13.
- Fequet, D., Hache, L., McCourt, S., Langlois, D., Dicaire, C., Premont, B., Jolicoeur, A., Minano, A., 2011. *Sea Ice Climatic Atlas for the Northern Canadian Waters 1981 – 2010*. Environment Canada. <http://www.ec.gc.ca/glaces-ice/default.asp?lang=En&n=4B35305B-1>. Accessed 21 July 2012.
- Fortier, M., Fortier, L., Michel, C., Legendre, L., 2002. Climatic and biological forcing of the vertical flux of biogenic particles under seasonal Arctic sea ice. *Mar. Ecol. Prog. Ser.* 225, 1-16.
- Gosselin, M., Legendre, L., Demers, S., Ingram, R.G., 1985. Responses of sea-ice microalgae to climatic and fortnightly tidal energy inputs (Manitounuk Sound, Hudson Bay). *Can. J. Fish. Aquat. Sci.* 42, 999-1006.
- Gosselin, M., Legendre, L., Therriault, J.C., Demers, S., Rochet, M., 1986. Physical control of the horizontal patchiness of sea-ice microalgae. *Mar. Ecol. Prog. Ser.* 29, 289-298.
- Gosselin, M., Legendre, L., Therriault, J.C., Demers, S., 1990. Light and nutrient limitation of sea-ice microalgae (Hudson Bay, Canadian Arctic). *J. Phycol.* 26, 220-232.

- Gradinger, R., Spindler, M., Henschel, D., 1991. Development of Arctic sea-ice organisms under graded snow cover. *Polar Res.* 10, 295-307.
- Granskog, M.A., Kaartokallio, H., Kuosa, H., Thomas, D.N., Ehn, J., Sonninen, E., 2005. Scales of horizontal patchiness in chlorophyll a, chemical and physical properties of landfast sea ice in the Gulf of Finland (Baltic Sea). *Polar Biol.* 28, 276-283.
- Holm-Hansen, O., Lorenzen, J., Holmes, R.W., Strickland, J.D., 1965. Fluorometric determination of chlorophyll. *ICES J. Mar. Sci.* 30, 3-15.
- Iacozza, J., Barber, D.G., 1999. An examination of the distribution of snow on sea-ice, *Atmos. Ocean* 37, 21-51.
- Iacozza, J., Barber, D.G., 2001. Ablation patterns of snow cover over smooth first-year sea ice in the Canadian Arctic. *Hydrol. Proc.* 15, 3559-3569.
- Juhl, A., Krembs, C., 2010. Effects of snow removal and algal photoacclimation on growth and export of ice algae. *Polar Biol.* 33, 1057-1065.
- Lavoie, D., Denman, K., Michel, C., 2005. Modeling ice algal growth and decline in a seasonally ice-covered region of the Arctic (Resolute Passage, Canadian Archipelago). *J. Geophys. Res.* 110, C11009, doi:10.1029/2005JC002922.
- Leu, E., Soreide, J.E., Hessen, D.O., Falk-Peterson, S., Berge, J., 2011. Consequences of changing sea-ice cover for primary and secondary producers in the European Arctic shelf Seas: Timing, quantity, and quality. *Prog. Oceanogr.* 90, 18-32.
- Light, B., Maykut, G.A., Grenfell, T.C., 2003. Effects of temperature on the microstructure of first-year Arctic sea ice. *J. Geophys. Res.* 108, C23051, doi: 10.1029/2001JC000887.
- McMinn, A., Ryan, K.G., Ralph, P.J., Pankowski, A., 2007. Spring sea ice photosynthesis, primary productivity and biomass distribution in eastern Antarctica, 2002-2004. *Mar. Biol.* 151, 985-995.
- Mundy, C.J., Barber, D.G., Michel, C., 2005. Variability of snow and ice thermal, physical and optical properties pertinent to sea ice biomass during spring, *J. Mar. Syst.* 58, 107-120.
- Mundy, C.J., Barber, D.G., Michel, C., Marsden, R.F., 2007a. Linking ice structure and microscale variability of algal biomass in Arctic first-year sea ice using an in situ photographic technique. *Polar Biol.* 30, 1099-1114.
- Mundy, C.J., Ehn, J.K., Barber, D.G., Michel, C., 2007b. Influence of snow cover and algae on the spectral dependence of transmitted irradiance through Arctic landfast first-year sea ice. *J. Geophys. Res.* 112, C03007, doi:10.1029/2006JC003683.

- Parsons, T.R., Maita, Y., Lalli, C.M., 1984. *Manual of Chemical and Biological Methods for Seawater Analysis*. Pergamon Press, New York.
- Perovich, D., 1996. *The Optical Properties of Sea Ice*, US Army Corps of Engineers. Cold Research and Engineering Laboratory, Monograph 96-1, 1-23.
- Robinson, D.H., Arrigo, K.R., Iturriaga, R., Sullivan, C.W. 1995. Adaptation to low irradiance and restricted spectral distribution by Antarctic microalgae from under-ice habitats. *J. Phycol.* 31, 508–520.
- Robineau, B., Legendre, L., Kishino, M., Kudoh, S., 1997. Horizontal heterogeneity of microalgal biomass in the first-year sea ice of Saroma-ko Lagoon (Hokkaido, Japan). *J. Mar. Syst.* 11, 81-91.
- Rózanska, M., Gosselin, M., Poulin, M., Wiktor, J.M, Michel, C., 2009. Influence of environmental factors on the development of bottom ice protist communities during the winter–spring transition. *Mar. Ecol. Prog. Ser.* 386, 43-59.
- Rysgaard, S., Kuhl, M., Hansen, J.W., 2001. Biomass, production and horizontal patchiness of sea ice microalgae in a high-Arctic fjord (Young Sound, NE Greenland). *Mar. Ecol. Prog. Ser.* 223, 15-26.
- Sturm, M., Massom, R.A., 2010. Snow and Sea Ice, in: Thomas D.N., Dieckmann G.S. (Eds.), *Sea Ice*, second edition. Wiley Blackwell Publishing, Malaysia, pp. 154-204.
- Zeebe, R.E., Eicken, H., Robinson, D.H., Wolf-Gladrow, D., Dieckmann, G.S., 1996. Modeling the heating and melting of sea ice through light absorption by microalgae. *J. Geophys. Res.* 101, 1163-1181.

CHAPTER FIVE: CONCLUSIONS AND RECOMMENDATIONS

5.1 Summary

Chapter one presents an introduction to the thesis topic and outlines the content of each chapter to follow.

Chapter two provides context on the research topic with a discussion of information relevant to the Arctic ice algae bloom, including the sea ice habitat. The chapter focuses on the formation, growth, and decay of sea ice and how this controls the optical and structural characteristics of the ice, the factors limiting biomass and causing bloom termination, and finally discussion of the methods of sampling algal populations.

Chapter three presents the use of transmitted irradiance to estimate ice algae biomass at one point location over time, providing the first truly representative time series estimates of biomass. Coincident measurement of select environmental variables permitted evaluation of physical limitations on algal accumulation and loss, which in turn contribute to biomass variability and the end of the spring bloom.

Chapter four builds off of the results of chapter three with the validated remote sensing technique now used to further investigate the strong association between ice algal biomass and snow depth that was outlined in the previous chapter. A collection of time series, transects, and snow clear experiments were used to investigate the nature of this association. Information from these data contribute to understanding sub-ice spatial variability of algal biomass and potential response of algae populations to a warming climate.

5.2 Future Recommendations

Deriving non-invasive biomass estimates from transmitted irradiance measurements is an effective means of sampling *in situ* populations and should be incorporated into future research on sea ice primary producers. Some precautions, however, should be taken with the application of this technique:

- 1) A universal optimal normalized difference index (NDI) is unlikely; instead transmitted irradiance should be calibrated to core based, or other traditionally derived, biomass values for each study completed at different times and locations. This may be a consequence of differences in pigment composition between populations that may cause alternative optimal NDIs. Future work on the effects of algal pigment composition on NDI value is recommended.
- 2) The use of transmitted irradiance to estimate ice algae biomass should be avoided under two circumstances. The first, when biomass is known to be very low, as a higher proportion of negative chlorophyll *a* (chl *a*) values tends to occur, potentially as a result of core based calibration. Secondly, when debris is present in the water column or ice, as the presence of non-algal absorptive particles will create misleading NDIs and therefore inaccurate biomass estimates. This last condition is especially important to note during advanced melt when algae slough off the sea ice and float between the sensor and ice surface, serving to create falsely high biomass values.
- 3) Although the Analytical Spectral Device Inc. (ASD) instrument, recording wavelengths 300 to 1050 nm, was effectively used in this research, use of an instrument specific to recording wavelengths of photosynthetically active

radiation (PAR) may reduce noise in the data. In addition, using an instrument more robust for the snow covered conditions encountered in Arctic research is suggested as the multiple ASD connections were a constant source of potential error.

Following these provisions, transmitted irradiance could be measured from automated under-water vehicles (AUVs) or remote operated vehicles (ROVs) to obtain biomass estimates over larger spatial scales. Also, fixing more permanent radiometers beneath the ice could provide temporal biomass estimates of greater frequency. Indeed, any application which avoids or minimizes sensor deployment through holes augured at the ice surface would improve the efficiency of the method.

The assessment of physical influences on ice algae biomass outlined in chapters three and four would be complemented by controlled experimentation in a laboratory. This would permit examination of the primary variables discussed, such as small scale bottom ice ablation and structural changes, biological melt, and brine drainage, in detail. Improved observation of environmental conditions would also add to the conclusions of this research, in particular the use of a non-invasive technique to document *in situ* fine scale changes in bottom ice thickness and temperature.

5.3 Conclusions

Chapter three outlines the steps required for calibration of transmitted irradiance to core based algal biomass following the procedure of Mundy et al. (2007). In this research the NDI using wavelengths 478 and 490 nm was found to be the most representative of ice algae biomass (NDI_X), differing slightly from the optimal NDI of Mundy et al. (2007)

study which used wavelengths 472 and 485. The development and termination of the spring ice algal bloom was successfully documented when NDI_X was then applied to calculate bottom-ice biomass at one location over time. Subsequent analysis of biomass variability at the time series was also investigated in chapter three, leading to the conclusion that bottom ice temperature was the primary physical control on biomass over the spring, in part because of its capacity to cause brine drainage events. This was followed by the negative influence of under-ice current velocity. Large changes to snow depth and therefore transmittance of PAR through the sea ice were also important factors during the early spring, and were instrumental in the timing of bloom termination.

The method developed in chapter three was applied to further document the association between biomass and snow depth, an environmental variable that exhibited a significant influence on biomass during the early period of the spring. Here, the presence of snow even in low amounts was found to promote greater accumulation of ice algae biomass throughout the spring, and extended the length of the algal bloom itself. Despite this positive influence of snow depth on biomass, the majority of algae during early spring were negatively associated with snow depth early on due to light limitation. This was followed however by a transition to a positive relationship and eventually a period of biomass decline independent of snow depth. The presence of snow cover was especially important during late spring (during the period of positive association) as algae were not able to persist without it at a time when ice was particularly warm due to cell loss associated with physical removal from the ice.

Effective remote estimation of ice algae biomass was proven with this M.Sc. research, as was the importance of the physical variables described above in causing

biomass variability and bloom termination through their control on the sea ice habitat.

The insights of this thesis will contribute to accurate estimates of sea ice primary production required in geochemical and ecosystem models and studies, and are important considerations when formulating predictions on the Arctic marine ecosystem's response to future habitat changes as a result of climate warming.

Literature Cited

Mundy, C.J., Ehn, J.K., Barber, D.G., Michel, C., 2007. Influence of snow cover and algae on the spectral dependence of transmitted irradiance through Arctic landfast first-year sea ice. *J. Geophys. Res.* 112, C03007, doi:10.1029/2006JC003683.

APPENDIX A: ABBREVIATIONS

Analysis of variance	ANOVA
Analytical Spectral Device Inc. spectrometer	ASD
Arctic-Ice Covered Ecosystem	Arctic-ICE
Automated underwater vehicle	AUV
Average brine volume	BV _{AVG}
Average daily change in chlorophyll <i>a</i> at snow clear sites	R _X
Average daily change in chlorophyll <i>a</i> at snow covered time series	R _{TS}
Bottom ice (10 cm) temperature	T ₁₀
Bottom ice temperature gradient	TG
Bottom ice (10 cm) salinity	S ₁₀
Coloured dissolved organic matter	CDOM
Chlorophyll <i>a</i>	chl <i>a</i>
Dimethylsulfoniopropionate	DMSP
Dimethylsulfoxide	DMSO
Exopolymeric substances	EPS
Filtered sea water	FSW
First-year sea ice	FYI
Integrated surface downwelling of photosynthetically active radiation	S _{PAR}
Integrated transmittance of photosynthetically active radiation	T _{PAR}
Mean daily sub-ice current velocity	MDV
Non-algal particle	NAP
Normalized difference index	NDI
Normalized difference index (λ 478 and 490 nm)	NDI _X
Photosynthetically active radiation (400 to 700 nm)	PAR
Principal component analysis	PCA
Remotely operated vehicle	ROV
Reverse cosine receptor	RCR
Snow depth	H _S
Snow depth category low	L
Snow depth category medium	M
Snow depth category high	H
Snow, Ice, and Permafrost Research Establishment	SIPRE
Surface downwelling irradiance	DW
Surface upwelling irradiance	UW